Sampling and Reconstruction of Spherical Signals for Applications in Cosmology, Acoustics and Beyond

Usama Elahi

January 2019

A thesis submitted for the degree of Doctor of Philosophy
of The Australian National University

Australian National University

Research School of Electrical, Energy and Materials Engineering
College of Engineering and Computer Science
The Australian National University

Declaration

The contents of this thesis are the results of original research and have not been submitted for a higher degree to any other university or institution.

Much of the work in this thesis has been published for publication as journal papers or conference proceedings. These papers are:

Journal articles

J1. **U. Elahi**, Z. Khalid, R. A. Kennedy, and J, D, McEwen, "An Optimal-Dimensionality Sampling for Spin-s Functions on the Sphere," *IEEE Signal Process. Lett.*, vol. 25, no. 10, pp. 1470-1474, OCT. 2018.

J2. **U. Elahi**, Z. Khalid, and R. A. Kennedy, "Band-limited Signal Extrapolation for inaccessible HRTF measurements on the Sphere ," *IEEE Trans. Signal Process.*, 2018. (submitted)

J3. **U. Elahi**, Z. Khalid, and R. A. Kennedy, "Design of a Spatially Constrained Anti-aliasing Filter using Slepian Functions in Spherical Microphone Arrays ," *IEEE Trans. Signal Process.*, 2019. (under preparation)

Conference papers

C1. **U. Elahi**, Z. Khalid, and R. A. Kennedy, "Comparative Analysis of Geometrical Properties of Sampling Schemes on the Sphere," in *Proc. Int. Conf. Signal Processing and Communication Systems ICSPCS'2016*, Gold Coast, Australia, pp. 1-7, Dec. 2016.

C2. **U. Elahi**, Z. Khalid, R. A. Kennedy, and J, D, McEwen "Iterative Residual Fitting for Spherical Harmonic Transform of Band-Limited Signals on the Sphere: Generalization and Analysis," in *Proc. IEEE Int. Conf. Sampling Theory and Applications, SampTA'2017*, Tallinn, Estonia, pp. 470-440, Mar. 2017.

C3. **U. Elahi**, Z. Khalid, and R. A. Kennedy, "An Improved Iterative Algorithm for Band-limited Signal Extrapolation on the Sphere," in *Proc. IEEE Int. Conf. Acoustics, Speech and Signal Processing, ICASSP'2018*, Calgary, Canada, pp. 4619-4623, Apr. 2018.

C4. **U. Elahi**, Z. Khalid, and R. A. Kennedy, "Spatially Constrained Anti-Aliasing Filter Using Slepian Eigenfunction Window on the Sphere," in *Proc. Int. Conf. Signal Processing and Communication Systems ICSPCS'2018*, Cairns, Australia, Dec. 2018.

C5. **U. Elahi**, Z. Khalid, and R. A. Kennedy, "Design of Spatially Constrained Anti-aliasing Filter using Slepian Functions on the Sphere," in *Proc. 27th European Signal Processing Conference, EUSIPCO'2019*, A Coruna, Spain, Sep. 2019. (submitted)

The following publications are also the results from my Ph.D. study but not included in this thesis:

C6. **U. Elahi**, Z. Khalid, and R. A. Kennedy, "On the choice of Kernel for signal interpolation on the sphere using reproducing kernel Hilbert Spaces," in *Proc. Int. Conf. Signal Processing and Communication Systems ICSPCS'2017*, Gold Coast, Australia, pp. 1-7 Dec. 2017.

The research presented in this thesis has been performed jointly with Dr. Zubair Khalid (Lahore University of Management and Sciences), Prof. Rodney A. Kennedy (The Australian National University) and Dr. Jason D. McEwen (University College London). The substantial majority of this work was my own.

Usama Elahi
Research School of Electrical, Energy and Materials Engineering,
The Australian National University,
Canberra,
ACT 2601,
Australia.

Acknowledgements

The work presented in this thesis would not have been possible without the support of a number of individuals and organizations and they are gratefully acknowledged below:

- I would like to thank my primary supervisor Prof. Rod Kennedy. He generously provided me with an abundance of opportunities, resources, sound advice and guidance. I am grateful to him for granting me freedom and flexibility in my research, as well as being willing to have in-depth discussions whenever I approached him for help.

- I would like to express my deepest gratitude to Dr. Zubair Khalid. His love for research and outstanding work ethic have inspired me throughout my PhD studies. He always made himself available; his patience, mentoring and friendship are also greatly appreciated.

- I would like to express my sincere thanks to members of my supervisory panel Dr. Salman Durrani and A/Prof. Parastoo Sadeghi for their guidance, support and encouragement throughout my PhD studies. They have also given me great support in providing academic advice and obtaining tutoring experience.

- I wish to thank Dr. Jason McEwen for providing remote supervision and guidance.

- It is my great pleasure to study in the Signal Processing Group at the Research School of Engineering. I would like to thank my friends and colleagues in the Signal Processing, Communications and Acoustics Groups for providing a friendly and supportive research environment.

- Special thanks to Khurram Shahzad (Communication Group) and Muhammad Hassan Iqbal (Laser Physics Centre) who I was fortunate to spend most of my PhD time with. Thank you Khurram and Hassan for being great friends, and for providing encouragement and much needed cricket relief during our studies.

- I would like to thank the ANU for awarding me the 2018 ANU Dean's Travel Grant for my visits to various international and national conferences. I would also like to acknowledge the support provided by the Australian Research Council's Discovery Projects funding scheme (Project No. DP150101011 and Project No. DP170101897).

- I would like to thank my lecturers and colleagues at the Department of Electrical Engineering, University of Engineering and Technology, Lahore, Pakistan. Dr. Syed Abdul Rahman Kashif for supervising my Masters project; these experiences were invaluable for developing my research skills. He along with Dr. Khalid Mahmud ul Hassan, in particular, inspired me to do a PhD and gave me a passion for signal processing. Thank you also to the many other excellent lecturers I had during my undergraduate and post-graduate studies.

- Thank you to my parents, Muhammad Azam and Rehana Parveen, who I would never have been able to start nor finish this thesis if it were not for their unwavering love, support and belief in me. My Mum has always been my greatest supporter and encourager. Thanks Mum for always being there for me. My Dad provided me all the help and means to travel abroad and pursue my dream of a PhD. My brother, Talha Ilahi and my sister, Ayma Azam, thank you for your encouragement and being a lot of fun when we catch up.

- I will like to thank my sister in law, Samreen Hameed, for giving us regular visits and support. Good luck for your upcoming PhD dissertation at Curtin University, Perth, Australia.

- Lastly, I would like to say special thanks to my wife, Fozia Hameed, for her constant encouragement, support, patience and always a wonderful company. I am in debt to her for providing me the soundness and calmness during the

toughest time in this journey. Thank you to my son, Aayan, for being the best thing to be home to.

Abstract

The main focus of this thesis is using the existing spherical signal processing techniques to sample and reconstruct data under different application driven scenarios. Spin-s functions are used in cosmology and an optimal sampling scheme to sample and reconstruct data using spin-s functions on the sphere is studied. Moreover, the problem of reconstruction in an environment where the samples on the sphere are inaccessible or not defined on a grid is also addressed. Lastly, the significance of spatial filtering is discussed in the field of acoustics where an anti-aliasing filter is designed to mitigate the effect of spatial aliasing in microphone arrays.

A sampling scheme is proposed for the representation of spin-s band-limited functions on the sphere, which requires optimal number of samples equal to the number of degrees of freedom. In comparison to the existing sampling designs, which require $\sim 2L^2$ samples for the representation of spin-s functions band-limited at L, the proposed scheme requires $L^2 - s^2$ samples for the accurate computation of the spin-s spherical harmonic transform (s-SHT). A method is developed to compute the s-SHT and samples are taken such that matrices involved in the computation of s-SHT are well conditioned. In order to improve the accuracy further, a multi-pass s-SHT method is also proposed. Geometrical properties like sampling efficiency, minimum geodesic distance, mesh norm and mesh ratio give us an insight of the nature of distribution of the points on the sphere. A comparative analysis with the existing schemes show that the proposed sampling design exhibits superior geometrical properties.

Algorithms for signal reconstruction on the sphere are developed and analysed for two different scenarios: i) when the measurements are not taken over a predefined grid and ii) when the estimation is done from incomplete measurements. For the first one, generalized iterative residual fitting (IRF) for the computation of the spherical harmonic transform (SHT) of band-limited signals on the sphere is presented. The proposed method is based on the partitioning of the subspace of

band-limited signals into orthogonal subspaces. There exist sampling schemes on the sphere which support accurate computation of SHT. The proposed IRF method enables accurate computation of SHTs of signals with randomly distributed sufficient number of samples. In order to improve the accuracy of the computation of the SHT, multi-pass IRF is proposed which adds multiple iterative passes to the IRF. An iterative algorithm for the extrapolation of band-limited signals from incomplete measurements on the sphere is proposed. The proposed algorithm improves the accuracy of the extrapolation of band-limited signals by using the information contained in the out-of-band harmonic coefficients of the signal to update the extrapolated signal at each iteration. The proposed algorithm does not only exploit the band-limited property of the signal at each iteration but also uses the harmonic coefficients outside the harmonic domain to improve the accuracy of signal extrapolation. To demonstrate the improvement in the accuracy, numerical experiments are conducted and a comparison is done with the results of the existing iterative conjugate gradient method.

The signal processing technique of spatial filtering is exploited in order to design an anti-aliasing filter for the applications in acoustics. In acoustics, the performance of spherical microphone arrays is typically limited by spatial aliasing which introduces side-lobes in the array beam pattern. In order to reduce the aliasing error, a spatially constrained anti-aliasing filter is proposed which approximates an ideal anti-aliasing filter used in literature as a weighted sum of concentrated eigenfunctions obtained by solving the Slepian concentration problem on the sphere. Three performance parameters namely white noise gain (WNG), directivity index (DI) and processing loss are employed to compare the performance of proposed filter with the ideal filter. A parameter-constrained filter design is also proposed by maximizing WNG subject to constraints on the DI and processing loss of the proposed filter.

List of Acronyms

FFT	Fast Fourier Transform
GL	Gauss-Legendre
SHT	Spherical Harmonic Transform
HRTF	Head-Related Transfer Function
CMB	Cosmic Microwave background
IRF	Iterative Residual Fitting
LSF	Least Square Fitting
WNG	White Noise Gain
DI	Directivity Index
3D	Three-Dimensional

Notations

x	scalar variable
$\boldsymbol{x}$	vector variable
$\hat{\boldsymbol{x}}$	unit vector
$\mathbf{X}$	matrix variable
$X_{x,y}$	element in row x and column y of $\mathbf{X}$
$\mathcal{X}$	operator
$\langle f, g \rangle$	inner product of two variables f and g
$\|(\cdot)\|$	L_2 norm
$\|(\cdot)\|$	absolute value of parameter $(\cdot)$
$\overline{(\cdot)}$	conjugate operation
$(\cdot)'$	transpose operation on vector
$(\cdot)^H$	Hermitian (conjugate transpose) operation of a matrix
$\lfloor (\cdot) \rfloor$	integer floor function
$\lceil (\cdot) \rceil$	integer ceiling function
$\delta_{p,q}$	Kronecker delta
$\delta(\cdot)$	Dirac delta
$\mathrm{tr}(\cdot)$	trace of a matrix

Contents

List of Figures

Chapter 1

Introduction

1.1 Motivation and Background

Signals are defined on the sphere in a variety of fields including medical imaging [1–3], geodesy and planetary studies [4–7], computer graphics and computer vision [8–11], acoustics [12], electromagnetic inverse problems [13], study and analysis of cosmic microwave background (CMB) in cosmology [14–21], astrophysics [22], 3D beamforming [23] and wireless channel modeling in communication systems [24, 25] to name a few. The main focus of this thesis is to develop such signal processing techniques that allow efficient measurements and accurate reconstruction of the signals on the sphere in an application-driven environment. Spherical harmonic (SH) functions [26] are a natural choice of basis functions for representing the signal on the sphere in all these applications.

Signal processing techniques have been explored and thoroughly investigated for single and multidimensional signals in the Euclidean domain, where the signals are assumed to be defined on the real line. For the processing of signals on the sphere, the mapping of data on the sphere to a two dimensional plane and applying signal processing methods developed in Euclidean domain is discouraged as the procedure produces large errors [27]. However, the signal processing techniques developed in the Euclidean domain can be extended and reformulated in order to design suitable techniques in the spherical domain [4, 18, 19, 28–50]. These include filtering [32, 37, 42], spectrum estimation [5, 27] and feature extraction [6, 31], convolution [40, 51, 52], Slepian concentration problem [53–56] on the sphere [5, 34, 57], finite-impulse-response (FIR) filtering [33], to name a few. Signals on sphere are

defined in both the spatial (spherical) and spectral (spherical harmonic) domains. The transformation between the two domains is enabled by spherical harmonic transform (SHT) [13, 26, 51, 58, 59] which is the analog of Fourier transform.

For harmonic analysis and signal representation (reconstruction), the ability to accurately compute the SHT of a signal from its samples taken over the sphere is of great importance. SHT must be computed numerically as in practice, only a finite number of samples of a signal in spatial domain are available. In the literature, over a number of decades, a number of sampling schemes on the sphere have been devised that permit accurate computation of SHT of a band-limited signal [51,59,60,60–71]. It is desirable to design such sampling schemes that should require the minimum possible number of samples for the accurate and efficient computation of SHT of a band-limited signal on sphere. Such a minimum number is referred as spatial dimensionality or optimal dimensionality—the numbers of degrees of freedom in harmonic space.

For the computation of the SHT, sampling theorems have been constructed [51, 59,62,68] using pre-defined sampling grids on the sphere, which lead to theoretically exact computation of the SHT. If the samples are taken arbitrary on the sphere, other numerical approaches can be deployed, such as approximate quadrature [61, 69]), least squares [66,67] or spherical designs [72,73], which nevertheless often lead to sufficiently accurate transform computations. Driscoll and Healy [51] developed a sampling theorem on the sphere which exploits an equiangular sampling grid to allow exact computation of signals band-limited to L on the sphere. The spatial dimensionality is $\sim 4L^2$ as the sampling scheme requires $2L$ iso-latitude rings of points, where the number of points in each ring, along longitude, are equal to $2L-1$. The well-known Gauss-Legendre (GL) quadrature on the sphere [74, 75] allows exact computation of SHT from $\sim 2L^2$ samples on the sphere, as the roots of Legendre polynomials of order L determine the non-uniformly spaced L iso-latitude rings. The number of points in each ring remain $2L-1$. The sampling theorem proposed by McEwen and Wiaux [59] requires $3(L-1)$ fewer samples than the GL approach and achieves spatial dimensionality $\sim 2L^2$. Recently a sampling scheme that attains optimal dimensionality$\sim L^2$ while allowing accurate computation of the SHT has been developed [63] and allows accurate computation for SHT even for very large values of band-limits.

For equiangular sampling schemes, least squares approaches have also been de-

veloped for the computation of SHT [66,67] and achieve good accuracy by exploiting $2L^2$ samples on the sphere. However, least square methods are increasingly complex and the accuracy and stability of the least squares approach cannot be guaranteed for higher band-limits. Spherical designs [76], which require computation of integrals over the sphere using quadrature based on uniform weighting [72,73], compute the SHT of a band-limited signal using $4L^2$ samples. Spherical designs with $4L^2$ samples have been constructed successfully for band-limit up to only $L = 100$ [76]. Spherical designs using $2L^2$ samples may be used [60], although this is not proven. The choice of the sampling scheme also depends on the geometrical properties such as sampling efficiency, minimum geodesic distance, mesh norm and mesh ratio, which give an insight of the nature of distribution of points on the sphere. These geometrical properties also enable us to analyse uniform distribution, dense sampling, regularity and flexibility in the samples placement for a given set of sampling points. The geometrical properties of different sampling schemes on the sphere have been analysed [60, 64] and bounds have been derived on geometrical properties [77–79].

Slepian eigenfunctions on the sphere [34, 57] provide an alternative basis for the reconstruction of signals on the sphere when the samples are taken over a specific region of the sphere. Slepian functions, which are obtained by the solution of the Slepian spatial-spectral concentration problem on the sphere, beside being orthogonal, are also optimally concentrated within the region on the sphere where they are defined [34,57] and hence, have been used for localized spatial and spectral analysis [80, 81], and signal estimation from incomplete measurements [27, 82, 83]. Slepian eigenfunctions find applications in geophysics [81, 84, 85], cosmology and planetary studies [86–88], optics [82] and computer graphics [89], to name a few.

In practice, there are applications in geophysics and acoustics where the measurements cannot be taken over the whole sphere. For example, in acoustics, head related transfer function (HRTF) measurements are not reliable in the South polar cap region due to reflections from the ground. Another example is the problem of polar gap in geophysics where the inclination of satellite orbit makes the satellite measurements on poles unreliable. To address the issue of unreliable and inaccessible samples on the sphere in these applications, many algorithms have been proposed for extrapolation of band-limited signals on the sphere [46, 90–93].

In acoustics, specially in array signal processing, array performance is limited

by spatial aliasing [94] as side lobes are generated in the array beam pattern. In literature, there exists certain sampling schemes that provide aliasing free sampling for band-limited array measurements [95], however, acoustics sound fields such as measurements of sound pressure produced by plane waves are not band-limited on the sphere, giving rise to spatial aliasing at higher frequencies in practice. Anti-aliasing filters are deployed to improve the performance of the microphone arrays in [95].

This thesis is predominantly focussed on the extension of existing spherical signal processing techniques in order to achieve accurate reconstruction of the signals on the sphere. In particular, we extend the optimal dimensionality sampling scheme [63] and propose a sampling scheme that requires the optimal number of samples for the representation of spin-s functions on the sphere (described in the next section). In addition, we analyze the iterative residual fitting (IRF) algorithm which is a well known reconstruction method when the data is not present on a pre-defined grid on the sphere. We also propose a new iterative extrapolation algorithm when the samples are not accessible on the sphere. We use the Slepian eigenfunctions to design a spatially constrained anti-aliasing filter in order to mitigate the effects of spatial aliasing in acoustics. In the remainder of this chapter, we first review the previous work on development of signal processing techniques for sampling and reconstructing signals on the sphere. Then we discuss the research problems considered in this thesis and finally we provide the summary of our contributions and an outline of this thesis.

1.1.1 Sampling of Spin-s Functions on the Sphere

Spin functions (generally referred to as spin-s functions) naturally arise in many applications including cosmology [96], astrophysics [97], fluid dynamics [98], global circulation modeling and models of stress propagation of Earth [99], to name a few. In particular, they play a pivotal role in the statistical studies of signals on the celestial sphere, such as cosmic microwave background (CMB) polarization and gravitational lensing [59, 62, 70]. In these applications, harmonic analysis is enabled through the spin-s spherical harmonic transform (s-SHT). Consequently, the ability to compute s-SHT of signal is of significant importance. It is desirable to design such sampling schemes that should require the minimum possible number of samples (spatial dimensionality) for the accurate and efficient computation of the

s-SHT of the signal and have superior geometrical properties [26,51,59,63,100–105]. For accurate computation of s-SHT of a band-limited spin-s function with band-limit L and spin s, the spatial dimensionality, is $(L^2 - s^2)$ — the number of degrees of freedom in harmonic space.

Discroll and Healy presented a sampling theorem on the sphere for an equiangular sampling grid of spatial dimensionality (asymptotically) $\sim 4L^2$ for the exact reconstruction of band-limited scalar ($s = 0$) functions on the sphere [51]. For the same equiangular sampling grid, algorithms for the computation of s-SHT and signal reconstruction of band-limited spin-s functions on the sphere $\mathbb{S}^2$ were developed in [101]. A stable, fast and exact algorithm for equiangular sampling of spatial dimensionality $\sim 4L^2$ for the evaluation of s-SHT of band-limited spin-s functions with spin ($s = \pm 2$) has also been proposed in [70]. These algorithms although enabling stable computation of s-SHT, have large pre-computation and storage requirements. In order to reduce the pre-computation requirements, by exploiting the relationship between the Wigner d-functions [26, 58] and the spin-s spherical harmonics, an accurate and exact algorithm to compute s-SHT using $\sim 4L^2$ samples is proposed in [62]. To reduce the number of samples, [100] developed a sampling theorem requiring $\sim 2L^2$ samples for the (theoretically) exact and stable computation of s-SHT. The well-known Gauss-Legendre quadrature on the sphere [75] also supports exact computation of s-SHT using $\sim 2L^2$ samples on the sphere. Recently, a library (Libsharp) [103,104] has been developed for the computation of s-SHT, where they reduce the number of samples of the Gauss-Legendre grid by approximately 30% by applying so-called polar optimization to reduce the number of samples around poles. To the best of our knowledge, none of the existing sampling schemes requires fewer than $\sim 2L^2$ samples for the accurate computation of s-SHT, well in excess of the optimal spatial dimensionality $(L^2 - s^2)$.

1.1.2 Algorithms for Reconstruction of Band-limited Functions on the Sphere

Sampling schemes have been devised in the literature for the accurate and efficient computation of SHTs. However, the samples may not be available, in practice (e.g., [3,67]), over the grid defined by these sampling schemes. To support the computation of SHTs in applications where samples or data-sets are not available on pre-defined grid, least squares fitting (LSF) methods have been investigated

for efficient computation of the SHTs [66–68, 106–109]. LSF methods formulate a large linear system of basis functions and then attempt to solve it efficiently. However, due to memory overflow, it is not suitable for systems with large band-limits, $L > 1024$ [110–112]. To solve this problem, an iterative residual fitting (IRF) method has been proposed in [110] as an extension of LSF and incorporates a divide and conquer technique for the computation of SHTs. The basic idea of IRF is to divide the subspace spanned by all spherical harmonics into smaller partitions and then perform least squares on each partition iteratively. Although IRF is fast, it creates a less accurate reconstruction [110] as the size of the harmonic basis increases for large band-limits. To improve the reconstruction accuracy, a multi-pass IRF approach is used which includes multiple passes for fitting. This is same as IRF but it involves multiple IRF operations rather than one. A variant of this scheme is presented in [110], where reconstruction for 3D surfaces is carried out by taking large number of samples.

There are also certain applications in geophysics and acoustics where the measurements cannot be taken over the whole sphere. For example, in acoustics, head related transfer function (HRTF) measurements are not reliable in the South polar cap region due to reflections from the ground. Another example is the problem of polar gap in geophysics where the inclination of satellite orbit makes the satellite measurements on poles unreliable. To address the issue of unreliable and inaccessible samples on the sphere in these applications, the problem of signal extrapolation on the sphere has been studied in literature and algorithms have been proposed for extrapolation of band-limited signals on the sphere [46, 90–93]. An analog of Papoulis algorithm [113] for continuous signals on the sphere exploiting the band-limiting characteristics of the signal is proposed in [90] and its integral equation formulation is developed in [91]. For discrete signals on the sphere, an iterative algorithm is presented in [92], which converges to minimum norm least-squares solution. Conjugate gradient extrapolation algorithm on the sphere has been presented in [46], which in comparison to the previously proposed algorithms, enables more accurate and fast extrapolation. Finally, [114] uses the Slepian functions [34] to develop an iterative algorithm for the extrapolation of band-limited signal on the sphere in the presence of noise.

1.1.3 Spatial Filtering on the Sphere

In acoustics, spherical microphone arrays have been used for sound field analysis [115], sound field recordings [116], [117] and beamforming [118], [119]. In array processing, the spherical harmonics transform (SHT) [26] is used to examine the array performance [119]. At high frequencies, however, the array performance is limited by spatial aliasing [94] as side lobes are generated in the array beam pattern. In literature, there exists certain sampling schemes that provide aliasing free sampling for band-limited array measurements [95], however, acoustics sound fields such as measurements of sound pressure produced by plane waves are not band-limited on the sphere, giving rise to spatial aliasing at higher frequencies in practice. In [94], a theoretical analysis of the spherical microphone reveals spatial aliasing as the significant factor impacting the performance of the antenna array. Several approaches to handle the spatial aliasing such as spatial anti-aliasing filters, using sensors with high directivity and reduction of spatial resolution at higher frequencies are presented in [120].

Anti-aliasing filters are deployed to reduce the energy content of the input signal at high frequencies and hence, improve the performance of the microphone arrays [95]. Anti-aliasing filtering takes place before sampling which is similar to the conventional time domain sampling. If the sound pressure is scanned using a single microphone array [121], [122] and the configuration of microphone is controlled in a way that before sampling, sound pressure can be spatially integrated, then such spatial filtering can be used for anti-aliasing [95]. In order to implement spatial integration, if a pressure sensor is used which covers a broad area and scans position on the same sphere, then the process of spatial filtering is equivalent to spherical correlation [71]. In order to reduce the errors introduced by spatial aliasing in spherical microphone arrays, the concept of spatial filtering is exploited in order to design anti-aliasing filters, where spatial truncation is applied by first designing an ideal filter and then applying window functions on this ideal filter in order to get spatially constrained anti-aliasing filters.

1.2 Overview and Contribution of Thesis

The main focus of this thesis is using the existing spherical signal processing techniques to sample and reconstruct data using spin-s functions on the sphere which

are predominantly used in cosmology. Moreover, the problem of reconstruction in an environment where the samples on the sphere are inaccessible or not defined on a grid is also addressed. Lastly, the significance of spatial filtering is discussed in the field of acoustics where an anti-aliasing filter is designed to mitigate the effect of spatial aliasing in microphone arrays.

1.2.1 Questions to be Answered

Following the literature review presented in Section 1.1, we pose the following questions that are answered in this thesis:

Q1. For band-limited spin-s functions, can we design a sampling scheme on the sphere with the optimal spatial dimensionality of $L^2 - s^2$?

Q2. Does the proposed scheme for band-limited spin-s functions enable an accurate computation of spin-s spherical harmonic transform?

Q3. Does the proposed scheme for band-limited spin-s functions exhibit superior geometric properties (such as mesh norm and mesh ratio) to existing schemes?

Q4. For the case where data is not present on a pre-defined grid, can we improve the error convergence rate using Iterative Residual Fitting (IRF)?

Q5. Can we develop an efficient extrapolation algorithm for reconstruction of band-limited signals in presence of incomplete measurements on sphere?

Q6. How can we use Slepian eigenfunction as window in order to design a spatially constrained anti-aliasing filter?

Q7. Can we improve the performance of a spatially constrained anti-aliasing filter so that it shows traits closer to that of the spatially unconstrained ideal filter in literature?

1.2.2 Thesis Contributions and Organization

Fig. 1.1 depicts the flowchart of the thesis. The mathematical background is presented in Chapter 2. The thesis develops sampling schemes for measuring signals on the sphere and subsequently reconstructing the signals by expansion in the spherical harmonic basis. The first original contribution in this thesis (Chapter 3)

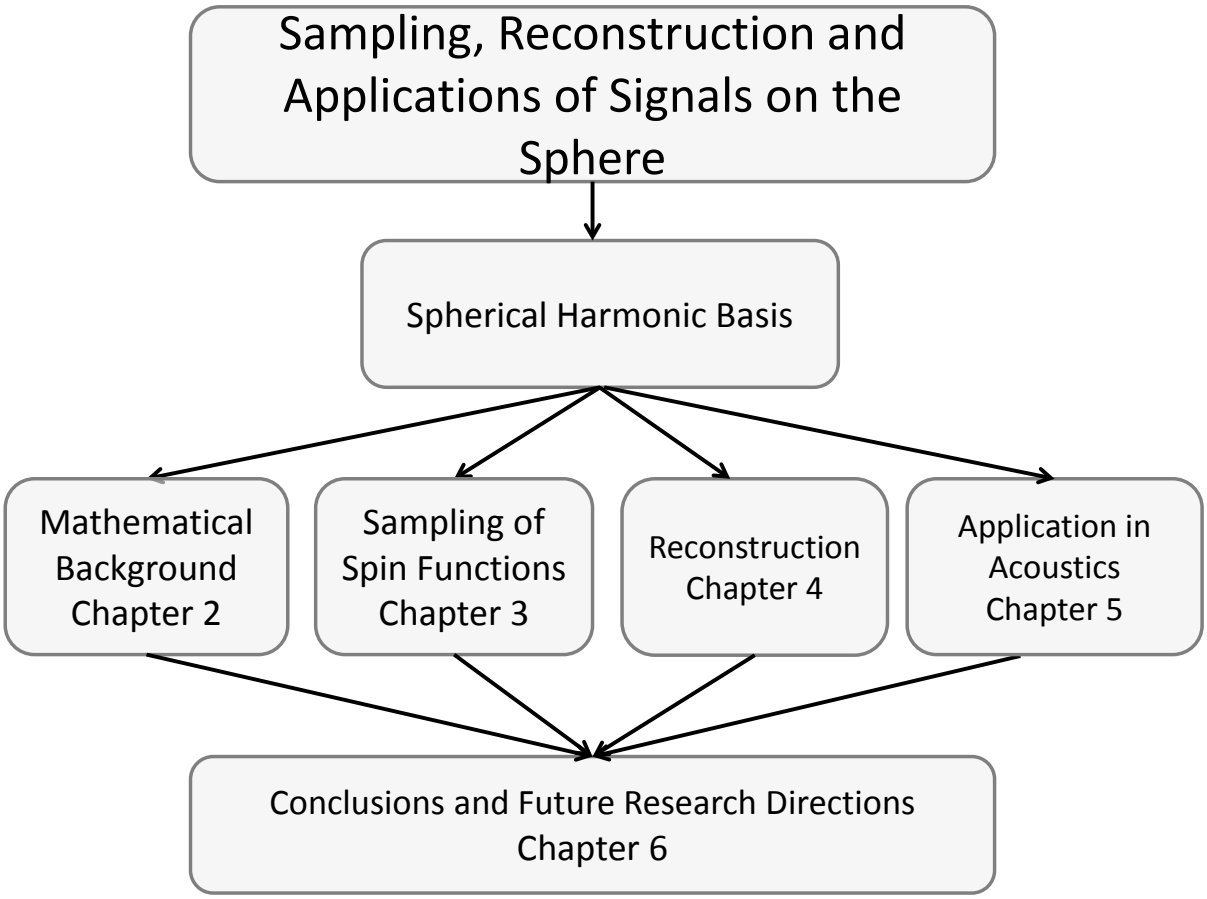

Figure 1.1: Thesis Flow Chart.

presents an optimal dimensionality sampling scheme on the sphere for sampling and reconstruction of the band-limited spin-s functions on the sphere. The geometrical properties of different sampling schemes are analysed and comparison is made with the proposed optimal dimensionality sampling scheme. In Chapter 4, we address the problem of reconstruction of signals on the sphere first in the absence of samples defined on a pre-defined grid and then in the presence of incomplete measurements. In Chapter 5, we design a spatially constrained anti-alaising filter using Slepian eigenfunctions on the sphere and apply it to mitigate the effect of spatial aliasing in the applications in acoustics. Finally, the conclusions and future research directions arising from the work presented in the contribution chapters (Chapters 3-5) are presented in Chapter 6. A more detailed summary of the contributions in each chapter is as follows:

Chapter 3 - Optimal Dimensionality Sampling Scheme for Spin-s functions on Sphere and Analysis of Geometrical Properties In Chapter 3, we propose a sampling scheme with optimal number of samples equal to the number of degrees of freedom of the function in harmonic space for the representation of spin-s band-limited functions on the sphere. Following the discussion in Section 1.1.1, we note that the existing sampling schemes on the sphere do not meet all the practical and signal processing requirements.

To summarize, our main contributions in this work are:

1. In comparison to the existing sampling designs, which require $\sim 2L^2$ samples for the representation of spin-s functions band-limited at L, the proposed scheme requires $L^2 - s^2$ samples for the accurate computation of the spin-s spherical harmonic transform (s-SHT).

2. For the proposed sampling scheme, we also develop a method to compute the s-SHT. We place the samples in our design scheme such that the matrices involved in the computation of s-SHT are well-conditioned.

3. We also present a multi-pass s-SHT to improve the accuracy of the transform.

4. We also show that the proposed sampling design exhibits superior geometrical properties compared to existing equiangular and Gauss-Legendre sampling schemes, and enables accurate computation of the s-SHT corroborated through numerical experiments.

The results in Chapter 3 have been presented in the following publications which are listed again for ease of reference:

J1. **U. Elahi**, Z. Khalid, R. A. Kennedy, and J, D, McEwen "An Optimal-Dimensionality Sampling for Spin-s Functions on the Sphere," *IEEE Signal Process. Lett.*, vol. 25, no. 10, pp. 1470-1474, OCT. 2018.

C1. **U. Elahi**, Z. Khalid, and R. A. Kennedy, "Comparative Analysis of Geometrical Properties of Sampling Schemes on the Sphere," in *Proc. Int. Conf. Signal Processing and Communication Systems ICSPCS'2016*, Gold Coast, Australia, pp. 1-7, Dec. 2016.

Chapter 4 - Signal Reconstruction on the Sphere

In Chapter 4, we pose two problems regarding reconstruction of the signals on the sphere. In the first part of Chapter 4, we reconstruct the signals on sphere in the absence of a pre-defined grid. We have presented the generalized iterative residual fitting (IRF) method for the computation of the spherical harmonic transform (SHT) of band-limited signals on the sphere. Proposed IRF is based on partitioning the subspaces of band-limited signals into orthogonal spaces. In the second part of Chapter 4, we reconstruct the signal from incomplete samples and propose an iterative extrapolation algorithm. The main contributions of this chapter are:

1. In order to improve the accuracy of the transform, we present a multi-pass IRF scheme and analyse it for different sampling schemes and for four different size partitions.

2. For different partitions and different sampling distributions, we analyse the residual (error) and demonstrate the convergence of the residual to zero.

3. We develop an iterative algorithm for extrapolation of band-limited signals on the sphere from limited or incomplete measurements. Existing schemes focus on the use of the band-limited property of the signal, that is, the signal extrapolation is carried out iteratively by forcing the harmonic coefficients outside the band-limit of the signal to zero at each iteration.

4. In the proposed algorithm, we do not only force the harmonic coefficients to zero but also use these to improve the extrapolation of the signal over the inaccessible region at each iteration.

5. We conduct numerical experiments in order to check the accuracy of the proposed algorithm and use Iterative Conjugate Gradient method as benchmark for comparison.

6. We also take HRTF measurements using synthetic head model and extrapolate the signal on the South pole. The numerical analysis show that the proposed algorithm enables more accurate extrapolation than the existing methods.

The results in Chapter 4 have been presented in the following publications which are listed again for ease of reference:

J2. **U. Elahi**, Z. Khalid, and R. A. Kennedy, "Band-limited Signal Extrapolation for inaccessible HRTF measurements on the Sphere ," *IEEE Trans. Signal Process.*, 2018. (submitted)

C2. **U. Elahi**, Z. Khalid, R. A. Kennedy, and J, D, McEwen "Iterative Residual Fitting for Spherical Harmonic Transform of Band-Limited Signals on the Sphere: Generalization and Analysis," in *Proc. IEEE Int. Conf. Sampling Theory and Applications, SampTA'2017*, Tallinn, Estonia, pp. 470-440, Mar. 2017.

C3. **U. Elahi**, Z. Khalid, and R. A. Kennedy, "An Improved Iterative Algorithm for Band-limited Signal Extrapolation on the Sphere," in *Proc. IEEE Int. Conf. Acoustics, Speech and Signal Processing, ICASSP'2018*, Calgary, Canada, pp. 4619-4623, Apr. 2018.

Chapter 5 - Spatial filtering for Applications in Acoustics

In Chapter 5, we design a spatially constrained anti-aliasing filter as a weighted sum of band-limited spatially (optimal) concentrated eigenfunctions obtained as the solution of Slepian concentration problem on the sphere. The main contributions in this chapter are:

1. Given the spatial constraints, the proposed filter approximates an ideal low-pass filter on the sphere in the least-squares sense.

2. The filter obtained as a result of this multiple regression depends on the value of band-limit, L and maximum concentration region known as polar cap parameterized by its central angle θ_c.

3. We examine the performance of the proposed filter by measuring parameters like white noise gain (WNG), directivity index (DI) and processing loss (γ), and compare the results with the ideal filter. We compare the performance of two filters first by varying polar cap of angle θ_c keeping band-limit, L constant and then varying band-limits keeping polar cap region constant.

4. By putting constraints on the directivity index and processing loss, we propose a parameter-constrained filter design and choose θ_c such that white noise gain of the proposed filter is maximized.

5. Our analysis show that based on the selected design requirements, the proposed spatially constrained anti-aliasing filter surpasses the ideal filter in performance.

6. We also propose to use suitably selected Slepian eigenfunction window for spatial truncation in order to get spatially constrained anti-aliasing filter from ideal filter.

7. Our analysis shows that for the reduction of side lobes produced by spatial aliasing error, anti-aliasing filter spatially truncated by the proposed eigenfunction window is a better choice than the rectangular and Hamming windows.

The results in Chapter 5 have been presented in the following publications which are listed again for ease of reference:

J3. **U. Elahi**, Z. Khalid, and R. A. Kennedy, "Design of a Spatially Constrained Anti-aliasing Filter using Slepian Functions in Spherical Microphone Arrays ," *IEEE Trans. Signal Process.*, 2019. (under preparation)

C4. **U. Elahi**, Z. Khalid, and R. A. Kennedy, "Spatially Constrained Anti-Aliasing Filter Using Slepian Eignefunction Window on the Sphere," in *Proc. Int. Conf. Signal Processing and Communication Systems ICSPCS'2018*, Cairns, Australia, Dec. 2018.

C5. **U. Elahi**, Z. Khalid, and R. A. Kennedy, "Design of Spatially Constrained Anti-aliasing Filter using Slepian Functions on the Sphere," in *Proc. 27th European Signal Processing Conference, EUSIPCO'2019*, A Coruna, Spain, Sep. 2019. (submitted)

Finally, Chapter 7 draws conclusions from this thesis and provides directions for future research work.

Chapter 2

Mathematical Preliminaries and Sampling Schemes on Sphere

In this chapter, we, first, provide mathematical background to clarify the adopted notation used in later chapters and then give a brief review of sampling schemes on the sphere.

2.1 Signals on the Sphere

We consider square integrable complex functions of the form $f(\hat{\boldsymbol{x}})$ defined on the unit sphere, denoted by $\mathbb{S}^2 \triangleq \{\hat{\boldsymbol{x}} \in \mathbb{R}^3 \colon |\hat{\boldsymbol{x}}| = 1\}$. Here $\hat{\boldsymbol{x}} = \hat{\boldsymbol{x}}(\theta, \phi) = (\sin\theta\cos\phi, \cos\theta\cos\phi, \cos\theta) \in \mathbb{S}^2 \subset \mathbb{R}^3$ denotes a point on the sphere, where $\theta \in [0, \pi]$ denotes the co-latitude and $\phi \in [0, 2\pi)$ is the longitude. The inner product of the two functions $f(\theta, \phi)$ and $g(\theta, \phi)$ defined on $\mathbb{S}^2$ is given by [26]

$$\langle f, g \rangle \triangleq \int_{\mathbb{S}^2} f(\theta, \phi)\overline{g(\theta, \phi)} \sin\theta \, d\theta \, d\phi, \tag{2.1}$$

where $\overline{(\cdot)}$ represents the complex conjugate operation and $\sin\theta \, d\theta \, d\phi$ is the differential area element on the sphere. The inner product given in (2.1) induces a norm $\|g\| \triangleq \langle g, g \rangle^{1/2}$. We refer to the functions with finite induced norms as signals on the sphere $\mathbb{S}^2$ [26]. Using the Fredholm integral equation as [26], also define a linear integral operator $\mathcal{D}$ with kernel $D(\hat{\boldsymbol{x}}, \hat{\boldsymbol{y}})$ as [26]

$$(\mathcal{D}f)(\hat{\boldsymbol{x}}) = \int_{\mathbb{S}^2} D(\hat{\boldsymbol{x}}, \hat{\boldsymbol{y}}) \, f(\hat{\boldsymbol{y}}) ds(\hat{\boldsymbol{y}}). \tag{2.2}$$

2.1.1 Spherical Harmonics

Spherical harmonics [26], $Y_\ell^m(\theta,\phi)$ of all integer degrees $\ell \geq 0$ and integer orders $m \leq |\ell|$ are defined as

$$Y_\ell^m(\theta,\phi) \triangleq \sqrt{\frac{2\ell+1}{4\pi}\frac{(\ell-m)!}{(\ell+m)!}} P_\ell^m(\cos\theta)\, e^{im\phi}, \tag{2.3}$$

where $P_\ell^m(\cdot)$ are the associated Legendre functions (with Condon-Shortley phase included) [26, 58]. The spherical harmonics are orthonormal over the sphere with $\langle Y_\ell^m, Y_p^q \rangle = \delta_{\ell,p}\delta_{m,q}$, where $\delta_{m,q}$ is the Kronecker delta function: $\delta_{m,q} = 1$ for $m = q$ and is zero otherwise. Spherical harmonics form a complete orthonormal set of basis functions, and therefore we can expand signal on sphere as

$$f(\theta,\phi) = \sum_{\ell=0}^{\infty} \sum_{m=-\ell}^{\ell} (f)_\ell^m Y_\ell^m(\theta,\phi), \tag{2.4}$$

where $(g)_\ell^m$ is the spherical harmonic coefficient of degree ℓ and order m and is given by the spherical harmonic transform (SHT) defined as

$$(f)_\ell^m \triangleq \langle f, Y_\ell^m \rangle = \int_{\mathbb{S}^2} f(\theta,\phi)\overline{Y_\ell^m(\theta,\phi)}\, \sin\theta\, d\theta\, d\phi. \tag{2.5}$$

2.2 Spin-s Functions on the Sphere

The spin-s functions on the sphere, denoted by ${}_sf \in L^2(\mathbb{S}^2)$ with integer spin s, are defined by their behaviour under local rotation, that is, the spin-s function transforms as

$${}_sf'(\theta,\phi) = e^{-is\gamma}\, {}_sf(\theta,\phi), \tag{2.6}$$

under a local rotation γ. ${}_sf'$ is the rotated function obtained by rotating ${}_sf$ by γ in the tangent plane at (θ,ϕ).

2.2.1 Spin-s Spherical Harmonic Transform

The spin-s spherical harmonic functions (or spin weighted spherical harmonics), denoted by ${}_sY_\ell^m$ for degree ℓ, order $|m| \leq \ell$ and integer spin $|s| \leq \ell$, are defined as

$$ {}_sY_\ell^m(\theta,\phi) \triangleq (-1)^s \sqrt{\frac{2\ell+1}{4\pi}}\, e^{im\phi} d_\ell^{m,-s}(\theta), \tag{2.7} $$

where $d_\ell^{m,m'}(\theta)$ denotes the Wigner-d function [26, 58]

$$ \begin{aligned} d_\ell^{m,m'}(\vartheta) = \sum_n (-1)^{n-m'+m} \times \frac{\sqrt{(\ell+m')!(\ell-m')!(\ell+m)!(\ell-m)!}}{(\ell+m'-n)!(n)!(\ell-n-m)!(n-m'+m)!} \\ \times \left(\cos\frac{\vartheta}{2}\right)^{2\ell-2n+m'-m} \left(\sin\frac{\vartheta}{2}\right)^{2n-m'+m}, \end{aligned} \tag{2.8} $$

where the summation over n is such that the factorial terms in the denominator remain non-negative. Spin-s spherical harmonics form a complete set of basis for spin-s functions on the sphere and therefore any spin-s function ${}_sf$ can be expanded as

$$ {}_sf(\theta,\phi) = \sum_{\ell=s}^{\infty} \sum_{m=-\ell}^{\ell} ({}_sf)_\ell^m \, {}_sY_\ell^m(\theta,\phi), \tag{2.9} $$

where $({}_sf)_\ell^m$ is the spin-s spherical harmonic coefficient of degree ℓ and order m and is given by the standard inner product for functions on the sphere [26]:

$$ ({}_sf)_\ell^m = \int_{\mathbb{S}^2} {}_sf(\theta,\phi) \overline{{}_sY_\ell^m(\theta,\phi)} \, \sin\theta \, d\theta \, d\phi, \tag{2.10} $$

where $\overline{(\cdot)}$ denotes the complex conjugate operation. These coefficients form the spectral (or harmonic) domain of the spin-s function and the transformation of the spin-s function to its harmonic coefficient given in (2.10) is referred to as spin-s spherical harmonic transform (s-SHT). Note that spin-s spherical harmonics are equal to (scalar) spherical harmonics for $s = 0$.

2.3 Band-limited Signals on the Sphere

The signal $f(\theta,\phi)$ is considered as band-limited at degree L if $(f)_\ell^m = 0$ for all $\ell \geq L$. For the representation of a band-limited signal using (2.4), the summation

over degree ℓ is truncated at $L-1$. We note that the set of bandlimited signals forms an L^2 dimensional subspace of $L^2(\mathbb{S}^2)$, which we denote by $\mathcal{H}_L$.

$$f(\theta,\phi) = \sum_{\ell=0}^{L-1} \sum_{m=-\ell}^{\ell} (f)_\ell^m Y_\ell^m(\theta,\phi). \tag{2.11}$$

The number of spherical harmonic coefficients required to represent $f(\theta,\phi)$, given in (2.11), is L^2, which also represents the optimal spatial dimensionality (also referred to as the optimal dimensionality), defined as the number of samples attainable by any sampling scheme that allows the accurate computation of the SHT of any band-limited signal on the sphere. Similarly, the spin-s function ${}_sf$ is said to be band-limited at L if $({}_sf)_\ell^m = 0$ for all $\ell \geq L$. Such band-limited spin-s functions form a subspace $\mathcal{H}_L \subset L^2(\mathbb{S}^2)$ of dimension $L^2 - s^2$.

2.4 Sampling Schemes on the Sphere

We focus on the recently developed sampling schemes on the sphere which permit accurate computation of SHT of a bandlimited signal from its samples. For a signal band-limited at L, we use N to denote the spatial dimensionality, that is the number of samples, required by each of the sampling scheme to compute SHT or equivalently represent the band-limited signal accurately.

2.4.1 Gauss-Legendre Quadrature based Sampling

This sampling scheme is devised on the basis of the well known Gauss-Legendre quadrature on the sphere [123] and is therefore referred to as Gauss-Legendre (GL) sampling scheme. The GL quadrature is used to construct a sampling theorem such that the SHT of a band-limited signal can be exactly computed from its samples. For a signal band-limited at L, this scheme takes samples on L iso-latitude rings with $2L-1$ equiangular placed samples along longitude ϕ, resulting in a total requirement of $N_{\mathrm{GL}} = L(2L-1)$ samples, for the exact computation of SHT. The location of the rings along co-latitude θ is given by the roots of the Legendre polynomials of order L as dictated by the Gauss-Legendre quadrature to discretize the integral given in (2.5). The variants of the Gauss-Legendre quadrature scheme have also been proposed (e.g., [124]) that require less number of samples. However, these sampling schemes do not support exact or sufficiently accurate computation

of SHT. As an example, the samples on the sphere for GL sampling scheme are shown in Fig.2.1(a) for $L = 10$.

2.4.2 Equiangular Sampling

For the exact computation of SHT of a signal band-limited at L, an equiangular scheme was first proposed in [51] which requires $2L$ iso-latitude equiangular spaced rings of samples with $2L$ equiangular samples along longitude ϕ. Recently, an equiangular scheme has been developed [59] that takes samples on an equiangular grid defined by the following sample positions:

$$\theta_t = \frac{\pi(2t+1)}{(2L-1)}, \qquad t = 0, 1, 2, ..., L-1, \tag{2.12}$$

and

$$\phi_k = \frac{2\pi k)}{(2L-1)}, \qquad k = 0, 1, 2, ..., 2L-2, \tag{2.13}$$

that is, it requires $L-1$ iso-latitude rings with $2L-1$ samples along longitude in each ring and a sample at one of the poles ($\theta = 0$ or $\theta = \pi$) and therefore reduces the number of equiangular samples required for the computation of SHT by a factor of two. In total, the number of samples required by equiangular scheme are $N_{\mathrm{E}} = (L-1)(2L-1)+1$, that is, $3(L-1)$ fewer samples in comparison to the GL scheme. As an example, the samples on the sphere for equiangular sampling scheme are shown in Fig.2.1(b) for $L = 10$.

2.4.3 Optimal-Dimensionality Sampling Scheme

The spatial dimensionality of both GL and equiangular sampling schemes is twice the optimal spatial dimensionality given by the dimensionality of $\mathcal{H}_L$, that is, the degree of freedom in harmonic space to represent a signal band-limited at spherical harmonic degree L. Recently, an optimal-dimensionality sampling scheme [63] has been proposed that requires L^2 points to compute the accurate SHT for signals band-limited at L and therefore the scheme has optimal spatial dimensionality. Although the SHT associated with the optimal dimensionality sampling is not theoretically exact, the accuracy of the SHT has been demonstrated for band-limits up to $L = 2048$ with errors on the order of numerical precision. Like GL

and equiangular sampling schemes, it is also an iso-latitude sampling scheme of the sphere and takes L rings along each latitude. Let $\theta_k, k = 0, 1, \cdots, L-1$ denotes the sample position of the ring along latitude, where these sample locations are chosen such that the accuracy of the computation of SHT is maximized. For a ring placed at θ_k, the samples in the ring along ϕ are given by

$$\phi_n^k = \frac{2\pi n}{2k+1}, \quad n = 0, 1, \ldots, 2k \tag{2.14}$$

that is $2k+1$ equiangular samples. In total, the number of samples required by optimal-dimensionality sampling scheme is

$$N_{\mathrm{O}} = \sum_{k=0}^{L-1} (2k+1) = L^2. \tag{2.15}$$

As an example, the samples on the sphere for optimal dimensionality sampling scheme are shown in Fig.2.1(c) for $L = 10$.

2.4.4 Spherical Designs

A set of points on the sphere is called a spherical design such that the integral of the signal of maximum spherical polynomial degree t or maximum band-limit $t+1$ over the sphere can be evaluated as an average value over the samples of the signal [60]. Since the spherical design is parameterized by t, the set of points is often referred to as spherical t-design. Spherical t-designs, by definition, enable exact evaluation of the integral of polynomial of maximum degree t. For the computation of SHT using the points given by spherical design, we first note that the SHT requires to evaluate the integral given in (2.5), where the integrand is the product of a signal band-limited at L and spherical harmonic $Y_\ell^m(\theta, \phi)$. Since we require to evaluate the integral for all $\ell < L$, $|m| \leq \ell$, the maximum polynomial degree of integrand is $2L-2$. Consequently, we require $(2L-2)$-spherical design for the sampling of band-limited signal such that the SHT can be computed accurately. In our work, we choose the spherical t-designs[1] [60] which takes $t^2/2 + t + O(1)$ samples. We use N_{SD} to denote the number of samples of $(2L-2)$-spherical design. Due to high computational cost associated with the computation of spherical design, we

[1]The spherical designs are available at `http://web.maths.unsw.edu.au/~rsw/Sphere/EffSphDes/index.html`.

note that the spherical t-designs have been proposed for maximum $t = 180$ and therefore the SHT can be computed for band-limits up to $L = 91$. As an example, the samples of the $(2L - 2)$-spherical design are shown in Fig.2.1(d) for $L = 10$.

2.4.5 Extremal Points on the Sphere

For a given band-limit L, the extremal (maximum determinant) systems are sets of L^2 extremal points on the sphere which, by definition, maximize the determinant of a basis matrix (see [64] for details). For spherical harmonic basis, extremal points are supported by interpolatory cubature rule with positive weights and therefore enables the accurate computation of SHT of a signal band-limited at L using $N_{\text{ES}} = L^2$ sampling points of extremal system. The sampling scheme based on the points[2] of the extremal system will be referred to as extremal system sampling scheme. As an example, the extremal points on the sphere are shown in Fig.2.1(e) for $L = 10$.

2.5 Summary

In this chapter, we have introduced the required mathematical background. The notation adopted in this chapter is used throughout this thesis. However, new notation or formulation, will be defined in later chapters as required. Also, a brief review of the sampling schemes on the sphere is given.

[2]We use the the points of extremal systems publicly available at `http://web.maths.unsw.edu.au/~rsw/Sphere/Extremal/New/extremal1.html`.

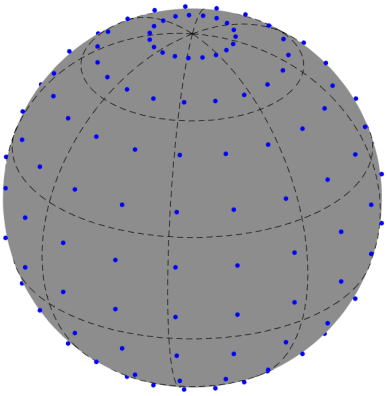

(a) Gauss-Legendre sampling

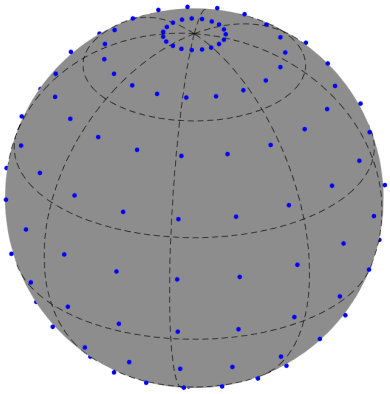

(b) Equiangular sampling

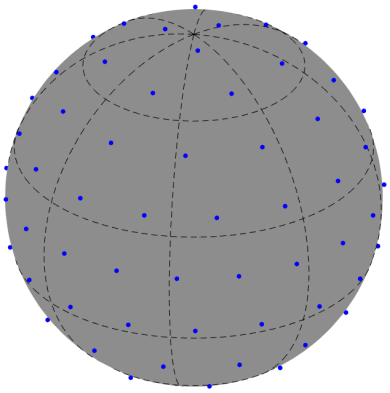

(c) Optimal-dimensionality sampling

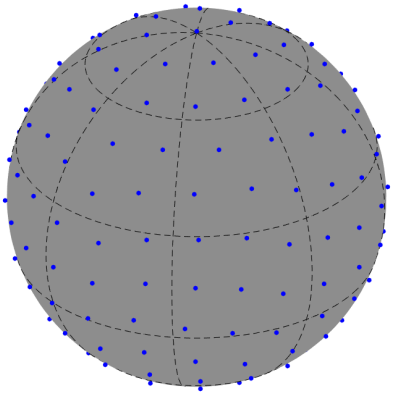

(d) Spherical design sampling

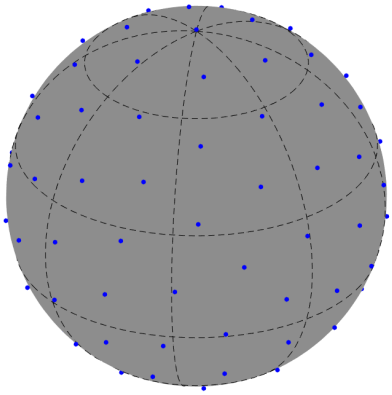

(e) Samples of extremal points

Figure 2.1: The sampling schemes on the sphere, (a) Gauss-Legendre quadrature based sampling, (b) equiangular sampling, (c) optimal dimensionality sampling scheme, (d) spherical desings and (e) extremal points, presented in Section III for the representation of the signal band-limited at $L = 10$.

Chapter 3

Optimal Dimensionality Sampling Scheme for Spin-s functions on Sphere and Analysis of Geometrical Properties

In this chapter, we propose a sampling scheme with optimal number of samples equal to the number of degrees of freedom of the function in harmonic space for the representation of spin-s band-limited functions on the sphere. In comparison to the existing sampling designs, which require $\sim 2L^2$ samples for the representation of spin-s functions band-limited at L, the proposed scheme requires $N_o = L^2 - s^2$ samples for the accurate computation of the spin-s spherical harmonic transform (s-SHT). For the proposed sampling scheme, we also develop a method to compute the s-SHT. We place the samples in our design scheme such that the matrices involved in the computation of s-SHT are well-conditioned. We also present a multi-pass s-SHT to improve the accuracy of the transform. We analyse geometrical properties like sampling efficiency, minimum geodesic distance, mesh norm and mesh ratio for the sampling schemes defined in the first part of this chapter and carry out the comparative analysis of the geometrical properties of the proposed sampling scheme on the sphere for spin-s functions and different values of integer spin, s. We show that the proposed sampling design exhibits superior geometrical properties compared to existing equiangular and Gauss-Legendre sampling schemes.

This chapter is organized as follows. In Section 3.1, existing sampling schemes in

literature and the importance of geometrical properties are discussed. The proposed optimal dimensionality sampling scheme and s-SHT is presented in Section 3.2. In Section 3.3, we define the geometrical properties and compare these properties for the proposed scheme with existing schemes in literature for different values of integer spin, s. Section 3.4 discusses the summary of the main contribution of this chapter.

3.1 Prior Work

Spin functions (generally referred to as spin-s functions) naturally arise in many applications including cosmology [96], astrophysics [97], fluid dynamics [98], global circulation modeling and models of stress propagation of earth [99], to name a few. In particular, they play a pivotal role in the statistical studies of signals on the celestial sphere, such as cosmic microwave background (CMB) polarization and gravitational lensing [59, 62, 70]. In these applications, harmonic analysis is enabled through the spin-s spherical harmonic transform (s-SHT). Consequently, the ability to compute s-SHT of signal is of significant importance. It is desirable to design such sampling schemes that should require the minimum possible number of samples (spatial dimensionality) for the accurate and efficient computation of the s-SHT of the signal and have superior geometrical properties [26,51,59,63,100–105]. For accurate computation of s-SHT of a band-limited spin-s function with band-limit L and spin s, the spatial dimensionality, denoted by N_o, is $(L^2 - s^2)$ — the number of degrees of freedom in harmonic space.

Discroll and Healy presented a sampling theorem on the sphere for an equiangular sampling grid of spatial dimensionality (asymptotically) $\sim 4L^2$ for the exact reconstruction of band-limited scalar ($s = 0$) functions on the sphere [51]. For the same equiangular sampling grid, algorithms for the computation of s-SHT and signal reconstruction of band-limited spin-s functions on the sphere $\mathbb{S}^2$ were developed in [101]. A stable, fast and exact algorithm for equiangular sampling of spatial dimensionality $\sim 4L^2$ for the evaluation of s-SHT of band-limited spin-s functions with spin ($s = \pm 2$) has also been proposed in [70]. These algorithms although enabling stable computation of s-SHT, have large pre-computation and storage requirements. In order to reduce the pre-computation requirements, by exploiting the relationship between the Wigner d-functions [26, 58] and the spin-

s spherical harmonics, an accurate and exact algorithm to compute s-SHT using $\sim 4L^2$ samples is proposed in [62]. To reduce the number of samples, Jason [100] developed a sampling theorem requiring $\sim 2L^2$ samples for the (theoretically) exact and stable computation of s-SHT. The well-known Gauss-Legendre quadrature on the sphere [75] also supports exact computation of s-SHT using $\sim 2L^2$ samples on the sphere. Recently, a library (Libsharp) [103, 104] has been developed for the computation of s-SHT, where they reduce the number of samples of the Gauss-Legendre grid by approximately 30% by applying so-called polar optimization to reduce the number of samples around poles.

Geometric properties such as sampling efficiency, minimum geodesic distance, mesh norm and mesh ratio of the set of sampling points give an insight of the nature of distribution of points on the sphere [60, 64, 77–79]. These geometrical properties also enable us to analyse uniform distribution, dense sampling, regularity and flexibility in the samples placement for a given set of sampling points. The geometrical properties of different sampling schemes on the sphere have been analysed [60, 64] and bounds have been derived on geometrical properties [77–79].

3.1.1 Research Questions

To the best of our knowledge, none of the existing sampling schemes requires fewer than $\sim 2L^2$ samples for the accurate computation of s-SHT, well in excess of the optimal spatial dimensionality. In this context, we address the following questions in this chapter:

- What information do geometrical properties provide about a certain sampling scheme?

- For band-limited spin-s functions, how can we design a sampling scheme on the sphere with optimal spatial dimensionality of $N_o = L^2 - s^2$?

- Does the proposed scheme enable accurate computation of spin-s spherical harmonic transform and exhibit superior geometric properties (such as mesh norm and mesh ratio) to existing schemes?

3.2 Optimal-Dimensionality Sampling and Spin-s Spherical Harmonic Transform

3.2.1 Sampling Scheme

We define an iso-latitude sampling scheme, denoted by $\mathfrak{S}_s^L$, on the sphere as

$$\mathfrak{S}_s^L \;=\; \big\{(\theta_t, \frac{2\pi p}{2t+1}) \;\big|\; t \;=\; |s|, |s|+1, \ldots, L-1, \quad p \;=\; 0, 1, \ldots, 2t\big\}, \quad (3.1)$$

which is comprised of $L-|s|$ iso-latitude rings of samples placed at $\theta_t\,, t = |s|, |s|+1, \ldots, L-1$ with $2t+1$ equally spaced sampling points along ϕ in the ring placed at θ_t. We discuss the location of iso-latitude rings later in this section. Since the sampling scheme takes N_o sample points on the sphere in total, equal to the number of degrees of freedom of the spin-s function band-limited at L, it is referred to as optimal-dimensionality sampling.

3.2.2 Spin-s Spherical Harmonic Transform – Formulation

We define the *iso-latitude Fourier transform* of the signal ${}_sf(\theta, \phi)$ along ϕ given by

$$\begin{aligned} G_m(\theta) &\triangleq \int_0^{2\pi} {}_sf(\theta,\phi) e^{-im\phi} d\phi \\ &= (-1)^s\, 2\pi \sum_{\ell=\Delta}^{L-1} \sqrt{\frac{2\ell+1}{4\pi}}\, ({}_sf)_\ell^m\, d_\ell^{m,-s}(\theta), \end{aligned} \quad (3.2)$$

where $\Delta = \max(|m|, |s|)$ and we have employed (2.7), (2.9) and orthogonality of complex exponentials in obtaining the second equality. Also define a vector of length $L-\Delta$ containing $G_m(\theta)$ evaluated at sample points of the proposed sampling scheme as

$${}_s\mathbf{g}_m \triangleq [G_m(\theta_\Delta),\, G_m(\theta_{\Delta+1}), \ldots, G_m(\theta_{L-1})], \quad (3.3)$$

which can be equivalently expressed using (3.2) as

$${}_s\mathbf{g}_m = (-1)^s\, {}_s\mathbf{D}_m\, {}_s\mathbf{f}_m. \quad (3.4)$$

where ${}_s\mathbf{D}_m \triangleq$

$$\begin{pmatrix} a_0 d_{\Delta}^{m,-s}(\theta_{\Delta}) & a_1 d_{\Delta+1}^{m,-s}(\theta_{\Delta}) & \cdots & a_{L-1} d_{L-1}^{m,-s}(\theta_{\Delta}) \\ a_0 d_{\Delta}^{m,-s}(\theta_{\Delta+1}) & a_1 d_{\Delta+1}^{m,-s}(\theta_{\Delta+1}) & \cdots & a_{L-1} d_{L-1}^{m,-s}(\theta_{\Delta+1}) \\ \vdots & \vdots & \ddots & \vdots \\ a_0 d_{\Delta}^{m,-s}(\theta_{L-1}) & a_1 d_{\Delta+1}^{m,-s}(\theta_{L-1}) & \cdots & a_{L-1} d_{L-1}^{m,-s}(\theta_{L-1}) \end{pmatrix}, \tag{3.5}$$

with $a_\beta = \sqrt{\pi(2\beta+1)}$ and

$${}_s\mathbf{f}_m = \left[({}_sf)_{\Delta}^m, ({}_sf)_{\Delta+1}^m, \ldots, ({}_sf)_{L-1}^m \right]^T, \tag{3.6}$$

is a vector of spin-s spherical harmonic coefficients of order $|m| < L$ and integer spin s.

Remark 3.1 (Requirements for the Computation of s-SHT) *The spherical harmonic coefficients contained in a vector ${}_s\mathbf{f}_m$ for each $|m| < L$ can be recovered by inverting the system in* (3.4) *provided (Requirement 1:) ${}_s\mathbf{g}_m$ is known and (Requirement 2:) ${}_s\mathbf{D}_m$ is invertible.*

3.2.3 Spin-s Spherical Harmonic Transform – Computation

By changing the order of summations in (2.9) and using (2.7) and (3.2), we re-write (2.9) for a band-limited spin-s function as

$${}_sf(\theta,\phi) = \frac{1}{2\pi} \sum_{m=-(L-1)}^{L-1} G_m(\theta) e^{im\phi}, \tag{3.7}$$

which indicates that ${}_sf(\theta,\phi)$ is a linear sum of $2L-1$ complex exponentials along ϕ. Due to this fact, the existing iso-latitude schemes require $2L-1$ samples in each of the iso-latitude rings in order to compute $G_m(\theta_t)$ and consequently ${}_s\mathbf{g}_m$ correctly and serve the requirement 1 (see Remark 3.1). However, if we know the spherical harmonic coefficients of all degrees (and orders) greater than given Δ', we can remove their contributions from the signal which consequently reduces the band-limit along ϕ and enable the computation of $G_m(\theta_t)$ by taking an FFT over $2\Delta'+1$ samples (instead of $2L-1$ samples) in a ring placed at θ_t. We further elaborate on this idea below.

We first compute the spin-s spherical harmonic coefficients of orders $|m| =$

$L-1$, which can be determined by computing ${}_s\mathbf{g}_{L-1} = {}_sG_{L-1}(\theta_{L-1})$ and ${}_s\mathbf{g}_{-(L-1)} = {}_sG_{-(L-1)}(\theta_{L-1})$ in (3.4) using an FFT over only one ring of $2L-1$ samples along ϕ placed at θ_{L-1}. Once $({}_sf)_{L-1}^{L-1}$ is computed, we update the signal at the samples in the rings placed at θ_t, $t = |s|, |s|+1, \ldots, L-2$ as

$$ {}_sf(\theta_t, \phi) \leftarrow {}_sf(\theta_t, \phi) - {}_s\tilde{f}_{L-1}(\theta_t, \phi) \tag{3.8} $$

where

$$ \begin{aligned} {}_s\tilde{f}_m(\theta, \phi) &\triangleq \sum_{\ell=\Delta}^{L-1} \left(({}_sf)_\ell^m \, {}_sY_\ell^m(\theta, \phi) + ({}_sf)_\ell^{-m} \, {}_sY_\ell^{-m}(\theta, \phi) \right) \\ &= \frac{1}{2\pi} \left(e^{im\phi} G_m(\theta) + e^{-im\phi} G_{-m}(\theta) \right) \end{aligned} \tag{3.9} $$

denotes the part of the signal ${}_sf(\theta, \phi)$ composed of contribution of spherical harmonics of order m and $-m$ and all degrees $\Delta \leq \ell \leq (L-1)$ for integer spin s. Once the signal is updated as given in (3.8), $2L-3$ samples are required instead of $2L-1$ to compute $G_m(\theta_t)$. For computing spin spherical harmonic coefficients of order $L-2$ and $-(L-2)$, we only need $2L-3$ samples along the ϕ-ring placed at θ_{L-2}. After computation, these can be used to update the signal at other sample positions. In this manner, we continue to evaluate the spin spherical harmonic coefficients for all degrees $\ell \geq |s|$ and all orders $|m| \leq \ell$. This proposed s-SHT is summarized in the form of procedure below.

Procedure 1 s-SHT

Require: $({}_sf)_\ell^m, \quad \forall\ |m| < L,\ \Delta \leq \ell < L$, given ${}_sf(\theta, \phi)$

procedure SPIN SHT(${}_sf(\theta, \phi)$)
  for $m = L-1, L-2, \ldots, 0$ **do**
    compute ${}_s\mathbf{g}_m$ and ${}_s\mathbf{g}_{-m}$ by evaluating $G_m(\theta_t)$ for $t = \Delta, \Delta+1, \ldots, L-1$
    compute ${}_s\mathbf{f}_m$ and ${}_s\mathbf{f}_{-m}$ by inverting (3.4)
    update ${}_sf(\theta_t, \phi) \leftarrow {}_sf(\theta_t, \phi) - {}_s\tilde{f}_m(\theta_t, \phi)$ for all $t = |s|, |s|+1, \ldots, \Delta-1$ and all associated sampling points along ϕ
  end for
  return $({}_sf)_\ell^m$
end procedure

3.2.4 Placement of Samples along Co-latitude

We yet need to determine the sampling points along co-latitude for the placement of iso-latitude rings. To serve the requirement 2 (see Remark 3.1), we propose a method, referred to as condition number minimization [63], to determine $L - |s|$ co-latitude sample points θ_t, $t = \{|s|, |s|+1, \ldots, L-1\}$ such that each matrix ${}_s\mathbf{D}_m$, given in (3.5), which depends on last $L - \Delta$ samples along co-latitude, is well-conditioned. Our method consider a set of $M \gg L$ equiangular samples (with uniform measure along θ) given by $\Theta(M) = \left\{\frac{t\,\pi}{M+1}\right\}$, $t = 1, 2, \ldots, M$ to choose sampling points θ_t, $t = |s|, |s|+1, \ldots, L-1$ using the following steps:

- Choose $\theta_L = \frac{\pi\lceil\frac{M}{2}\rceil}{M+1}$, that is, farthest from the poles in the set $\Theta(M)$, which is a natural choice for the ring of $2L-1$ samples along ϕ.
- For each $m = L-2, L-3, \ldots, |s|$, choose θ_m from the set $\Theta(M)$ which minimizes the condition number of the matrix ${}_s\mathbf{D}_m$.

Such placement of iso-latitude rings ensures that each matrix ${}_s\mathbf{D}_m$ for at least each $|m| = |s|, |s|+1, \ldots, L-1$ is well-conditioned and therefore enables the accurate computation of s-SHT. We note that the proposed condition number minimization method, although computationally intensive, is only required to be used once for each s and band-limit L to determine sample positions along co-latitude.

3.2.5 Multi-pass s-SHT

The s-SHT presented here computes the spherical harmonic coefficients for each order m in a sequence $|m| = L-1, L-2, \ldots, 0$. Since the error in the computation of m-th order coefficients contributes to the error in the computation of coefficients of order $m-1$, there tends to be error accumulation in the inherent sequential computation of s-SHT. We propose a multi-pass s-SHT which iteratively minimizes the building-up of error and therefore improves the accuracy of the s-SHT.

For a spin-s function band-limited at L and discretized over the sampling scheme $\mathfrak{S}_s^L$, we compute its spherical harmonic coefficients, denoted by $({}_s\breve{f}_1)_\ell^m$ using proposed s-SHT and define the residual as

$$r_k(\theta,\phi) = {}_sf(\theta,\phi) - \sum_{\ell=s}^{L-1}\sum_{m=-\ell}^{\ell} ({}_s\breve{f}_k)_\ell^m\, {}_sY_\ell^m(\theta,\phi) \tag{3.10}$$

that is, an error between the signal ${}_sf$ and the signal synthesized from the spherical harmonic coefficients. Here $k = 1, 2, \ldots,$ indicates the iteration number. We carry out s-SHT of the residual to compute its spherical harmonic coefficients, denoted by $(r_k)_\ell^m$ and update $({}_s\breve{f}_k)_\ell^m$ as

$$({}_s\breve{f}_{k+1})_\ell^m = ({}_s\breve{f}_k)_\ell^m + (r_k)_\ell^m. \tag{3.11}$$

In multi-pass s-SHT, we propose to use (3.10) and (3.11) iteratively to compute $({}_s\breve{f}_k)_\ell^m$ for $k = 1, 2, \ldots,$ until the following stopping criterion is met

$$\max_{(\theta,\phi\in\mathfrak{S}_s^L)} \big|r_{k+1}(\theta,\phi)\big| > \max_{(\theta,\phi\in\mathfrak{S}_s^L)} \big|r_k(\theta,\phi)\big|. \tag{3.12}$$

Later, we illustrate, through numerical experiments, that the multi-pass s-SHT improves the accuracy over the (single-pass) s-SHT.

3.2.6 Numerical Accuracy

In our experiment to evaluate the accuracy of the proposed spin-s SHT, we generate the spin spherical harmonic coefficients $({}_sf_{\rm a})_\ell^m$ of our test signal for $|s| < \ell < L$, $|m| \leq \ell$ with real and imaginary parts uniformly distributed in the interval $[-1,\, 1]$ and then use (2.9) to obtain the signal over samples of the proposed scheme $\mathfrak{S}_s^L$. We then apply the proposed s-SHT and multi-pass s-SHT to reconstruct the spin-s spherical harmonic coefficients denoted by $({}_sf_{\rm r})_\ell^m$. For each $L = 8, 16, 32, 64$ and $s = 1, 2, 4$, we repeat this experiment 10 times to obtain the average value of the maximum and mean errors, defined as

$$\epsilon_{\rm max} \triangleq \max \big|{}_sf_{\rm a}(\theta,\phi) - {}_sf_{\rm r}(\theta,\phi)\big|, \tag{3.13}$$

$$\epsilon_{\rm mean} \triangleq \frac{1}{N_o} \sum_{(\theta,\phi)} \big|{}_sf_{\rm a}(\theta,\phi) - {}_sf_{\rm r}(\theta,\phi)\big|, \tag{3.14}$$

which are plotted in Fig. 3.1 that illustrates that the proposed transforms enable accurate computation of s-SHT and multi-pass s-SHT improves the reconstruction accuracy. It is observed that the reconstruction errors grow with the increase in integer spin s, which is due to the fact that matrix ${}_sD_m$ defined in (3.5) becomes ill-conditioned as s increases irrespective of the placement of samples by the condition number minimization method.

3.3 Analysis of Geometrical Properties

For each of the sampling scheme on the sphere presented in chapter 2, we here analyse the geometrical properties of the sampling scheme and review the accuracy and computational complexity of the s-SHT associated with each of the sampling scheme. In this section, we first define the geometrical properties: sampling efficiency, minimum geodesic distance, mesh norm and mesh ratio for the scalar spin-s functions ($s = 0$) and shows the significance of the geometrical properties in the nalysis of the sampling schemes and then compare geometrical properties of the proposed sampling scheme with those for the the existing equiangular [59] and Gauss-Legendre sampling schemes [75, 103].

3.3.1 Sampling Efficiency

The sampling efficiency, defined as a ratio of the dimensionality of the subspace formed by the band-limited signals, that is the number of coefficients required to represent a band-limited signal in the harmonic domain, to the number of samples required to accurately compute s-SHT, is the fundamental property of any sampling scheme. For a band-limit L, we define the sampling efficiency, denoted by ${}_sE_L$, of any sampling scheme as the ratio of the dimensionality (N_o) of subspace formed by band-limited spin-s functions to the number of samples required to accurately compute s-SHT.

3.3.2 Minimum Geodesic Distance and Packing Radius

For a set of sampling points on the sphere, the minimum geodesic distance is defined as the minimum distance between any two points in the set. It is also defined as twice the packing radius on the sphere. It is desirable to design a sampling scheme on the sphere such that the minimum geodesic distance is maximized (well-known sphere packing problem). For points of an extremal system for a band-limit L, the minimum geodesic distance is lower bounded by $\pi/2(L-1)$ [78]. For a set of sampling points on the sphere denoted by ζ, the minimum geodesic distance is defined as

$$ {}_s\sigma(\zeta) \triangleq \min_{\hat{\boldsymbol{x}},\, \hat{\boldsymbol{y}} \in \zeta} d_S(\hat{\boldsymbol{x}}, \hat{\boldsymbol{y}}), \tag{3.15} $$

where $d_S(\hat{\boldsymbol{x}}, \hat{\boldsymbol{y}})$ denotes the geodesic (great circle or spherical) distance between two points $\hat{\boldsymbol{x}}(\theta_x, \phi_x)$ and $\hat{\boldsymbol{y}}(\theta_y, \phi_y)$ and is given by

$$ \begin{aligned} d_S(\hat{\boldsymbol{x}}, \hat{\boldsymbol{y}}) &= \cos^{-1}(\hat{\boldsymbol{x}} \cdot \hat{\boldsymbol{y}}) \\ &= \cos^{-1}\big(\cos\theta_x \cos\theta_y + \sin\theta_x \sin\theta_y \cos(\phi_x - \phi_y)\big). \end{aligned} \tag{3.16} $$

Since the sampling schemes under consideration do not have the same sampling efficiency, we need to incorporate sampling efficiency in defining the minimum geodesic distance for a meaningful comparison of different sampling schemes. We define the normalized minimum geodesic distance as

$$ {}_s\sigma_n(\zeta) \triangleq \frac{1}{{}_sE_L}\sigma(\zeta) = \frac{1}{{}_sE_L} \min_{\hat{\boldsymbol{x}},\, \hat{\boldsymbol{y}} \in \zeta} d_S(\hat{\boldsymbol{x}}, \hat{\boldsymbol{y}}), \tag{3.17} $$

3.3.3 Mesh Norm

For a set ζ of points on the sphere, mesh norm is defined as the largest geodesic distance from a point $\hat{\boldsymbol{x}} \in \mathbb{S}^2$ to the nearest point in the set ζ. For a set ζ of sampling points of the sampling scheme parameterized by L, we define the mesh norm as

$$ {}_s\lambda(\zeta) \triangleq \frac{1}{{}_sE_L} \max_{\hat{\boldsymbol{x}} \in \mathbb{S}^2} \min_{\hat{\boldsymbol{y}} \in \zeta} \; d_S(\hat{\boldsymbol{x}}, \hat{\boldsymbol{y}}). \tag{3.18} $$

where ${}_sE_L$ is the sampling efficiency of the sampling scheme and $d_S(\hat{\boldsymbol{x}}, \hat{\boldsymbol{y}})$ is given in (3.16). We note that the mesh norm is also referred to as the covering radius as the spherical caps of radius equal to mesh norm and centered at sampling points covering the whole sphere. It is desirable to design a sampling scheme that minimizes the mesh norm [64]. For points of an extremal system for a band-limit L, Reimer [79] obtained an upper bound on the mesh norm of any system of points associated with positive weight cubature rule for a band-limit L. The upper bound is $\lambda(\zeta) \leq 2j_o/(L-1) \approx 4.8097/(L-1)$, where j_o is the smallest positive zero of the Bessel function J_o.

3.3.4 Mesh Ratio

Mesh ratio is the ratio of the covering to the packing radius of the identical spherical caps on the surface of a sphere. For a set ζ of sampling points on the sphere, we define the mesh ratio as

$$ {}_s\Gamma(\zeta) = \frac{2\,{}_s\lambda(\zeta)}{{}_s\sigma_n(\zeta)} > 1, \tag{3.19}$$

where we have used normalized geodesic distance in the formulation of mesh ratio as we also normalize the mesh norm with the sampling efficiency. Since the mesh ratio serves as a good measure of the quality of the uniform distribution of points, the sampling schemes should have smaller mesh norm.

Analysis

For each of the sampling schemes presented in chapter 2, we plot the normalized minimum geodesic ${}_s\sigma_n(\zeta)$ for different band-limits $10 \leq L \leq 50$ and integer spin $s = 0$ in Fig. 3.2(a), where it can be observed that extremal system of points, spherical design and optimal dimensionality, all have well separated points on the sphere. The nomralized minimum geodesic distance curves, obtained by using the points of equiangular and Gauss-Legendre quadrature based sampling schemes, are well below the lower bound values for all degrees $10 \leq L \leq 50$. It is because, these sampling schemes exhibit dense sampling near the poles. For each of the sampling schemes, we numerically compute the mesh norm by 1) randomly taking the M number of uniformly distributed number of points on the sphere, 2) taking the minimum distance between the sampling points and the randomly chosen points on the sphere and 3) then obtaining the maximum over the minimum distances. We choose M such that the numerically computed mesh norms by taking M random points and $2M$ random points do not differ more than 1%.

We plot the mesh norm for different sampling schemes in Fig. 3.2(b). It is evident that extremal system of points has the smallest mesh norm. As compared to equiangular and GL sampling schemes, spherical designs and optimal dimensionality sampling schemes have smaller mesh norm. In Fig. 3.2(c), we plot the mesh ratio for different sampling schemes and different band-limits, where we observe that the mesh ratio for equiangular and GL sampling schemes increase with the

band-limit, whereas the mesh ratio remains (almost) constant with the increase in band-limit. It can also be observed that the extremal system sampling scheme has the smallest mesh ratio.

Among the geometrical properties analysed for different sampling schemes, sampling efficiency and mesh norm encapsulates the other properties and therefore serve as the measures of the uniform distribution of sampling points. Analysis of geometrical properties of the sampling scheme reveals that the mesh ratio grow with the band-limit for the equiangular and Gauss-Legendre sampling schemes which is a consequence of the fact that these sampling schemes require dense sampling at the poles. In contrast, the optimal dimensionality, spherical design and extremal systems sampling schemes exhibit desired geometrical properties. Furthermore, the optimal dimensionality and extremal system sampling schemes have almost twice of the sampling efficiency attained by equiangular, Gauss-Legendre and spherical design sampling schemes. The mesh ratio achieved by optimal dimensionality is a little higher than extremal system, yet, it is very small compared to the equiangular schemes.

In Fig. 3.3, we plot these properties for proposed sampling scheme and compare results with equiangular sampling and Gauss-Legendre sampling schemes for band-limits $8 \leq L \leq 64$ and integer spin $s = 1, 2, 4$, where it can observed that the proposed optimal dimensionality scheme exhibit superior geometrical properties primarily due to the dense sampling near the poles required by the existing schemes.

3.4 Summary of Contributions

In this chapter, we have proposed an optimal-dimensionality sampling scheme for the accurate reconstruction of band-limited spin-s functions on the sphere and developed a method to compute s-SHT associated with the proposed sampling scheme. We have placed the samples such that the linear system of equations involved in the computation of s-SHT are well-conditioned. For the accurate computation of s-SHT of the spin-s function band-limited at L, the proposed sampling scheme requires optimal $N_o = L^2 - s^2$ samples equal to the number of degrees of freedom of the signal in harmonic space. In comparison, the existing schemes require $\sim 2L^2$ samples. We have also developed a multi-pass s-SHT that iteratively improves the accuracy of the transform, demonstrated the accuracy of the s-SHT.

We show that the proposed sampling scheme is superior to existing schemes in terms of geometrical properties such as geodesic distance, mesh norm and mesh ratio.

Addressing Q1 posed in Section 1.2.1:

- For the accurate computation of s-SHT of the spin-s function band-limited at L, the proposed sampling scheme requires optimal $N_o = L^2 - s^2$ samples equal to the number of degrees of freedom of the signal in harmonic space. In comparison, the existing schemes require $\sim 2L^2$ samples.

Addressing Q2 posed in Section 1.2.1:

- We have also developed a multi-pass s-SHT that iteratively improves the accuracy of the transform, demonstrated the accuracy of the s-SHT.
- Numerical experiments show the accuracy of the proposed s-SHT and multi-pass s-SHT.

Addressing Q3 posed in Section 1.2.1:

- We have done analysis and show that the proposed sampling scheme is superior to existing schemes in terms of geometrical properties such as geodesic distance, mesh norm and mesh ratio.

Note that in the later chapters, we will only consider the scalar functions (i.e., $s = 0$) on the sphere, so for ease, notation SHT will be used instead of s-SHT ($s = 0$).

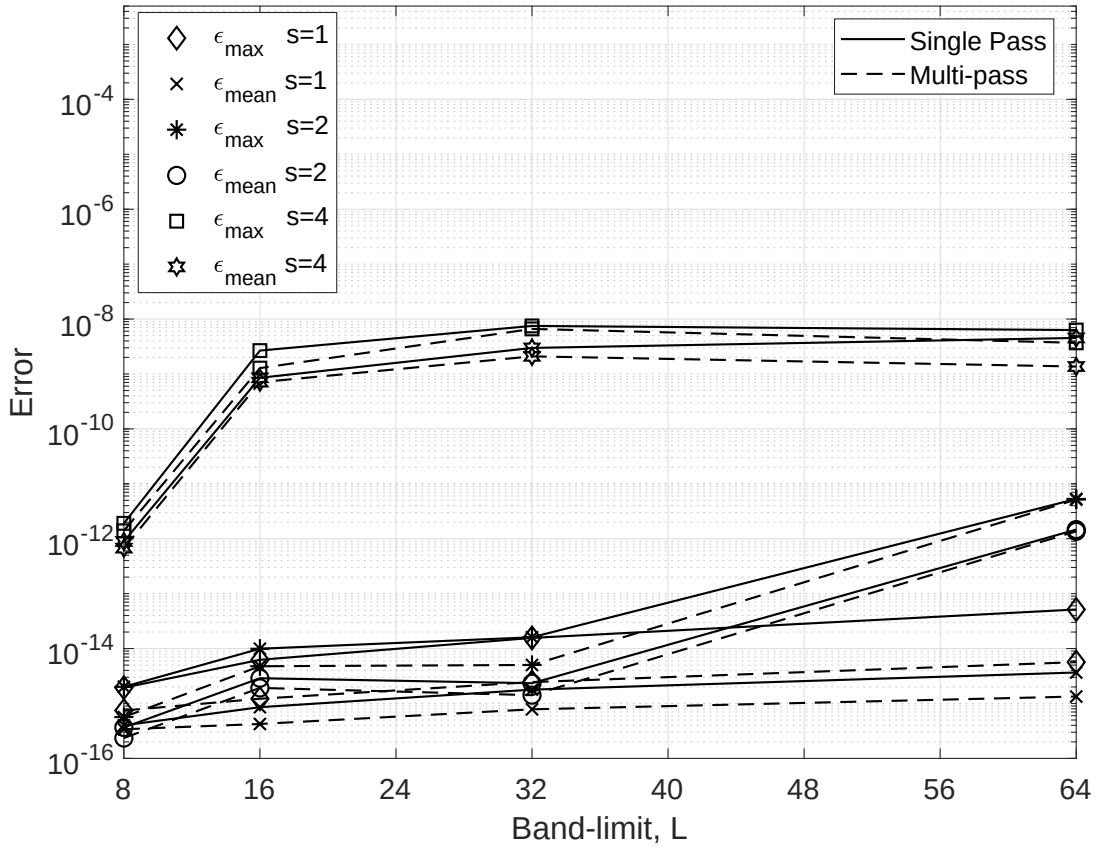

Figure 3.1: Numerical accuracy of the proposed s-SHT: the maximum error $\epsilon_{\max}$ and the mean error ϵ_{mean} for band-limits $L = (8, 16, 32, 64)$ and integer spin $s = (1, 2, 4)$.

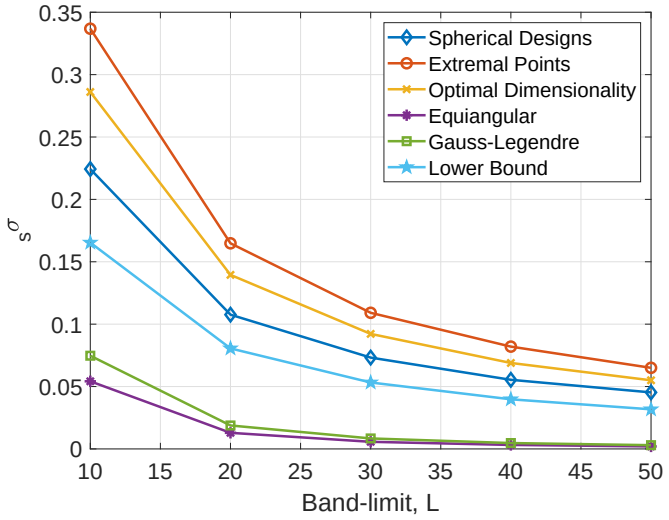

(a)

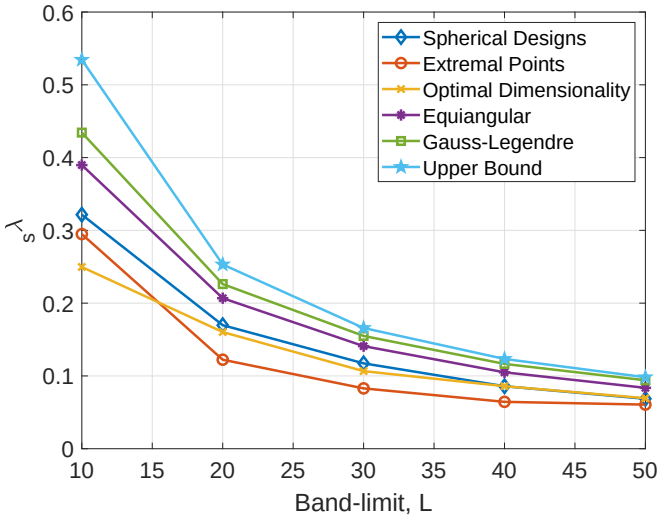

(b)

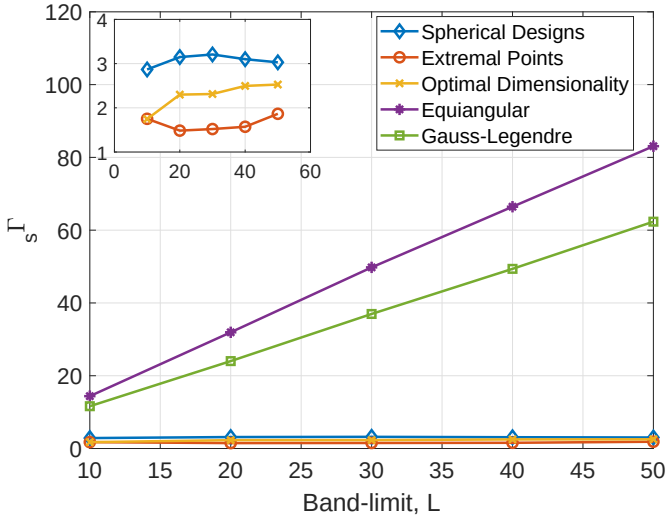

(c)

Figure 3.2: The geometrical properties: (a) Minimum Geodesic Distance ${}_s\sigma(\zeta)$, (b) Mesh norm ${}_s\lambda(\zeta)$ and (c) Mesh Ratio ${}_s\Gamma(\zeta)$ for band-limits $10 \leq L \leq 50$, integer spin $s = 0$ and different sampling schemes.

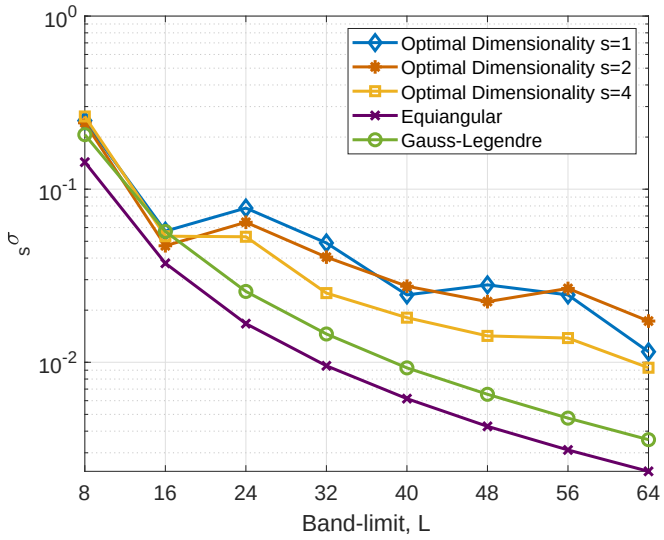

(a)

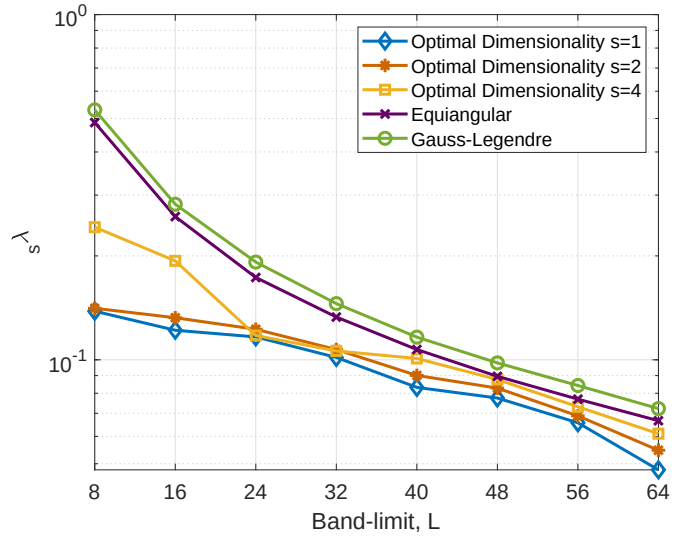

(b)

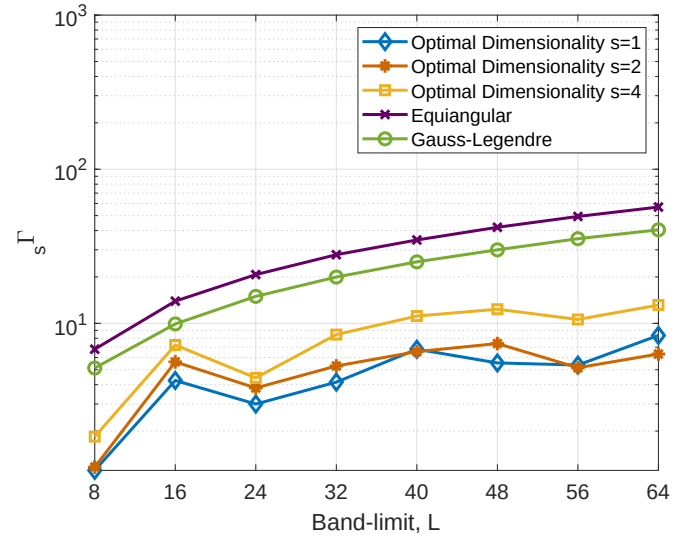

(c)

Figure 3.3: The geometrical properties: (a) Minimum Geodesic Distance ${}_s\sigma(\zeta)$, (b) Mesh norm ${}_s\lambda(\zeta)$ and (c) Mesh Ratio ${}_s\Gamma(\zeta)$ for proposed, equiangular and Gauss-Legendre sampling schemes.

Chapter 4

Signal Reconstruction on the Sphere

In this chapter, we study two scenarios for the reconstruction of the signal on the sphere: i) when the measurements are not taken on a pre-defined grid on the sphere (first part of the chapter) and ii) when the estimation is done from incomplete measurements (second part of the chapter).

In the first part of this chapter, we present the generalized iterative residual fitting (IRF) for the computation of the spherical harmonic transform (SHT) of band-limited signals on the sphere. The proposed method is based on the partitioning of the subspace of band-limited signals into orthogonal subspaces. There exist sampling schemes on the sphere which support accurate computation of SHT. However, there are applications where samples (or measurements) are not taken over the predefined grid due to nature of the signal and/or acquisition set-up. To support such applications, the proposed IRF method enables accurate computation of SHTs of signals with randomly distributed sufficient number of samples. In order to improve the accuracy of the computation of the SHT, we also present the so-called multi-pass IRF which adds multiple iterative passes to the IRF. We analyse the multi-pass IRF for different sampling schemes and for different size partitions. Furthermore, we conduct numerical experiments to illustrate that the multi-pass IRF allows sufficiently accurate computation of SHTs.

In the second part of the chapter, we develop an algorithm for the extrapolation of band-limited signals on the sphere. The proposed algorithm improves the accuracy of the extrapolation of band-limited signal by using the information contained in the out-of-band harmonic coefficients of the signal to update the extrapolated

signal at each iteration. The estimation of signals on the sphere from incomplete measurements finds applications in acoustics, cosmology and geophysics. The proposed algorithm does not only exploit the band-limited property of the signal, that is, force the harmonic coefficients outside the band-limit to zero, at each iteration as carried out in the existing algorithms but also uses the harmonic coefficients outside the harmonic domain to improve the accuracy of signal extrapolation. To demonstrate the improvement in the accuracy enabled by the proposed algorithm, we conduct numerical experiments and compare the results of the proposed algorithm with the existing iterative conjugate gradient method.

This chapter is organized as follows. We present the necessary literature review for signal reconstruction on sphere in Section 4.1. In Section 4.2, we state the first problem under consideration in this chapter and formulate IRF and multi-pass IRF methods. Analysis of different partitions is also done. The second problem of extrapolation (reconstruction of signals from incomplete measurement)is discussed in detail in Section 4.3 and an iterative algorithm is proposed and formulated for signal extrapolation on the sphere. We then analyse the methods discussed in the two parts of this chapter and evaluate reconstruction errors under different experimental settings in Section 4.4.

4.1 Prior Work

Sampling schemes have been devised in the literature for the accurate and efficient computation of SHTs [51, 59, 63] which require samples on the whole sphere.. However, the samples may not be available, in practice (e.g., [3, 67]), over the grid defined by these sampling schemes. To support the computation of SHTs in applications where samples or data-sets are not available on the pre-defined grid, least squares fitting (LSF) methods have been investigated for efficient computation of the SHTs [66–68, 106–109]. LSF methods formulate a large linear system of basis functions and then attempt to solve it efficiently. However, due to memory overflow, it is not suitable for systems with large band-limits, $L > 1024$ [110–112]. To solve this problem, an iterative residual fitting (IRF) method has been proposed in [110] as an extension of LSF and incorporates a divide and conquer technique for the computation of SHTs. The basic idea of IRF is to divide the subspace spanned by all spherical harmonics into smaller partitions and then perform least squares

on each partition iteratively. Although IRF is fast, it creates a less accurate reconstruction [110] as the size of the harmonic basis increases for large band-limits. To improve the reconstruction accuracy, a multi-pass IRF approach is used which includes multiple passes for fitting. This is same as IRF but it involves multiple IRF operations rather than one. A variant of this scheme is presented in [110], where reconstruction for 3D surfaces is carried out by taking large number of samples.

There are applications in geophysics and acoustics where the measurements cannot be taken over the whole sphere. For example, in acoustics, head related transfer function (HRTF) measurements are not reliable in the South polar cap region due to reflections from the ground. Another example is the problem of polar gap in geophysics where the inclination of satellite orbit makes the satellite measurements on poles unreliable. To address the issue of unreliable and inaccessible samples on the sphere in these applications, we consider the problem of signal extrapolation on the sphere in the second part of this chapter. In literature, many algorithms have been proposed for extrapolation of band-limited signals on the sphere [46, 90–93]. An analog of Papoulis algorithm [113] for continuous signals on the sphere exploiting the band-limiting characteristics of the signal is proposed in [90] and its integral equation formulation is developed in [91]. For discrete signals on the sphere, an iterative algorithm is presented in [92], which converges to minimum norm least-squares solution. Conjugate gradient extrapolation algorithm on the sphere has been presented in [46], which in comparison to the previously proposed algorithms, enables more accurate and fast extrapolation. [114] uses the slepian functions [34] to develop an iterative algorithm for the extrapolation of band-limited signal on the sphere in the presence of noise.

4.2 Part I — Generalized Iterative Residual Fitting

In the first part of the chapter, we present an IRF method for the computation of the SHT of a band-limited signal in a general setting that partitions the subspace of band-limited signals into orthogonal subspaces, where each orthogonal subspace can be spanned by different numbers of basis functions. We also formulate multi-pass IRF to improve the accuracy of computation of the SHT. We analyze multi-pass IRF for different choices of partitioning of the subspace and sampling

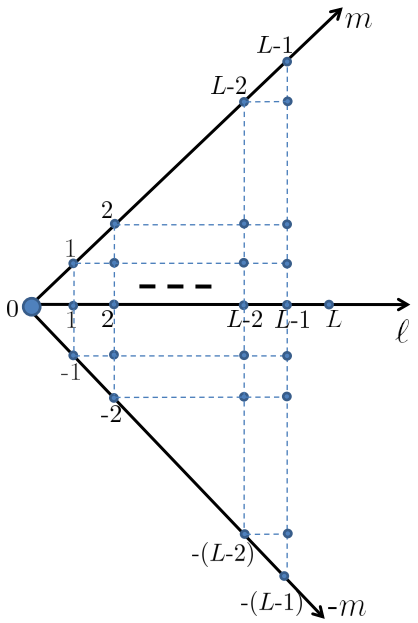

Figure 4.1: Spherical harmonic domain representation of a band-limited signal in $\mathcal{H}_L$.

schemes [59,63,110,125] and show that the computation of the SHT converges in all cases. We also show that the convergence is fast for the partition choice considered in this work. Here we present the generalization of the IRF method [3,110] for the computation of the SHT of the band-limited signal $g \in \mathcal{H}_L$ from its samples.

4.2.1 Iterative Residual Fitting (IRF) – Formulation

The IRF method is based on the idea to partition the subspace $\mathcal{H}_L$ into smaller subspaces and carry out least-squares estimation on these partitions iteratively. In this way, a large linear problem is divided into manageable small subsets of linear problems. The subspace $\mathcal{H}_L$ has graphical representation of the form shown in Fig. 4.1, which also represents the SH (spectral) domain formed by the SH coefficients of the band-limited signal in $\mathcal{H}_L$. We partition $\mathcal{H}_L$ into K *orthogonal* subspaces $\mathcal{H}_L^k$, $k = 1, 2, \cdots, K$, each of dimension N_k. We analyse different choices for partitioning later in the chapter. We index the SH functions that span the subspace $\mathcal{H}_L^k$ as Y_{kj}, $j = 1, 2, \cdots, N_k$. We also define $(g)_{kj} = \langle g, Y_{kj} \rangle$.

Given M samples (measurements) of the band-limited signal $g \in \mathcal{H}_L$, we wish to compute SH coefficients. By defining a vector

$$\mathbf{G} \triangleq \big[g(\hat{\boldsymbol{x}}_1), \ldots, g(\hat{\boldsymbol{x}}_M)\big]^T, \tag{4.1}$$

of M measurements (samples) of the signal $g \in \mathcal{H}_L$ on the sphere and the matrix $\mathbf{Y}_k$, with entries $\{\mathbf{Y}_k\}_{p,q} = Y_{kq}(\theta_p, \phi_q)$, of size $M \times N_k$ containing SH functions that span the subspace $\mathcal{H}_L^k$ evaluated at M sampling points, the vector $\mathbf{g_k} = [g_{k1}, g_{k2}, \cdots, g_{kN_k}]^T$ of SH coefficients can be *iteratively* computed (estimated) in the least-squares sense as

$$\tilde{\mathbf{g}}_k = (\mathbf{Y}_k^H \mathbf{Y}_k)^{-1}\ \mathbf{Y}_k^H\ \mathbf{r}_k, \tag{4.2}$$

where $(.)^H$ represents the Hermitian of a matrix and

$$\mathbf{r}_k = \mathbf{G} - \sum_{k'=1}^{k-1} \mathbf{Y}_{k'}\ \tilde{\mathbf{g}}_{k'}, \quad \mathbf{r}_0 = \mathbf{G} \tag{4.3}$$

is the residual between the samples of the signal and the signal obtained by using the coefficients $\tilde{\mathbf{g}}_{k'}$ for $k' = 1, 2, \ldots, k-1$ and the estimation of coefficients is carried out iteratively for $k = 1, 2, \ldots, K$. We note that the computational complexity for (4.2) for each k would be of the order of $max(\mathbb{O}(MN_k^2), \mathbb{O}(N_k^3)) = \mathbb{O}(MN_k^2)$. The computational complexity to compute (4.3) is $\mathbb{O}(ML^2)$. We later analyse the estimation accuracy of the IRF method for different sampling schemes on the sphere and different partitions of the subspace $\mathcal{H}_L$ of band-limited signals. For a special case of partitioning the subspace $\mathcal{H}_L$ into L subspaces $\mathcal{H}_L^k$ based on the degree of spherical harmonics $\ell = 0, 1, \ldots, L-1$, it has been shown that the iterative residual fitting allows sufficiently accurate estimation of SH coefficients [110].

The proposed IRF method enables accurate computation of the SHT of signals with a sufficient number of randomly distributed samples. The IRF algorithm finds significance use in applications where samples on the sphere are not taken over a predefined grid. For example, the samples are taken over the cortical surface in medical imaging [3], where IRF allows sufficient accurate parametric modeling of cortical surfaces.

4.2.2 Multi-Pass IRF and Residual Formulation

To improve the estimation accuracy, we employ the so-called multi-pass IRF [110] which is based on the use of IRF method in an iterative manner. In multi-pass IRF, the IRF algorithm is run for a number of iterations, denoted by $i = 1, 2, \ldots$. To clarify the concept, we incorporate the iteration index i in the formulation in

(4.2) and (4.3) as

$$\tilde{\mathbf{g}}_k(i) = (\mathbf{Y}_k^H \mathbf{Y}_k)^{-1}\ \mathbf{Y}_k^H\ \mathbf{r}_k(i), \tag{4.4}$$

$$\begin{aligned} \mathbf{r}_k(i) &= \mathbf{G} - \sum_{i'=1}^{i-1} \sum_{k'=1}^{k-1} \mathbf{Y}_{k'}\ \tilde{\mathbf{g}}_{k'}(i'), \\ \mathbf{r}_0(i) &= \mathbf{r}_K(i-1),\ \mathbf{r}_0(1) = \mathbf{G}. \end{aligned} \tag{4.5}$$

After i-th iteration, $\tilde{\mathbf{g}}_k$ can be computed for each $k = 1, 2, \ldots, K$ as

$$\tilde{\mathbf{g}}_k(i) = \sum_{i'=1}^{i} \tilde{\mathbf{g}}_k(i'). \tag{4.6}$$

By defining

$$\mathbf{A}_k \triangleq (\mathbf{Y}_k^H\ \mathbf{Y}_k)^{-1}\ \mathbf{Y}_k^H, \quad \mathbf{C}_k \triangleq \mathbf{Y}_k\ \mathbf{A}_k, \tag{4.7}$$

the residual after the i-th iteration is given by

$$r_K(i) = \left(\prod_{k=1}^{K} (1 - \mathbf{C_k}) \right)^i \mathbf{G}. \tag{4.8}$$

In general, the residual in (4.8) depends on the distribution of sampling points and nature of partitioning of $\mathcal{H}_L$. In the next section, we show that the residual converges to zero for a variety of sampling schemes and different partitions.

4.2.3 Partition Choices

In order to understand the partitioning of $\mathcal{H}_L$, we refer to the graphical representation of $\mathcal{H}_L$ shown in Fig. 4.1, which describes the position of spherical harmonic coefficients with respect to degree $\ell \in (0, 1, \ldots, L-1)$ and order $m \leq |\ell|$. We give numbers to the spectral harmonic coefficients (basis functions) shown in Fig. 4.1 from 1 to L^2 in a way that we start the domain from $\ell = 0, m = 0$ and then traverse the whole domain by $m = -\ell$ to $m = \ell$ for increasing values of ℓ. In a similar way, we can also traverse the whole domain by fixing m for all values of ℓ. We analyse four different type of partitions, whose sizes vary with the increasing or decreasing

values of degrees ℓ and orders m. The size of each partition is denoted by N_k. In all the partitions, the generalized IRF is run for all values of k and for a fixed value of i.

Partition Choice 1

We first consider the partitioning of $\mathcal{H}_L$ based on the spherical harmonic degree [110]. We take $K = L$ partitions $\mathcal{H}_L^k$ each for degree $\ell = k - 1$ such that the subspace $\mathcal{H}_L^k$ is spanned by spherical harmonics of degree $k-1$. Consequently, the dimension of each subspace is $N_k = 2k - 1$. As mentioned earlier, the IRF has been applied already for this choice of partition [110]. We show through numerical experiments that alternative choices for partitioning result in faster convergence and more accurate computation of the SHT.

Partition Choice 2

For partition choice 2, we combine the k-th partition choice 1 and $K - k + 1$-th partition choice 1, to obtain $\frac{L}{2}$ or $\frac{L+1}{2}$ partitions for even or odd band-limit L respectively. For even L, each partition 2 $\mathcal{H}_L^k$ is of size $N_k = 2L$ for $k = 1, 2, \ldots, \frac{L}{2}$. For odd L, we have $\frac{L+1}{2}$ partitions with $N_k = 2L$ for $k = 1, 2, \ldots, \frac{L-1}{2}$ and one partition of size $N_{\frac{L+1}{2}} L$.

Partition Choice 3

Here, we consider partitioning with respect to each order $|m| < L$ (see Fig. 4.1). Consequently, we have $2L - 1$ partitions, one for each order $|m| < L$ and spanned by SH functions of order m.

Partition Choice 4

Partition choice 4 is obtained by combining the partitions in partition choice 3. We obtain L partitions by combining partition choice 3 for m and $-(L - m)$ for $m = 1, 2, \ldots L - 1$. With such combining, we have L partitions of $\mathcal{H}_L$ each of size L. We defer the analysis until Section 4.4.

4.3 Part II — Signal Extrapolation

In the second part of the chapter, we develop an iterative algorithm for the signal extrapolation over the inaccessible region on the sphere. The proposed method takes samples according to the equiangular sampling scheme which supports exact computation of SHT on the sphere. Existing schemes focus on the use of the band-limited property of the signal, that is, the signal extrapolation is carried out iteratively by forcing the harmonic coefficients outside the band-limit of the signal to zero at each iteration. In the proposed algorithm, we do not only force the harmonic coefficients to zero but also use these to improve the extrapolation of the signal over the inaccessible region at each iteration. We conduct numerical experiments and compare the accuracy of the proposed algorithm with iterative conjugate gradient algorithm proposed in [46]. We also take HRTF measurements using synthetic head model [126], extrapolate the signal on the South pole and show that the proposed algorithm enables more accurate extrapolation than the existing methods.

4.3.1 Proposed Extrapolation Algorithm - Preliminaries

Samples are taken over the whole sphere for the accurate computation of SHT or signal reconstruction. However, in some applications, samples over some region of the sphere cannot be taken due to practical limitations [90, 93]. These applications require signal processing methods or algorithms to extrapolate the signal over the inaccessible region [46, 90–93]. We consider the same problem in this work and propose an iterative algorithm for signal extrapolation which, in comparison with the existing methods, enables more accurate extrapolation.

For a band-limited signal $f \in L^2(\mathbb{S}^2)$ with maximum spherical harmonic degree L, we assume that the measurements or samples are available over some region $\mathcal{R} \subset \mathbb{S}^2$. We assume that the measurements are not available over inaccessible region $\mathcal{R}^c = \mathbb{S}^2 \backslash R \subset \mathbb{S}^2$. For a spatial region $\mathcal{R}$, we define a space-limiting operator $D_{\mathcal{R}}$ with kernel given by

$$D_{\mathcal{R}}(, \hat{\boldsymbol{y}}) \triangleq I_{\mathcal{R}}(\hat{\boldsymbol{x}})\delta(\hat{\boldsymbol{x}}, \hat{\boldsymbol{y}}), \tag{4.9}$$

where $\delta(x, y)$ denotes the Dirac delta function [26] and

$$I_{\mathcal{R}}(\hat{\boldsymbol{x}}) \triangleq \begin{cases} 1 & \hat{\boldsymbol{x}} \in \mathcal{R}, \\ 0 & \hat{\boldsymbol{x}} \in \mathcal{R}^c, \end{cases} \tag{4.10}$$

is an indicator function of the region R. Using the operator $D_{\mathcal{R}}$, we define the problem under consideration is to extrapolate the signal $f \in \mathcal{H}_L$ when only $f_{\mathcal{R}}(\hat{\boldsymbol{x}}) \triangleq (D_{\mathcal{R}} f)(\hat{\boldsymbol{x}})$ is known and $f_{\mathcal{R}^c}(\hat{\boldsymbol{x}}) \triangleq (D_{\mathcal{R}^c} f)(\hat{\boldsymbol{x}})$ is unreliable or not known. With these definitions, we can express f as

$$f(\hat{\boldsymbol{x}}) = f_{\mathcal{R}}(\hat{\boldsymbol{x}}) + f_{\mathcal{R}^c}(\hat{\boldsymbol{x}}), \tag{4.11}$$

with representation in harmonic domain given by

$$\big(f\big)_\ell^m = \big(f_{\mathcal{R}}\big)_\ell^m + \big(f_{\mathcal{R}^c}\big)_\ell^m. \tag{4.12}$$

We note that the signals $f_{\mathcal{R}}$ and $f_{\mathcal{R}^c}$ are not band-limited due to the space-limiting operation.

4.3.2 Proposed Signal Extrapolation - Formulation

To reconstruct the original signal $f(\hat{\boldsymbol{x}})$, we assume that the signal is sampled over the sampling grid Ω_M where we assume $M > L$[1]. Since the original signal f is band-limited at L, we have $\big(f\big)_\ell^m = 0$ for all $\ell \geq L$, equation (4.12) implies

$$\big(f_{\mathcal{R}^c}\big)_\ell^m = -\big(f_{\mathcal{R}}\big)_\ell^m, \quad L \leq \ell < M,\ |m| \leq \ell. \tag{4.13}$$

We also define function $h(\hat{\boldsymbol{x}})$ as

$$h(\hat{\boldsymbol{x}}) \triangleq f_{\mathcal{R}^c}(\hat{\boldsymbol{x}}) I_{\mathcal{R}}(\hat{\boldsymbol{x}}), \tag{4.14}$$

which can be written in the harmonic domain as

$$\big(h\big)_\ell^m = \sum_{\ell' m'}^{M-1} \big(f_{\mathcal{R}^c}\big)_{\ell'}^{m'} \big(Z\big)_{\ell',\ell}^{m',m}, \tag{4.15}$$

[1]Due to the fact that the known signal $f_{\mathcal{R}}$ is not band-limited.

where $\sum_{\ell' m'}^{M-1} \triangleq \sum_{\ell'}^{M-1} \sum_{m'=-\ell'}^{\ell}$ and

$$\begin{aligned}\big(Z\big)_{\ell',\ell}^{m',m} &= \big(I_{\mathcal{R}}(\hat{\boldsymbol{x}}) Y_{\ell'}^{m'}(\hat{\boldsymbol{x}})\big)_{\ell}^{m}, \\ &= \sum_{\ell'' m''}^{M-1} \big(I_{\mathcal{R}^c}\big)_{\ell''}^{m''} T_{\ell,m}^{\ell',m',\ell'',m''}. \end{aligned} \tag{4.16}$$

Here

$$T_{\ell,m}^{\ell',m',\ell'',m''} = \int_{\mathbb{S}^2} Y_{\ell'}^{m'}(\hat{\boldsymbol{x}}) Y_{\ell''}^{m''}(\hat{\boldsymbol{x}}) \overline{Y_{\ell}^{m}(\hat{\boldsymbol{x}})}\, ds(\hat{\boldsymbol{x}}). \tag{4.17}$$

4.3.3 Proposed Signal Extrapolation - Algorithm

Since $f_{\mathcal{R}^c} = 0$ on R by definition, we have $h(\hat{\boldsymbol{x}}) = 0$ as defined in (4.14), which implies $\big(h\big)_{\ell}^{m} = 0$. Consequently, we have the following system

$$\sum_{\ell' m'}^{M-1} \big(f_{\mathcal{R}^c}\big)_{\ell'}^{m'} \big(Z\big)_{\ell',\ell}^{m',m} = 0, \tag{4.18}$$

which can be equivalently expressed as

$$\mathbf{Z}\mathbf{f} = 0, \tag{4.19}$$

where $\mathbf{Z}$ is an $M^2 \times M^2$ matrix containing all the spherical harmonic coefficients of the expression derived in (4.16) and $\mathbf{f}$ is vector of length M^2 containing spherical harmonic coefficients $\big(f\big)_{\ell}^{m}$. During the construction of $\mathbf{f}$ in our proposed algorithm, we use (4.13) to replace the unknown coefficients with the negative of the known coefficients in each iteration. In order to solve the system in (4.19), we divide the matrix $\mathbf{Z}$ and vector $\mathbf{f}$ into two partitions of different sizes namely $\mathbf{Z}_a, \mathbf{Z}_b$ and $\mathbf{f}_a, \mathbf{f}_b$ respectively. The system now is

$$[\mathbf{Z}_a | \mathbf{Z}_b] \begin{bmatrix} \mathbf{f}_a \\ \hline \mathbf{f}_b \end{bmatrix} = 0. \tag{4.20}$$

Note that we ensure the system proposed in (4.20) is always overdetermined by selecting a suitable band-limit which is $M = \lceil \sqrt{2}L \rceil$. Using (4.13) and (4.20), the unknown coefficients can be determined by

$$\mathbf{f}_a = \Lambda \mathbf{f}_b, \tag{4.21}$$

where $\Lambda = (-1)(\mathbf{Z}_a^T\mathbf{Z}_a)^{-1}\mathbf{Z}_a^T\mathbf{Z}_b$. In our algorithm, we take samples of f over the equiangular sampling grid Ω_M where $M > L$. We first pre-compute $\big(Z\big)_{\ell',\ell}^{m',m}$ using (4.16) and form matrix $\mathbf{Z}$ to determine Λ. We apply the space limiting operator defined in (4.9) to get space-limited function $\hat{f}(\hat{\boldsymbol{x}})$. In order to find the vector $\mathbf{f}$ in (4.19), we take the SHT of space-limited function $\hat{f}(\hat{\boldsymbol{x}})$, first modify it using (4.13) and then modify it again by updating $\mathbf{f}_a$ after computing $\mathbf{f}_a$ using (4.21). We take the inverse SHT of $\mathbf{f}$ and update the space-limited function. We use the same procedure iteratively for K number of iterations and summarize the evaluation of the unknown coefficients in the form of procedure 2 given below[2].

Procedure 2 Iterative Extrapolation

Require: $\big(f\big)_\ell^m, \quad \forall\ 0 \leq \ell < L,\ |m| \leq \ell$

procedure ITERATIVE EXTRAPOLATION($f_{\mathcal{R}}(\hat{\boldsymbol{x}})$)
  $\hat{f}(\hat{\boldsymbol{x}}) = f_{\mathcal{R}}(\hat{\boldsymbol{x}})$
  compute $\mathbf{Z}$ using (4.16) and evaluate Λ
  for $k = 1, 2, \ldots, K$ **do**
    compute $\mathbf{f}$ from $\hat{f}(\hat{\boldsymbol{x}})$ using SHT
    update $\mathbf{f}$ using (4.13)
    compute $\mathbf{f}_a$ using (4.21)
    update $\mathbf{f}$ with $\mathbf{f}_a$
    compute $\hat{g}(\hat{\boldsymbol{x}})$ as inverse SHT of $\mathbf{f}$
    update $\hat{f}(\hat{\boldsymbol{x}}) \leftarrow \hat{f}(\hat{\boldsymbol{x}}) + (D_{\mathcal{R}^c}\hat{g})(\hat{\boldsymbol{x}})$
  end for
  evaluate $\big(f\big)_\ell^m$ by taking SHT of $\hat{f}(\hat{\boldsymbol{x}})$
  return $\big(f\big)_\ell^m$
end procedure

4.4 Analysis

4.4.1 Analysis of Multi-Pass IRF

Here we analyse the accuracy of the computation of the SHT, that is, the computation of SH coefficients, of the band-limited signal sampled over different sampling schemes. For the distribution of samples on sphere, we consider equiangular sampling [127] and optimal-dimensionality sampling [63] in our analysis as these schemes support the accurate computation of the SHT for band-limited signals.

[2]We represent the inverse SHT of $\mathbf{f}$ as $\hat{g}(\hat{\boldsymbol{x}})$.

Among the sampling schemes on the sphere, which do not support the highly accurate computation of the SHT, we consider the HEALPix sampling scheme [125] and random samples with uniform distribution with respect to the differential measure $\sin\theta d\theta d\phi$. In order to analyse accuracy, we take a test signal $g \in \mathcal{H}_L$ by first generating the spherical harmonic coefficients $\big(g\big)_\ell^m$ with real and imaginary part uniformly distributed in $[-1, 1]$ and using (2.4) to obtain the signal over the samples for each sampling scheme. For a meaningful comparison, we take approximately the same number of points for each sampling scheme. We apply the proposed multi-pass IRF for each choice of partition and each sampling scheme to compute the estimate of SH coefficients $\big(\tilde{g}\big)_\ell^m$ and record the maximum error between reconstructed and original SH coefficients given by

$$\epsilon_{\max} \triangleq \max_{\ell<L,\,|m|\leq\ell} |\big(g\big)_\ell^m - \big(\tilde{g}\big)_\ell^m|, \tag{4.22}$$

which is plotted in logarithmic scale in Fig. 4.2 for band-limit $L = 15$. Different partition choices and different sampling schemes (see caption for number of samples for each sampling scheme) against the number of iterations of the proposed multi-pass IRF are plotted, where it can be observed that 1) the error converges to zero (10^{-16}, double precision) for all partition choices and sampling schemes, and 2) the error converges quickly for partition choice 4.

We also validate the formulation of the residual in (4.8) by computing after each iteration of the multi-pass IRF. To illustrate the effect of the number of samples on the accuracy of the proposed multi-pass IRF, we have taken $2L^2$, $4L^2$ and $6L^2$ samples of optimal dimensionality sampling [63] and plot the error $\epsilon_{\max}$ in Fig. 4.2(d)-(f), where it is evident that the error converges quickly for a greater number of samples. The convergence of the error is in agreement with the formulation of the residual in (4.8), however, convergence changes with the sampling scheme and nature of the partition of the subspace of band-limited signals.

4.4.2 Analysis of the Proposed Extrapolation Algorithm

In this section, we conduct two numerical experiments to illustrate the accuracy of the proposed iterative extrapolation method. We compare the proposed algorithm with the the iterative conjugate gradient method [46]. In both the experiments, we

consider the accessible region as

$$\mathcal{R} = \left\{ \hat{\boldsymbol{x}}(\theta, \phi) \in \mathbb{S}^2 | 0 \leq \theta \leq \ \pi - \theta_c \right\}, \tag{4.23}$$

where θ_c represents the excluded polar cap region, that is, it represents the region where the measurements are unreliable or unaccessible. In both the experiments, we compute the mean extrapolation error defined as

$$\epsilon_{\text{mean}} \triangleq \frac{1}{L^2} \sum_{\ell,m}^{L-1} |\big(f\big)_\ell^m - \big(\hat{f}\big)_\ell^m|, \tag{4.24}$$

where we take the mean of the absolute difference between actual $\big(f\big)_\ell^m$ and the extrapolated values $\big(\hat{f}\big)_\ell^m$ in the harmonic domain.

Experiment 1: In the first experiment, we consider random complex valued band-limited test signal with band-limit $L = 30$. We generate such test signal first randomly selecting $\big(f\big)_\ell^m$ with real and imaginary parts uniformly distributed in the interval $[-1, 1]$ and then synthesizing signal over Ω_M using (2.4). For different values of $\theta_c = \pi/8, \pi/6$, and $M = 60$, we apply the proposed algortihm and iterative conjugate gradient method to extrapolate the signal in region $\mathcal{R}^c$ and compute the error as defined in (4.24). We run both the algorithms for $K = 100$ number of iterations and plot the mean error in Fig. 4.3, where it is evident that the proposed algorithm enables more accurate extrapolation.

Experiment 2: In the second experiment, we apply the proposed method to extrapolate the head related transfer function (HRTF) on the sphere. We use spherical head model [126] to obtain synthetic HRTF data for the following parameters: head radius, $a = 0.09$ m, distance from head, $r = 1$ m, audible frequency range, $f_r = [5, 20]$ kHz, and speed of sound, $c = 340$ ms^{-1}. The effective HRTF band-limit is estimated by $L(\lambda) = \lceil \frac{e\pi a f_r}{c} \rceil + 1$, where λ is a wave number and is directly proportional to the frequency f_r. HRTF measurements are not reliable in South polar cap region due to the reflections from the ground and hence the samples cannot be taken near the South pole. For a given frequency, f_r, we obtain the HRTF measurements, $h(\hat{\boldsymbol{x}})$ over the sampling grid Ω_M and compute spherical harmonic coefficients, $\big(h\big)_\ell^m$ using (2.5). We then apply the proposed algorithm to extrapolate the signal in the region beyond $\theta_c = \pi/6$ and compute the mean error as defined in (4.24). The results of extrapolation of HRTF measurements of different

frequencies $f_r = 5$ kHz,10 kHz, effective band-limits, $L = 15, 27$ and $M = 40, 70$ for $K = 100$ using the proposed and iterative conjugate gradient method are plotted in Fig. 4.4. Again the numerical analysis reveals that the proposed method gives more accurate result than the well-known iterative conjugate gradient method.

4.5 Summary of Contributions

In this chapter, we pose two problems regarding reconstruction of the signals on the sphere. In the first part, we present the generalized iterative residual fitting (IRF) method for the computation of the spherical harmonic transform (SHT) of band-limited signals on the sphere. Proposed IRF is based on partitioning the subspace of band-limited signals into orthogonal spaces. In order to improve the accuracy of the transform, we have also presented a multi-pass IRF scheme and analysed it for different sampling schemes and for four different size partitions. We have performed numerical experiments to show that accurate computation of the SHT is achieved by multi-pass IRF. For different partitions and different sampling distributions, we have analysed the residual (error) and demonstrated the convergence of the residual to zero. It has been demonstrated that the rate of convergence of error depends on the sampling scheme and choice of partition.

In the second part of this chapter, we develop an iterative algorithm for extrapolation of band-limited signals on the sphere from limited or incomplete measurements. Existing schemes focus on the use of the band-limited property of the signal, that is, the signal extrapolation is carried out iteratively by forcing the harmonic coefficients outside the band-limit of the signal to zero at each iteration. In the proposed algorithm, we do not only force the harmonic coefficients to zero but also use these to improve the extrapolation of the signal over the inaccessible region at each iteration. We conduct numerical experiments in order to check the accuracy of the proposed algorithm and use Iterative Conjugate Gradient method as benchmark for comparison. We also take HRTF measurements using synthetic head model and extrapolate the signal on the South pole. The numerical analysis show that the proposed algorithm enables more accurate extrapolation than the existing methods.

Addressing Q4 posed in Section 1.2.1:

- It has been demonstrated that the rate of convergence of error depends on

the sampling scheme and choice of partition. For different partitions and different sampling distributions, we have analysed the residual (error) and demonstrated the convergence of the residual to zero.

Addressing Q5 posed in Section 1.2.1:

- We develop an iterative algorithm for extrapolation of band-limited signals on the sphere from limited or incomplete measurements. We conduct numerical experiments in order to check the accuracy of the proposed algorithm and use Iterative Conjugate Gradient method as benchmark for comparison. We also take HRTF measurements using synthetic head model and extrapolate the signal on the South pole. The numerical analysis show that the proposed algorithm enables more accurate extrapolation than the existing methods.

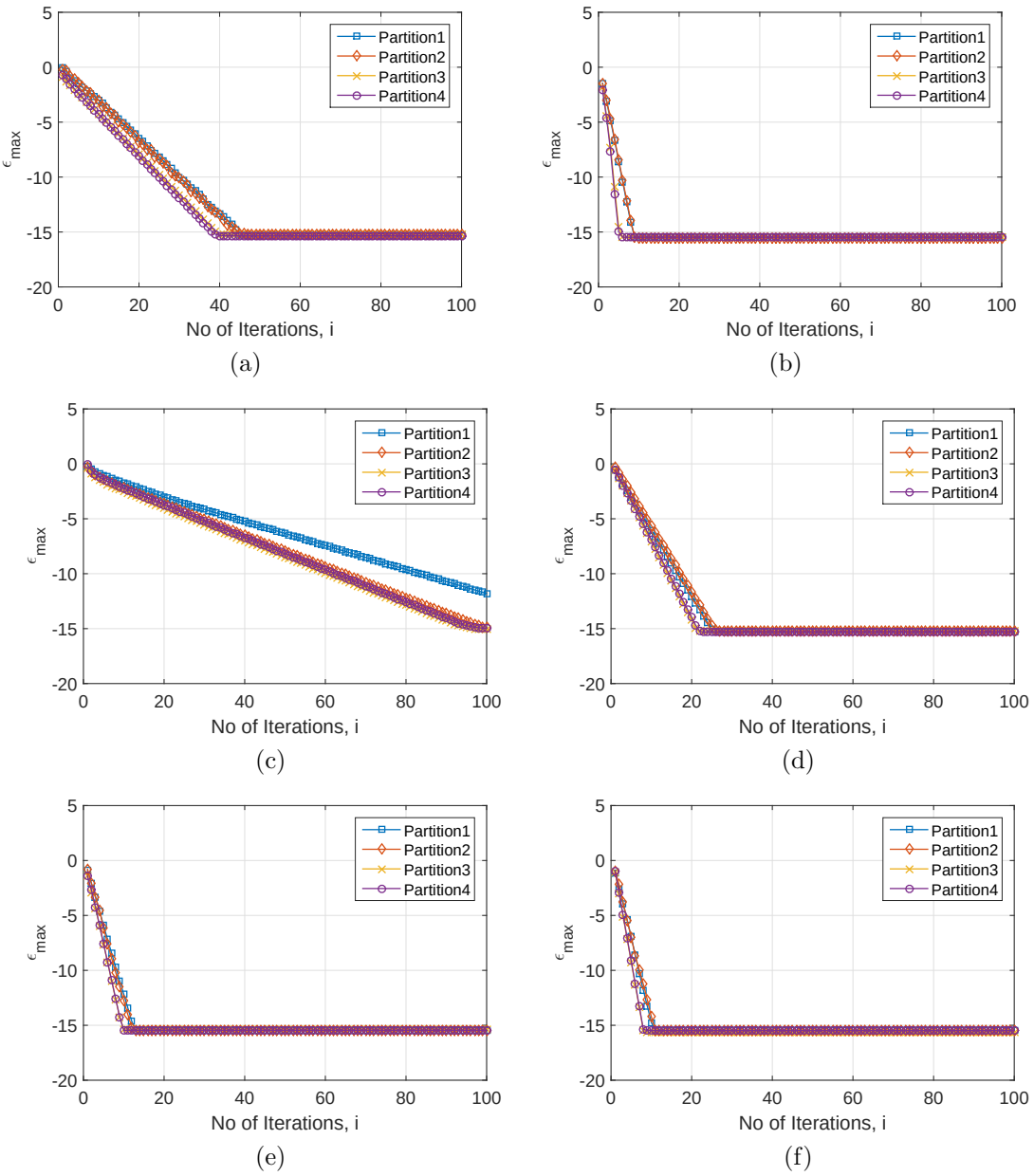

Figure 4.2: Maximum reconstruction error $\epsilon_{\max}$, given in (4.22), between the original and reconstructed SH coefficients of a band-limited signal with $L = 15$. Reconstructed SH coefficients are obtained using the proposed multi-pass IRF, where the samples of the signal are taken as (a) 991 samples of the Equiangular sampling scheme, (b) 972 samples of the HEALpix sampling scheme, (c) 900 random samples (d) 450 (e) 900 and (f) 1350 samples of the optimal dimensionality sampling scheme.

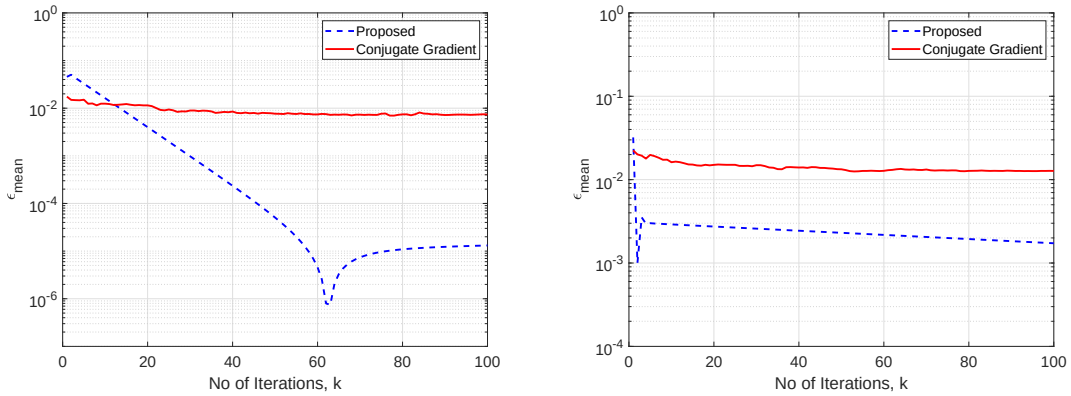

Figure 4.3: Mean extrapolation error ϵ_{mean} given in (4.24), for Experiment 1, for a random signal, band-limited at $L = 30$ and sampled over Ω_M with $M = 60$ for (a) $\theta_c = \pi/8$ and (b) $\theta_c = \pi/6$.

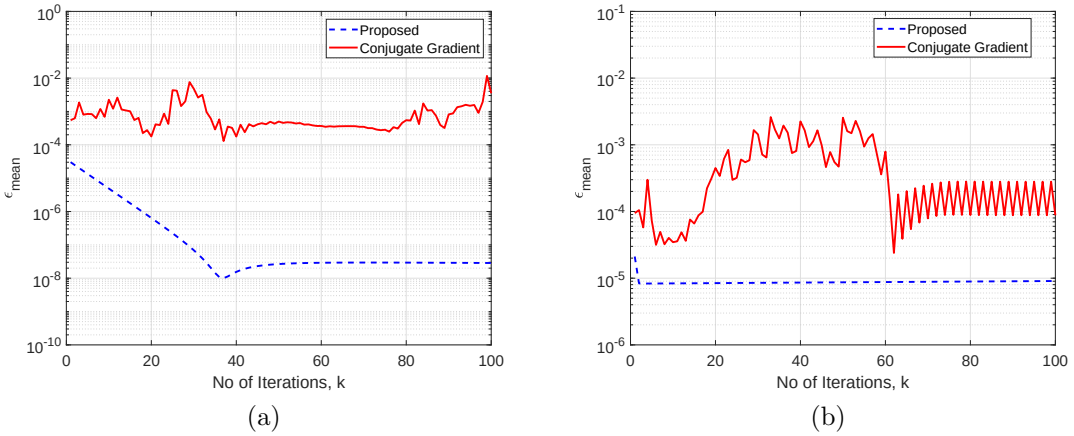

Figure 4.4: Mean extrapolation error ϵ_{mean} given in (4.24), for Experiment 2, for HRTF measurements over $\mathcal{R}$ with $\theta_c = \pi/6$ taken at (a) frequency $f_a = 5kHz$, effective band-limit $L = 15$ and $M = 40$ and (b) frequency f_r=10kHz, effective band-limit $L = 27$ and $M = 70$.

Chapter 5

Spatial Filtering for Applications in Acoustics

Spherical microphone arrays sample the sound field on the sphere in both space and time. The performance of spherical microphone arrays is typically limited by spatial aliasing which introduces side-lobes in the array beam pattern. In order to reduce the aliasing error, anti-aliasing filters, both ideal and spatially constrained, have been presented in the literature. In this chapter, we propose the design of spatially constrained filter which approximates an ideal anti-aliasing filter used in literature as a weighted sum of concentrated eigenfunctions obtained by solving the Slepian concentration problem on the sphere. Three performance parameters namely white noise gain (WNG), directivity index (DI) and processing loss are employed to compare the performance of proposed filter with the ideal filter. We propose a parameter-constrained filter design by maximizing WNG subject to constraints on the directivity index and processing loss of the proposed filter. We also propose a Slepian eigenfunction window which spatially truncates the ideal anti-aliasing filter used in literature to design a spatially constrained anti-aliasing filter. For windowing, we provide an illustration to show that the aliasing on the beam pattern is reduced by the use of the proposed anti-aliaisng filter and compare the results with the spatially constrained filters obtained by applying rectangular and Hamming windows.

The chapter is organised as follows. The problem under question is posed by reviewing literature in Section 5.1. Sampling scheme used, aliasing function and spatial filtering are reviewed in detail in Section 5.2. The proposed constrained filter designs are discussed in Section 5.3, where we also analyse the performance

of the filter based on WNG, DI and processing loss. Construction of the eigenfunction window and use of window functions in producing spatially constrained anti-aliasing filters are also discussed in detail. An array example is also provided to see the effect of aliasing and benefit of anti-aliasing filter. In Section 5.3 the research contributions are discussed.

5.1 Prior Work

In many real world applications, signals are naturally defined on the sphere. Particularly, in acoustics, spherical microphone arrays have been used for sound field analysis [115], sound field recordings [116], [117] and beamforming [118], [119]. In array processing, the spherical harmonics transform (SHT) [26] is used to examine the array performance [119]. At high frequencies, however, the array performance is limited by spatial aliasing [94] as side lobes are generated in the array beam pattern. In literature, there exists certain sampling schemes that provide aliasing free sampling for band-limited array measurements [95], however, acoustics sound fields such as measurements of sound pressure produced by plane waves are not band-limited on the sphere, giving rise to spatial aliasing at higher frequencies in practice.

In [94], a theoretical analysis of the spherical microphone reveals spatial aliasing as the significant factor impacting the performance of the antenna array. Several approaches to handle the spatial aliasing such as spatial anti-aliasing filters, using sensors with high directivity and reduction of spatial resolution at higher frequencies are presented in [120]. Anti-aliasing filters are deployed to improve the performance of the microphone arrays in [95], where spatial truncation is applied by first designing an ideal filter and then applying window functions on ideal filter in order to get spatially constrained anti-aliasing filters. In [128], a spatially constrained anti-aliasing filter based on spatial truncation of ideal filter by Slepian eigenfunction window obtained as a solution of Slepian concentration problem on the sphere [38], [34] is proposed.

5.2 Spatial Aliasing and Filtering on the sphere

5.2.1 Aliasing Function

Spatial aliasing affects the performance of spherical microphone arrays at high frequencies. In the literature, there are sampling schemes which provide aliasing free sampling for band-limited functions on the sphere. The sound pressure, however is not a band-limited function on sphere and hence measurements are affected by spatial aliasing at higher frequencies [117]. A detailed analysis of the nature of aliasing error in spherical microphone arrays is given in [94]. We adopt equiangular sampling scheme proposed in [59] as it requires least number of samples for exact computation of SHT defined in (2.5) of a band-limited signal on the sphere and use Ω_M to denote the set of equiangular sampling points taken on L iso-latitude rings. We sample the function (such as sound pressure) by N microphone arrays at positions Ω_j and its spherical coefficients are estimated by using (2.4) as

$$\begin{aligned}\big(\hat{f}\big)_\ell^m &= \sum_{j=1}^{N} \omega_j f(\theta_j,\phi_j)\overline{Y_\ell^m(\theta_j,\phi_j)},\\ &= \sum_{\ell'=0}^{\infty}\sum_{m'=-\ell'}^{\ell'} \big(f\big)_{\ell'}^{m'} \sum_{j=1}^{N} \omega_j Y_{\ell'}^{m'}(\theta'_j,\phi'_j)\overline{Y_\ell^m(\theta_j,\phi_j)},\end{aligned} \tag{5.1}$$

where ω_j are the weights which depend on the sampling scheme chosen and

$$\sum_{j=1}^{N} \omega_j Y_{\ell'}^{m'}(\theta'_j,\phi'_j)\overline{Y_\ell^m(\theta_j,\phi_j)} = \begin{cases}\delta_{\ell\ell'}\delta_{mm'} \ \ell,\ell' \leq L,\\ \epsilon_{\ell,m,\ell',m'} \ \ell \leq L < \ell',\end{cases} \tag{5.2}$$

where $\delta_{\ell\ell'}\delta_{mm'}$ represent the Kronecker delta function and $\epsilon_{\ell,m,\ell',m'}$ is the aliasing error.

5.2.2 Spatial Filtering and Ideal Anti-Aliasing Filter

Let f represents the sound pressure and the measurements are taken by rotating the microphone around the sphere. The spatial filtering can be obtained by using spherical correlation of pressure function f and a azimuthally symmetric spatial

filter, denoted by h as [71]

$$F(\alpha,\beta,\gamma) = \int_{\mathbb{S}^2} f(\Omega)\overline{\Lambda(\alpha,\beta,\gamma)h(\Omega)}\sin\theta d\theta d\phi, \tag{5.3}$$

where $\Omega \in \mathbb{S}^2$ represents the position on the sphere and $\Lambda(\alpha,\beta,\gamma)$ is the rotation operator in $SO(3)$, where α and γ represents rotation along the z-axis and β rotation along the y-axis. The spherical correlation in (5.3) can be re-written as [71]

$$F(\Lambda) = \sum_{\ell=0}^{\infty}\sum_{m=-\ell}^{\ell}\sum_{m'=-\ell}^{\ell} \big(f\big)_\ell^m \overline{\big(h\big)_\ell^m D_{\ell'}^{mm'}}(\Lambda), \tag{5.4}$$

where $D_\ell^{mm'}(\Lambda)$ are the wigner-D functions [26], which are basis functions for the fourier transform on the rotation group $SO(3)$. Because of azimuthal symmetry, h is invariant under rotation along the z-axis ($\gamma = 0$), that is, $\Lambda(\alpha,\beta,\gamma) = \Lambda(\alpha,\beta)$, F is mapped to $\mathbb{S}^2$ as

$$\begin{aligned} F(\alpha,\beta) &= \sum_{\ell=0}^{\infty}\sum_{m=-\ell}^{\ell} \big(f\big)_\ell^m \overline{\big(h\big)_\ell^0 D_\ell^{m0}}(\alpha,\beta,0), \\ &= \sum_{\ell=0}^{\infty}\sum_{m=-\ell}^{\ell} \big(f\big)_\ell^m \overline{\big(h\big)_\ell^0}\sqrt{\frac{4\pi}{2\ell+1}} Y_\ell^m(\alpha,\beta), \\ &= \sum_{\ell=0}^{\infty}\sum_{m=-\ell}^{\ell} \big(F\big)_\ell^m Y_\ell^m(\alpha,\beta), \end{aligned} \tag{5.5}$$

where

$$\big(F\big)_\ell^m = \big(f\big)_\ell^m \overline{\big(h\big)_\ell^0}\sqrt{\frac{4\pi}{2\ell+1}}. \tag{5.6}$$

It can be seen that aliasing error will diminish if such a filter h can be designed which has low or zero values at high frequencies in the harmonic domain. Following (5.5), an ideal anti-aliasing filter can be designed as

$$\big(h\big)_\ell^0 = \begin{cases} \sqrt{\frac{2\ell+1}{4\pi}} & 0 \le \ell \le L, \\ 0 & \ell > L, \end{cases} \tag{5.7}$$

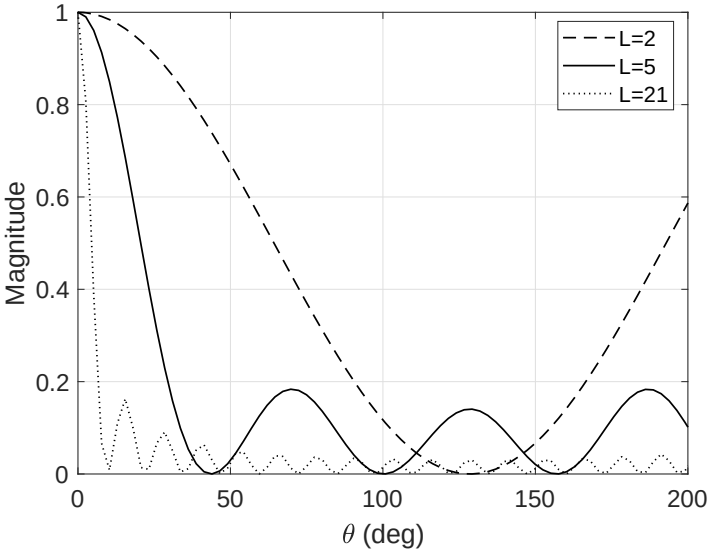

Figure 5.1: Magnitude of the ideal anti-aliasing filter as a function of elevation angle θ for various values of L.

and the spatial filter h can be obtained by taking inverse SHT as

$$\begin{aligned} h(\theta,\phi) &= \sum_{\ell=0}^{L} \sqrt{\frac{2\ell+1}{4\pi}} Y_\ell^0(\theta,\phi), \\ &= \frac{L}{4\pi(\cos\theta - 1)} [P_L(\cos\theta) - P_{L-1}(\cos\theta)]. \end{aligned} \tag{5.8}$$

Fig. 5.1 shows the magnitude of the ideal anti-aliasing filter as a function of the elevation angle θ , for different band-limits L , normalized to have a unity gain at $\theta = 0$.

5.3 Spatially Constrained Anti-aliasing Filter

Using an ideal filter means building such a microphone which has a sensing surface covering the entire sphere which is not cost efficient. Practically, we want such a sensor which is more spatially constrained and cover only a small section of the sphere. In order to experience minimum possible aliasing, it is desirable to design such a spatially constrained filter whose performance matches an ideal filter. In this chapter, we use eigenfunctions obtained by solving the Slepian concentration problem on the sphere [34, 38, 129] to design spatially constrained anti-aliasing filter. We also use the highest energy eigenfunction as window and obtain spatially

constrained anti-aliasing filter. The proposed eigenfunction filter and use of eigenfunction as window to design spatially constrained anti-aliasing filter are discussed in the following parts of this chapter.

5.3.1 Slepian Concentration Problem - Band-limited Eigenfunctions

As a solution of the eigenvalue problem associated with the Slepian concentration problem on the sphere [34,38,129], we obtain band-limited functions on the sphere that maximizes the ratio of the energy in the desired polar cap region (parameterized by angle θ_c and is defined as $R_{\theta_c} = \{(\theta, \phi) \in \mathbb{S}^2, 0 \leq \theta \leq \theta_c\}$) to the energy over the whole sphere. The azimuthally symmetric eigenfunctions g with band-limit L and energy concentration within the polar cap of angle θ_c are obtained as a solution of the following algebraic eigenvalue problem [34]

$$\mathbf{K}\mathbf{g} = \lambda\mathbf{g}, \tag{5.9}$$

where $\mathbf{g} = [(g)_0^0, (g)_1^0, \cdots, (g)_L^0]$ is a column vector of size $(L+1)$ containing spherical harmonic coefficients of zero order of g and $\mathbf{K}$ is real and symmetric matrix with dimensions $(L+1) \times (L+1)$ with entries given by

$$\begin{aligned} K_{\ell,\ell'} &= 2\pi \int_0^{\theta_c} Y_\ell^0(\theta, 0) Y_{\ell'}^0(\theta, 0) \sin\theta d\theta, \\ &= \frac{\sqrt{(2\ell+1)(2\ell'+1)}}{2} \sum_{n=\ell-\ell'}^{n=\ell+\ell'} \begin{pmatrix} \ell & n & \ell' \\ 0 & 0 & 0 \end{pmatrix}^2 \\ &\times [P_{n-1}(\cos\theta) - P_{n+1}(\cos\theta)], \end{aligned} \tag{5.10}$$

where the term in the parenthesis are Wigner-3j symbols which are required to be evaluated for the computation of $\mathbf{K}$. The eigenvalue problem in (5.9) can also be solved by eigen decomposition of a matrix $\mathbf{S}$ of size $(L+1) \times (L+1)$ commuting it with $\mathbf{K}$, that is, $\mathbf{KS} = \mathbf{SK}$. $\mathbf{S}$ is a tridiagonal matrix having the following entries [34, 129]

$$S_{\ell,\ell+1} = \frac{(\ell+1)(\ell(\ell+2) - (L)(L+2))}{\sqrt{(2\ell+1)(2\ell+3)}},$$

$$S_{\ell,\ell} = -\ell(\ell+1)\cos(\theta_c), \quad S_{\ell,\ell'} = 0. \tag{5.11}$$

The eigen decomposition of $\mathbf{S}$ gives $L+1$ eigenvectors of the form $\mathbf{g}_\alpha$. Since the eigenvalue problem in (5.9) is formulated in the spectral domain, each eigenvector represents the spectral domain (spherical harmonic coefficients) of the associated azimuthally symmetric eigenfunction $g_\alpha(\theta)$ in the spatial domain. We have the following orthonormality and orthogonality relations for the eigenfunctions

$$\mathbf{g}_\alpha^{\prime\mathbf{T}}\mathbf{g}_\alpha = \langle g_\alpha, g'_\alpha \rangle = \delta_{\alpha\alpha'}, \quad \mathbf{g}_\alpha^{\prime\mathbf{T}}\mathbf{K}\mathbf{g}_\alpha = \lambda\delta_{\alpha\alpha'}, \tag{5.12}$$

where $(\cdot)^T$ represents the transpose operation and $0 \leq \lambda_\alpha \leq 1$ associated with the eigenfunction represents a measure of energy concentration of the eigenfunction in the polar cap region R_{θ_c}.

5.3.1.1 Proposed Filter Design

In order to design the proposed spatially constrained anti-aliasing filter, we take the most N_t concentrated eigenfunctions obtain as a solution of Slepian concentration problem for band-limit L and polar cap region R_{θ_c}. We note that the sum of eigenvalues $N_t = \lceil \frac{(L+1)\theta_c}{\pi} \rceil$ serves as a good measure to approximate the number of concentrated eigenfunctions [80]. We propose to design the band-limited filter $\tilde{h}$, parameterized by band-limit L and θ_c defining the polar cap region, as a weighted sum of N_t eigenfunctions. We formulate this construction in the harmonic domain as

$$\big(\tilde{h}\big)_\ell^0 = \beta_1\big(\mathbf{g_1}\big)_\ell^0 + \beta_2\big(\mathbf{g_2}\big)_\ell^0 + \cdots + \beta_{N_t}\big(\mathbf{g_{N_t}}\big)_\ell^0, \tag{5.13}$$

where β represents the corresponding weights and are evaluated such that the proposed filter approximates the ideal filter in the least-squares sense. Since we use the eigenfunctions that are characterized by both L and θ_c, we note that the proposed filter depends on L and θ_c, that is, $\tilde{h} = \tilde{h}(L, \theta_c)$. The rationale behind the proposed construction is to use spatially concentrated eigenfunctions to approximate the band-limited filter and enabling the control on the spatial resolution θ_c of the filter. We note that we recover the ideal filter, that is, $\tilde{h}(L, \pi) = h$, when $\theta_c = \pi$ (the polar cap region is whole sphere $R_\pi = \mathbb{S}^2$).

5.3.1.2 Parameter constrained Filter Design and Analysis

Using the proposed construction of the filter, we also present a parameter constrained filter design taking into account the array performance parameters. The performance parameters under study are white noise gain (WNG), directivity index (DI) [130] and processing loss [131]. To maintain consistency in the analysis, we normalise the harmonic coefficients of both the ideal and the proposed filter to have unit energy, that is, $||h|| = ||\tilde{h}|| = 1$. Here we define the performance parameters and compare the performance of the ideal and proposed filter based on these parameters under certain settings. Later, we apply constraints on the proposed spatially constrained anti-aliasing filter and design an optimal parameter-constrained filter that maximizes WNG.

White Noise Gain (WNG): WNG is a measure of the improvement in signal to noise ratio at the array output compared to the array input. Assume an array of band-limit L with $P \geq L^2$ microphones, the WNG with the array looking at the arrival direction (θ_i, ϕ_i) of the plane wave can be written as [130]

$$WNG = \frac{P}{4\pi^2} \frac{|\sum_{\ell=0}^{L} c_\ell \ (2\ell+1)|^2}{\sum_{\ell=0}^{L} \frac{|c_\ell|^2}{|b_\ell|^2} \ (2\ell+1)}, \tag{5.14}$$

where c_ℓ is equal to $\overline{(\tilde{h})_\ell^0}\sqrt{\frac{4\pi}{2\ell+1}}$ and b_ℓ for the rigid sphere is calculated from [94].

Directivity Index (DI): The directivity index (DI) gives a measure to improved directivity of the array compared to an omnidirectional microphone [130] and can be written as the ratio of the array output in the look direction and the array output integrated over all directions. Assume that the array look direction is , (θ_i, ϕ_i)=(0,0), that is, the z-axis direction, and the directive index can be written as

$$DI = \frac{|\sum_{\ell=0}^{L} c_\ell \ (2\ell+1)|^2}{\sum_{\ell=0}^{L} |c_\ell|^2 \ (2\ell+1)}. \tag{5.15}$$

Processing Loss (γ): A certain amount of the signal is lost when a field is filtered.

We quantify such processing loss, γ, as

$$\gamma = 1 - \zeta, \quad \zeta = \sum_{\ell}^{L-1} \frac{c_\ell^2}{L}, \tag{5.16}$$

where ζ is the damping factor which provide information about the extent of dampness in amplitude in the filtering.

Analysis — Proposed Filter

Based on three performance parameters defined previously, we compare the performance of the proposed spatially constrained filter with the ideal filter under two experimental settings in Fig. 5.2 and Fig. 5.3. Fig. 5.2 compares the performance of the ideal filter and the proposed filter designed for band-limit $L = 20$ and polar cap regions, where θ_c is chosen in the range $\pi/18 \leq \theta_c \leq 2\pi/3$. It can be seen that WNG of the proposed filter is better than the ideal filter for selected values of θ_c. The directivity index of the proposed filter approaches the value attained by the ideal filter as θ_c increases from 0 to π. Processing loss (γ) of the ideal filter is zero and it can be seen that processing loss approaches the ideal filter for some values of θ_c. To analyse the impact of changing band-limits of the filter while keeping the same polar cap region in the design, we compare the performance parameters in Fig. 5.3 for $\theta_c = \pi/4$ and band-limit $5 \leq L \leq 40$.

Constrained Filter Design

In constrained design of the filter, $\tilde{h}(L, \theta_c)$, we find θ_c by formulating the following optimization problem

$$\begin{aligned} \underset{\tilde{h}}{\text{maximize}} \quad & WNG \\ \text{subject to} \quad & \zeta \geq 0.99, \\ & DI = \delta_L, \end{aligned} \tag{5.17}$$

where δ_L denotes the directivity index of ideal filter for a band-limit, L. Since the optimization problem in (5.17) is intractable, we solve it numerically and choose

such θ_c for which

$$|\sum_{\ell=0}^{L-1} c_{\ell_{proposed}}\ (2\ell+1)|^2 > (0.99L),$$

$$\delta_L\ \sum_{\ell=0}^{L-1} |c_{\ell_{proposed}}|^2\ (2\ell+1) > |\sum_{\ell=0}^{L-1} c_{\ell ideal}\ (2\ell+1)|^2. \tag{5.18}$$

where we put constraints on the processing loss and take the directivity index of the proposed filter to be equal to that of the ideal filter as our design requirements are limited to maximizing the WNG. After putting constraints and optimizing WNG, we have a filter which has a better WNG compared to the spatially unconstrained ideal filter for any band-limit L and the optimized polar cap, $\hat{\theta}_c$ as shown in Fig. 5.4.

5.3.2 Spatially Constrained Anti-Aliasing Filters — Windowing

Another way to design a spatially constrained anti-aliaisng filter is to spatially truncate the ideal filter by applying a window of width θ_c. In the following, we will study three type of windows namely rectangular window, Hamming window and the Slepian eigenfunction window [95, 129].

5.3.2.1 Rectangular Window

The rectangular window performs spectral truncation upto a certain band-limit, L and its spectral form is given by

$$\big(h\big)_\ell^0 = \begin{cases} 1 & 0 \leq \ell \leq L, \\ 0 & \text{otherwise.} \end{cases} \tag{5.19}$$

5.3.2.2 Hamming Window

The Hamming window in Eucledian domain [132] is defined in terms of the width of the main lobe θ_c as follows

$$h(\theta, \theta_c) = \begin{cases} 0.54 + 0.46\cos(\pi\theta/\theta_c) & 0 \leq \theta \leq \theta_c, \\ 0 & \text{otherwise.} \end{cases} \tag{5.20}$$

5.3.2.3 Slepian Eigenfunction Window

The eigen decomposition of $\mathbf{S}$ gives L+1 eigen vectors of the form $\mathbf{g}_\alpha$ and one with the largest eigenvalue gives the spectral domain representation, $(h)_\ell^0 = g_\ell^0$ of desired eigenfunction window, that is for $N_t = 1$. For $L = 5$, it is observed from Fig. 5.1 that ideal filter designed in (5.8) has significant values below the first zero at $\theta = 44°$. In order to design spatially constrained filter, we apply rectangular, Hamming and proposed eigenfunction windows of width $\theta_c = 44°$ to the ideal filter in (5.8). Fig. 5.5 shows the magnitude of the spherical harmonic coefficients of these spatially constrained windows plotted against degrees ℓ and for comparison the coefficients of ideal filter are also plotted. It can be seen that eigenfunction windows out-performs rectangular and Hamming windows attenuating most of the higher frequency harmonics above $\ell = L$. Note that increasing the window width will further improve the attenuation and reduce the overall aliasing error.

Array Processing Analysis — Windowing

In this example, we consider a spherical microphone array which samples the sound pressure, $p(kr, \Omega)$ of a plane wave sound field on the sphere, where k is the wave number and r is the radius of the rigid sphere [130]. A single unit amplitude plane wave is assumed to be arriving from direction $\Omega_o = (\pi/2, 0)$ and the plane wave decomposition is analysed in directions, $\Omega_t \in (\pi/2, [0, 2\pi])$. In array processing, aliasing errors are produced at high frequencies, particularly for $kr > 7$ [95]. In this example, significant aliasing errors are expected as a fourth order array with frequency $kr = 7$ is analysed. The array output for a practical array of order $\ell \leq L$ is calculated as

$$\begin{aligned} y &= \int_{\mathbb{S}^2} p(kr, \Omega)\overline{w(\Omega)}\, \sin\theta \, d\theta \, d\phi, \\ &= \sum_{\ell=0}^{L-1} \sum_{m=-\ell}^{\ell} (p)_\ell^m(kr)\overline{w_\ell^m(kr)}, \end{aligned} \tag{5.21}$$

where $\big(p\big)_\ell^m(kr) = b_\ell(kr)Y_\ell^m(\Omega_o)$ are the estimated spherical harmonic coefficients of sound pressure, p and $\overline{w_\ell^m(kr,\Omega_t)} = Y_\ell^m(\Omega_t)/b_\ell(kr)$ are the Fourier coefficients of plane wave decomposition weights, w. Note that b_ℓ for the rigid sphere is calculated from [94]. The estimated pressure coefficients include aliasing and to remove the aliasing error, the coefficients are filtered by anti-aliasing filters described in section III-C using (5.6). The array directivity for various array look directions Ω_t is then calculated as

$$y(\Omega_t) = \sum_{\ell=0}^{L-1}\sum_{m=-\ell}^{\ell} \big(\tilde{p}\big)_\ell^m(kr)\overline{w_\ell^m(kr,\Omega_t)}, \tag{5.22}$$

where $\big(\tilde{p}\big)_\ell^m(kr)$ are the estimated pressure coefficients obtained after low pass effect of anti-aliasing filters. In Fig. 5.6, we plot the array directivity for five different cases in form of polar plots. Fig. 5.6(a) shows array directivity when there is no aliasing error, that is, $\big(\tilde{p}\big)_\ell^m = \big(p\big)_\ell^m$. Directivity including aliasing error without using any anti-aliasing filter is shown in Fig. 5.6(b) where it is seen that there is a significant increase in the sidelobes due to the spatial aliasing introduced by significant high frequency harmonics. Fig. 5.6(c), Fig. 5.6(d) and Fig. 5.6(e) shows array directivity pattern when we perform spatial truncation of the ideal filter by using rectangular window, Hamming window and eigenfunction window of width $\theta_o = 44°$, respectively. It is observed from the polar plots obtained by applying sptaially constrained anti-alisaing filters that there is a significant reduction in the sidelobes introduced by aliasing errors in Fig. 5.6(b). Also, the spatially constrained anti-aliasing filter obtained by applying eigenfunction window provides higher attenuation and better results than the rectangular and Hamming windows based spatially constrained anti-aliasing filters.

5.4 Summary of Research Contribution

In this chapter, we design a spatially constrained anti-aliasing filter as a weighted sum of band-limited spatially (optimal) concentrated functions. Given the spatial constraints, the proposed filter approximates an ideal low-pass filter on the sphere in the least-squares sense. The weights are applied to the band-limited eigenvectors or eigenfunctions obtained by the solution of the Slepian concentration problem on the sphere. The filter obtained as a result of this multiple regression depends on

the value of band-limit, L and maximum concentration region known as polar cap parameterized by its central angle θ_c. We choose $N_t < L + 1$ maximally concentrated eigenvectors where we choose N_t such that we only use spatially concentrated functions in the design. We examine the performance of the proposed filter by measuring parameters like white noise gain (WNG), directivity index (DI)and processing loss (γ), and compare the results with the ideal filter. We compare the performance of two filters first by varying polar cap of angle θ_c keeping the band-limit L constant and then varying band-limits keeping the polar cap region constant. By putting constraints on the directivity index and processing loss, we propose a parameter-constrained filter design and choose θ_c such that white noise gain of the proposed filter is maximized. Our analysis show that based on the selected design requirements, the proposed spatially constrained anti-aliasing filter surpasses the ideal filter in performance. We also propose to use suitably selected Slepian eigenfunction window ($N_t = 1$) for spatial truncation in order to get spatially constrained anti-aliasing filter from ideal filter and compare the results with the rectangular and Hamming windows proposed in literature. Our analysis shows that for the reduction of side lobes produced by spatial aliasing error, anti-aliasing filter spatially truncated by the proposed eigenfunction window is a better choice than the rectangular and Hamming windows.

Addressing Q6 posed in Section 1.2.1:

- We have designed a spatially constrained anti-aliasing filter by spatially truncating ideal filter applying Slepian eigenfunction window of certain width $\theta_c = 44^\circ$ and compare the result using array processing example with the rectangular and Hamming windows proposed in literature. Our analysis show that the anti-aliasing filter design using the proposed Slepian eigenfunction window reduces the side lobes significantly as compared to other filters.

Addressing Q7 posed in Section 1.2.1:

- We design a spatially constrained anti-aliasing filter as a weighted sum of band-limited spatially (optimal) concentrated functions. Given the spatial constraints, the proposed filter approximates an ideal low-pass filter on the sphere in the least-squares sense. We choose $N_t < L + 1$ maximally concentrated eigenvectors where we choose N_t such that we only use spatially concentrated functions in the design. By putting constraints on the directivity index and processing loss, we propose a parameter-constrained filter

design and choose θ_c such that white noise gain of the proposed filter is maximized. Our analysis show that based on the selected design requirements, the proposed spatially constrained anti-aliasing filter surpasses the ideal filter in performance.

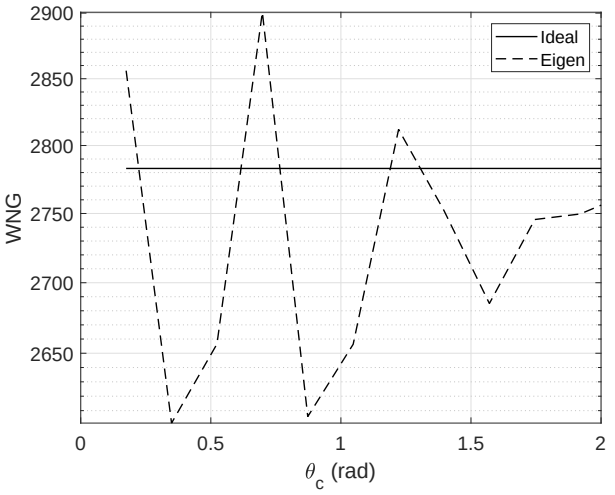

(a)

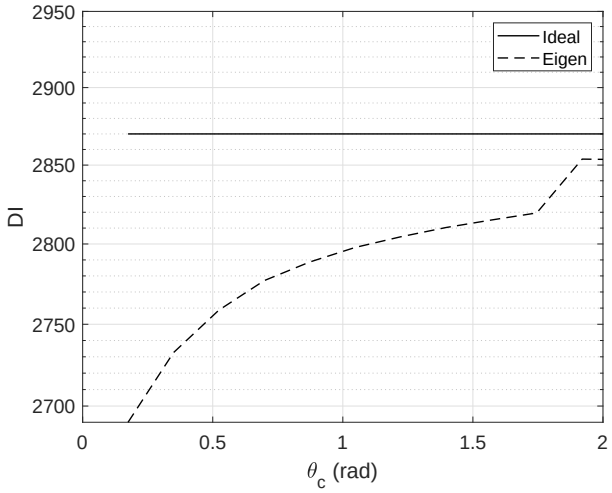

(b)

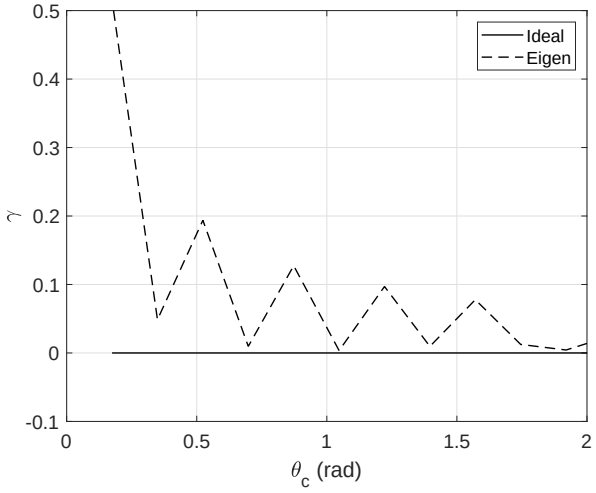

(c)

Figure 5.2: Performance parameters, (a) white noise gain (WNG), (b) directivity index (DI) and (c) processing loss (γ), of ideal and proposed spatially constrained filter having fixed band-limit, $L = 20$ and plotted for random polar cap regions of angle, $\pi/18 \leq \theta_c \leq 2\pi/3$.

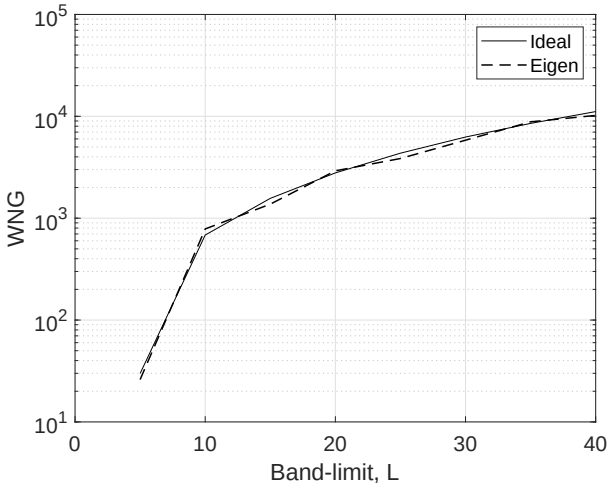

(a)

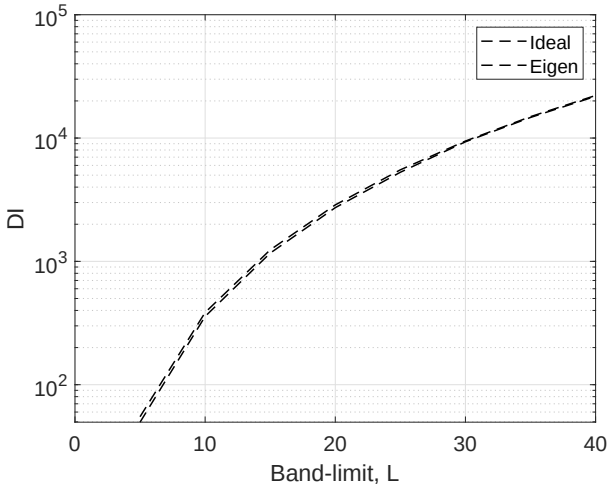

(b)

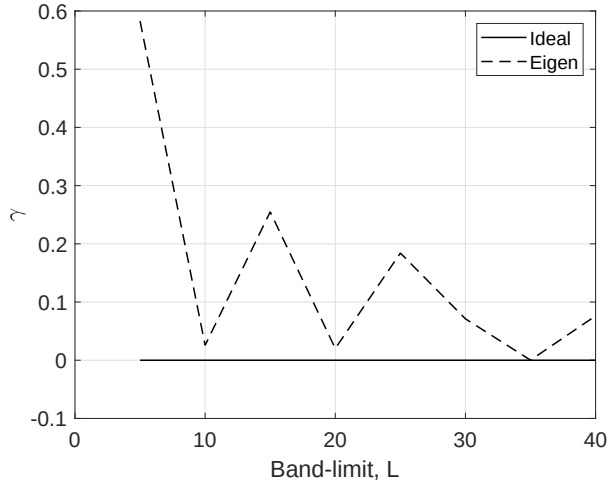

(c)

Figure 5.3: Performance parameters, (a) white noise gain (WNG), (b) directivity index (DI) and (c) processing loss (γ), of ideal and proposed spatially constrained for band-limit, $5 \leq L \leq 40$ and $\theta_c = \pi/4$.

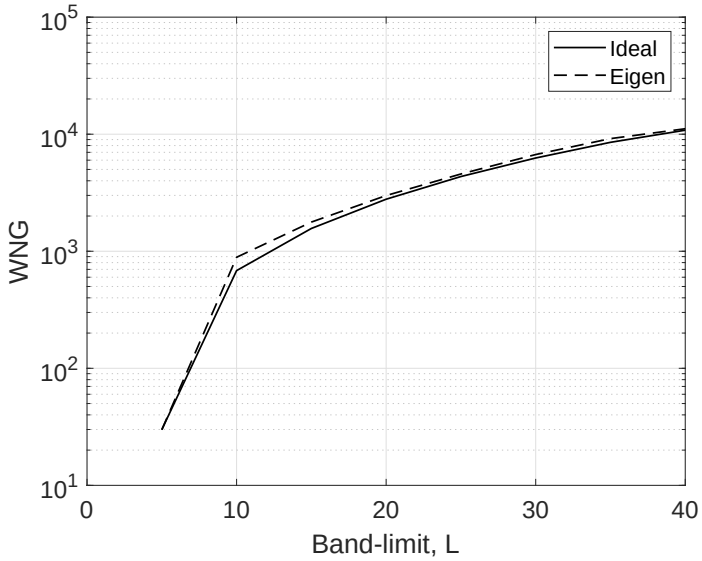

Figure 5.4: The optimized WNG of the proposed eigen filter against ideal filter, plotted for chosen optimized polar cap, $(\hat{\theta}_c)$ for $5 \leq L \leq 40$.

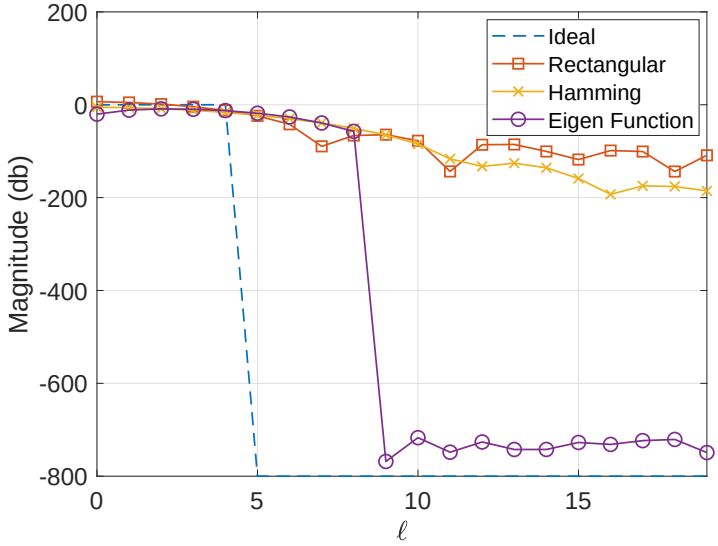

Figure 5.5: Magnitude of ideal anti-aliasing filter for $L = 5$ and spatially constrained filters using rectangular window, Hamming window and proposed Slepian eigenfunction window of width $\theta_c = 44°$.

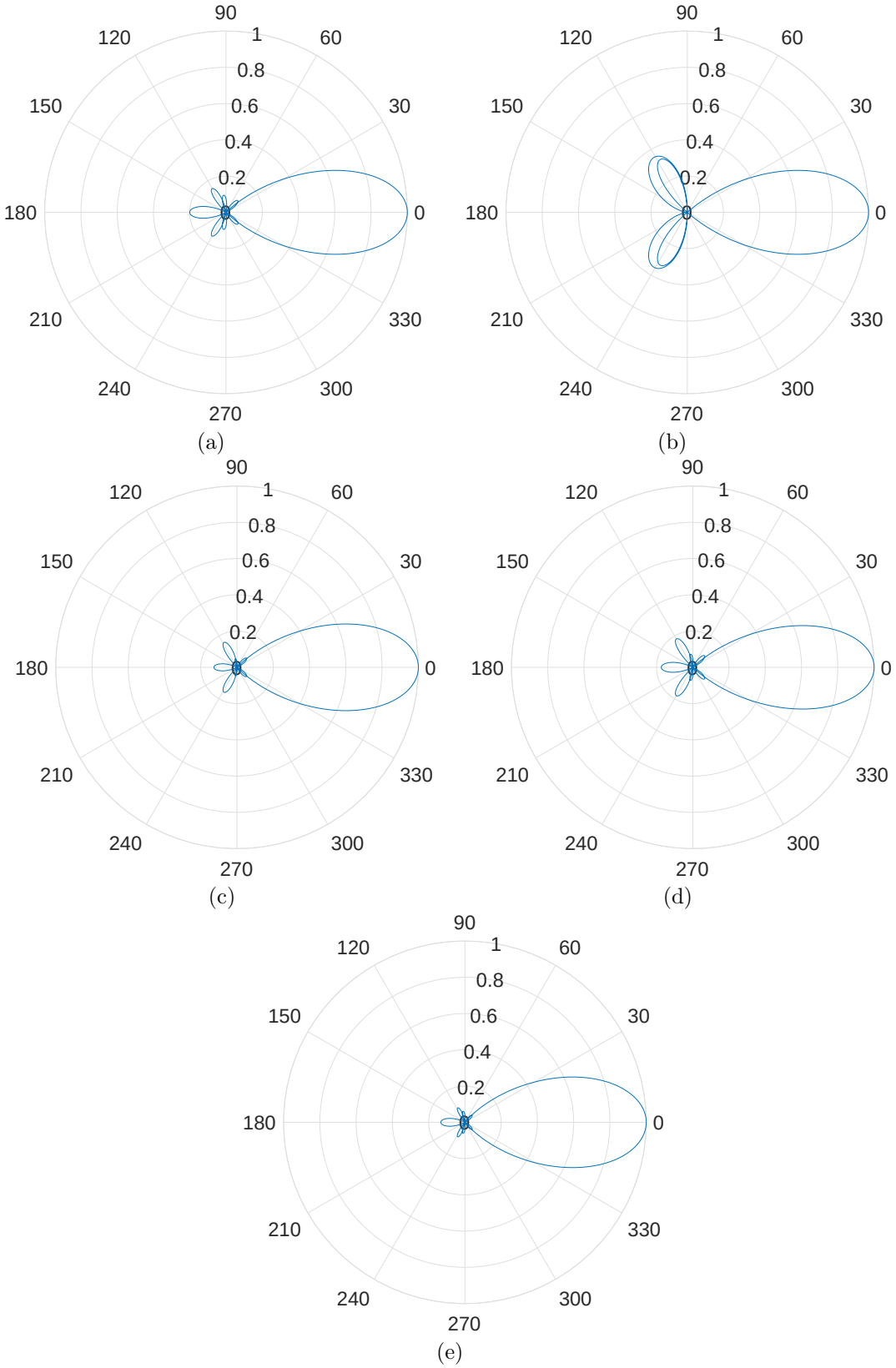

Figure 5.6: Magnitude of the fourth order plane wave decomposition array directivity with (a) ideal sampling, no aliasing error (b) sampling without anti-aliasing filter (c) sampling with rectangular window spatially constrained anti-aliasing filter (d) sampling with Hamming window spatially constrained anti-aliasing filter (e) sampling with proposed Slepian eigenfunction window spatially constrained anti-aliasing filter.

Chapter 6

Conclusions and Future Research Directions

In this chapter, general conclusions have been drawn from the thesis. The specific contribution of each chapter and its summary can be found at the end of each chapter, thus are not repeated here. We also outline some future research directions arising from this work.

6.1 Conclusions

The main focus of this thesis is the extension of existing spherical signal processing techniques in order to achieve accurate reconstruction of the signals on the sphere and use the current techniques to devise methods which are useful in practical applications.

In Chapter 3, we proposed an optimal-dimensionality sampling scheme for the accurate reconstruction of band-limited spin-s functions on the sphere and developed a method to compute s-SHT associated with the proposed sampling scheme. We placed samples such that the system under consideration remains well-conditioned. We showed that the accurate computation of s-SHT can be achieved by using optimal $L^2 - s^2$ samples. In order to improve the accuracy, a multi-pass s-SHT algorithm has been proposed. We show that the proposed sampling scheme is superior to existing schemes in terms of geometrical properties such as geodesic distance, mesh norm and mesh ratio.

In Chapter 4, we discuss two problems regarding reconstruction of the signals on the sphere. In the first part, we present the generalized iterative residual fit-

ting (IRF) method for the computation of the spherical harmonic transform (SHT) of band-limited signals on the sphere. In order to improve the accuracy of the transform, we have also presented a multi-pass IRF scheme and analysed it for different sampling schemes and for four different size partitions. For different partitions and different sampling distributions, we have analysed the residual (error) and demonstrated the convergence of the residual to zero. In the second part of that chapter, we develop an iterative algorithm for extrapolation of band-limited signals on the sphere from limited or incomplete measurements. Existing schemes focus on the use of the band-limited property of the signal, that is, the signal extrapolation is carried out iteratively by forcing the harmonic coefficients outside the band-limit of the signal to zero at each iteration. In the proposed algorithm, we do not only force the harmonic coefficients to zero but also use these to improve the extrapolation of the signal over the inaccessible region at each iteration. The numerical analysis show that the proposed algorithm enables more accurate extrapolation than the existing methods.

In Chapter 5, we design a spatially constrained anti-aliasing filter as a weighted sum of band-limited spatially (optimal) concentrated functions. Given the spatial constraints, the proposed filter approximates an ideal low-pass filter on the sphere in the least-squares sense. We choose $N_t < L + 1$ maximally concentrated eigenvectors where we choose N_t such that we only use spatially concentrated functions in the design. We examine the performance of the proposed filter by measuring parameters like white noise gain (WNG), directivity index (DI) and processing loss (γ), and compare the results with the ideal filter. By putting constraints on the directivity index and processing loss, we propose a parameter-constrained filter design and choose θ_c such that white noise gain of the proposed filter is maximized. Our analysis show that based on the selected design requirements, the proposed spatially constrained anti-aliasing filter surpasses the ideal filter in performance. We also propose to use suitably selected Slepian eigenfunction window ($N_t = 1$) for spatial truncation in order to get spatially constrained anti-aliasing filter from ideal filter. Our analysis shows that for the reduction of side lobes produced by spatial aliasing error, anti-aliasing filter spatially truncated by the proposed eigenfunction window is a better choice than the rectangular and Hamming windows.

6.2 Future Research Directions

A number of interesting future research directions arise from the work presented in this thesis.

- In Chapter 3, the proposed sampling scheme attain an optimal number of samples and have the lowest attainable reconstruction error. We have also observed the variation of reconstruction error by varying the integer spin, s. As integer spin, s increases, the condition number of the inverting matrix ${}_sD_m$ becomes very large and hence the systems becomes ill-conditioned. Future research should consider pre-conditioning techniques in order to maintain the well-conditioned state of the under determined system.

- Signals in some real world applications are not band-limited and hence future research related to sampling schemes on the sphere should consider signals that are not band-limited. We need to devise methods and model sampling schemes with more relaxed assumptions.

- Geometrical properties give us an insight into the nature of the distribution of the points of a sampling scheme. Future work should involve taking samples considering perfect geometrical distribution in mind, for example, samples on a sphere can be taken by keeping the minimum geodesic distance the same between the two points on the sphere.

- In Chapter 4, we analysed multi-pass IRF by dividing the subspace into different partitions. We observe that the residual error converges to zero faster for some partitions. Future research work should analyse this feature.

- Following the work done in Chapter 4, we can devise similar methods to achieve interpolation or extrapolation on the sphere. One such example is sinc interpolation in the Euclidian domian. To the best of our knowledge, sinc interpolation algorithm has not been devised in spherical settings.

- In acoustics, work can be done in the spherical settings, for example we should devise methods to improve the complexity ($O(L^6)$) of the algorithms used to detect the direction of arrival (DOA) from a source.

Bibliography

[1] M. K. Chung, K. J. Worsley, B. M. Nacewicz, K. M. Dalton, and R. J. Davidson, "General multivariate linear modeling of surface shapes using surfstat," *NeuroImage*, vol. 53, no. 2, pp. 491–505, 2010.

[2] P. Yu, P. E. Grant, Q. Yuan, H. Xiao, F. Segonne, R. Pienaar, E. Busa, J. Pacheco, N. Makris, R. L. Buckner, P. Golland, and B. Fischl, "Cortical surface shape analysis based on spherical wavelets," *IEEE Trans. Med. Imag.*, vol. 26, no. 4, pp. 582–597, Apr. 2007.

[3] M. K. Chung, Kim M. Dalton, Li Shen, Alan C. Evans, and Richard J. Davidson, "Weighted fourier series representation and its application to quantifying the amount of gray matter," *IEEE Trans. Med. Imag.*, vol. 26, no. 4, pp. 566–581, Apr. 2007.

[4] M. Simons, S. C. Solomon, and B. H. Hager, "Localization of gravity and topography: constraints on the tectonics and mantle dynamics of Venus," *Geophys. J. Int.*, vol. 131, no. 1, pp. 24–44, Oct. 1997.

[5] M. A. Wieczorek and F. J. Simons, "Localized spectral analysis on the sphere," *Geophys. J. Int.*, vol. 162, no. 3, pp. 655–675, May 2005.

[6] P. Audet, "Directional wavelet analysis on the sphere: Application to gravity and topography of the terrestrial planets," *J. Geophys. Res.*, vol. 116, Feb. 2011.

[7] A. Amirbekyan, V. Michel, and F. J. Simons, "Parametrizing surface wave tomographic models with harmonic spherical splines," *Geophys. J. Int.l*, vol. 174, no. 2, pp. 617–628, Jan. 2008.

[8] R. Ng, R. Ramamoorthi, and P. Hanrahan, "Triple product wavelet integrals for all-frequency relighting," *ACM Trans. Graph.*, vol. 23, no. 3, pp. 477–487, Aug. 2004.

[9] P. Schröder and W. Sweldens, "Spherical wavelets: Efficiently representing functions on a sphere," in *Wavelets in the Geosciences*, Roland Klees and Roger Haagmans, Eds., vol. 90 of *Lecture Notes in Earth Sciences*, pp. 158–188. Springer, Berlin Heidelberg, 2000, (Reprinted from Computer Graphics Proceedings, 1995, 161-172, ACM Siggraph.).

[10] C. H. Brechbühler, G. Gerig, and O. Kübler, "Parametrization of closed surfaces for 3-D shape description," *Computer Vision and Image Understanding*, vol. 61, no. 2, pp. 154–170, Mar. 1995.

[11] C. Han, B. Sun, R. Ramamoorthi, and E. Grinspun, "Frequency domain normal map filtering," *ACM Trans. on Graphics*, vol. 26, no. 3, pp. 28:1–28:12, July 2007.

[12] Wen Zhang, Mengqiu Zhang, Rodney A Kennedy, and Thushara D Abhayapala, "On high resolution head-related transfer function measurements: An efficient sampling scheme," *IEEE/ACM Trans. Audio, Speech, Language Process.*, vol. 20, no. 2, pp. 575–584, Dec. 2012.

[13] D. Colton and R. Kress, *Inverse Acoustic and Electromagnetic Scattering Theory*, Springer-Verlag, Berlin, second edition, 1998.

[14] C. Armitage and B. D. Wandelt, "Deconvolution map-making for cosmic microwave background observations," *Phys. Rev. D*, vol. 70, no. 12, pp. 123007:1–123007:7, Dec. 2004.

[15] K. W. Ng, "Full-sky correlation functions for CMB experiments with asymmetric window functions," *Phys. Rev. D*, vol. 71, no. 8, pp. 083009:1–083009:9, Apr. 2005.

[16] J. D. McEwen, P. Vielva, Y. Wiaux, R. B. Barreiro, L. Cayón, M. P. Hobson, A. N. Lasenby, E. Martínez-González, and J. L. Sanz, "Cosmological applications of a wavelet analysis on the sphere," *J. Fourier Anal. and Appl.*, vol. 13, no. 4, pp. 495–510, Aug. 2007.

[17] J. D. McEwen, M. P. Hobson, A. N. Lasenby, and D. J. Mortlock, "A high-significance detection of non-Gaussianity in the Wilkinson Microwave Anisotropy Probe 1-yr data using directional spherical wavelets," *Mon. Not. R. Astron. Soc.*, vol. 359, no. 4, pp. 1583–1596, 2005.

[18] J. L. Starck, Y. Moudden, P. Abrial, and M. Nguyen, "Wavelets, ridgelets and curvelets on the sphere," *Astron. & Astrophys.*, vol. 446, no. 3, pp. 1191–1204, Feb. 2006.

[19] Y. Wiaux, L. Jacques, and P. Vandergheynst, "Correspondence principle between spherical and Euclidean wavelets," *Astrophys. J.*, vol. 632, no. 1, pp. 15–28, Oct. 2005.

[20] D. N. Spergel, R. Bean, O. Doré, M. R. Nolta, C. L. Bennett, J. Dunkley, G. Hinshaw, N. Jarosik, E. Komatsu, L. Page, H. V. Peiris, L. Verde, M. Halpern, R. S. Hill, A. Kogut, M. Limon, S. S. Meyer, N. Odegard, G. S. Tucker, J. L. Weiland, E. Wollack, and E. L. Wright, "Three-year Wilkinson Microwave Anisotropy Probe (WMAP) observations: Implications for cosmology," *The Astrophysical Journal Supplement Series*, vol. 170, no. 2, pp. 377–408, 2007.

[21] Y. Fantaye, C. Baccigalupi, S.M. Leach, and A.P.S. Yadav, "Cmb lensing reconstruction in the presence of diffuse polarized foregrounds," *J. Cosmol. Astropart. Phys.*, vol. 2012, no. 12, pp. 017, July 2012.

[22] N. Jarosik, C. L. Bennett, J. Dunkley, B. Gold, M. R. Greason, M. Halpern, R. S. Hill, G. Hinshaw, A. Kogut, E. Komatsu, D. Larson, M. Limon, S. S. Meyer, M. R. Nolta, N. Odegard, L. Page, K. M. Smith, D.N. Spergel, G. S. Tucker, J. L. Weiland, E. Wollack, and E. L. Wright, "Seven-year Wilkinson Microwave Anisotropy Probe (WMAP) observations: Sky maps, systematic errors, and basic results," *Astrophys. J.*, vol. 192, no. 2, pp. 1–14, 2011.

[23] D. B. Ward, R. A. Kennedy, and R. C. Williamson, "Theory and design of broadband sensor arrays with frequency invariant far-field beam patterns," *J. Acoust. Soc. Am.*, vol. 97, no. 2, pp. 1023–1034, Feb. 1995.

[24] T. S. Pollock, T. D. Abhayapala, and R. A. Kennedy, "Introducing space into MIMO capacity calculations," *J. Telecommun. Syst.*, vol. 24, no. 2, pp. 415–436, Oct. 2003.

[25] Y. F. Alem, Z. Khalid, and R. A. Kennedy, "3D spatial fading correlation for uniform angle of arrival distribution," *IEEE Commun. Lett.*, vol. 19, pp. 1073–1076, June 2015.

[26] R. A. Kennedy and P. Sadeghi, *Hilbert Space Methods in Signal Processing*, Cambridge University Press, Cambridge, UK, March 2013.

[27] M. A. Wieczorek and F. J. Simons, "Minimum variance multitaper spectral estimation on the sphere," *J. Fourier Anal. Appl.*, vol. 13, no. 6, pp. 665–692, 2007.

[28] J. P. Antoine and P. Vandergheynst, "Wavelets on the 2-sphere: A group-theoretical approach," *Appl. Comput. Harmon. Anal.*, vol. 7, no. 3, pp. 262–291, 1999.

[29] D. Marinucci, D. Pietrobon, A. Balbi, P. Baldi, P. Cabella, G. Kerkyacharian, P. Natoli, D. Picard, and N. Vittorio, "Spherical needlets for cosmic microwave background data analysis," *Mon. Not. R. Astron. Soc.*, vol. 383, no. 2, pp. 539–545, 2008.

[30] J. D. McEwen, M. P. Hobson, and A. N. Lasenby, "A directional continuous wavelet transform on the sphere," *Arxiv preprint astro-ph/0609159*, 2006.

[31] J. D. McEwen, M. P. Hobson, D. J. Mortlock, and A. N. Lasenby, "Fast directional continuous spherical wavelet transform algorithms," *IEEE Trans. Signal Process.*, vol. 55, no. 2, pp. 520–529, Feb. 2007.

[32] J. D. McEwen, M. P. Hobson, and A. N. Lasenby, "Optimal filters on the sphere," *IEEE Trans. Signal Process.*, vol. 56, no. 8, pp. 3813–3823, Aug. 2008.

[33] R. Kakarala and P. Ogunbona, "A phase-sensitive approach to filtering on the sphere," *IEEE Trans. Signal Process.*, vol. 60, no. 12, pp. 6330–6339, Dec. 2012.

[34] F. J. Simons, F. A. Dahlen, and M. A. Wieczorek, "Spatiospectral concentration on a sphere," *SIAM Rev.*, vol. 48, no. 3, pp. 504–536, 2006.

[35] Y. Wiaux, L. Jacques, P. Vielva, and P. Vandergheynst, "Fast directional correlation on the sphere with steerable filters," *Astrophys. J.*, vol. 652, no. 1, pp. 820–832, Nov. 2006.

[36] Y. Wiaux, J. D. McEwen, P. Vandergheynst, and O. Blanc, "Exact reconstruction with directional wavelets on the sphere," *Mon. Not. R. Astron. Soc.*, vol. 388, no. 2, pp. 770–788, 2008.

[37] B. T. T. Yeo, W. Ou, and P. Golland, "On the construction of invertible filter banks on the 2-sphere," *IEEE Trans. Image Process.*, vol. 17, no. 3, pp. 283–300, Mar. 2008.

[38] Z. Khalid, S. Durrani, P. Sadeghi, and R. A. Kennedy, "Spatio-spectral analysis on the sphere using spatially localized spherical harmonics transform," *IEEE Trans. Signal Process.*, vol. 60, no. 3, pp. 1487–1492, Mar. 2012.

[39] Z. Khalid, P. Sadeghi, R. A. Kennedy, and S. Durrani, "Spatially varying spectral filtering of signals on the unit sphere," *IEEE Trans. Signal Process.*, vol. 61, no. 3, pp. 530–544, Feb. 2013.

[40] P. Sadeghi, R. A. Kennedy, and Z. Khalid, "Commutative anisotropic convolution on the 2-sphere," *IEEE Trans. Signal Process.*, vol. 60, no. 12, pp. 6697–6703, Dec. 2012.

[41] Z. Khalid, R. A. Kennedy, S. Durrani, P. Sadeghi, Y. Wiaux, and J. D. McEwen, "Fast directional spatially localized spherical harmonic transform," *IEEE Trans. Signal Process.*, vol. 61, no. 9, pp. 2192–2203, 2013.

[42] Z. Khalid, S. Durrani, R. A. Kennedy, and P. Sadeghi, "On the construction of low-pass filters on the unit sphere," in *Proc. IEEE Int. Conf. Acoust., Speech, Signal Process., ICASSP'2011*, Prague, Czech Republic, May 2011, pp. 4356–4359.

[43] W. Huang, Z. Khalid, and R. A. Kennedy, "Efficient computation of spherical harmonic transform using parallel architecture of cuda," in *5th International Conference on Signal Processing and Communication Systems, ICSPCS'2011*, Honolulu, HI, Dec. 2011, p. 6.

[44] Z. Khalid, S. Durrani, R. A. Kennedy, and P. Sadeghi, "Revisiting Slepian concentration problem on the sphere for azimuthally non-symmetric regions," in *5th International Conference on Signal Processing and Communication Systems, ICSPCS'2011*, Honolulu, HI, Dec. 2011, p. 7.

[45] Z. Khalid, S. Durrani, P. Sadeghi, and R. A. Kennedy, "Concentration uncertainty principles for signals on the unit sphere," in *Proc. IEEE Int. Conf. Acoust., Speech, Signal Process., ICASSP'2012*, Mar. 2012, pp. 3717–3720.

[46] Z. Khalid, R. A. Kennedy, S. Durrani, and P. Sadeghi, "Conjugate gradient algorithm for extrapolation of sampled bandlimited signals on the 2-sphere," in *Proc. IEEE Int. Conf. Acoust., Speech, Signal Process., ICASSP'2012*, Kyoto, Japan, Mar. 2011.

[47] Z. Khalid, S. Durrani, P. Sadeghi, and R. A. Kennedy, "Ambiguity function and Wigner distribution on the sphere," in *Proc. IEEE Int. Conf. Acoust., Speech, Signal Process., ICASSP'2012*, Kyoto, Japan, Mar. 2011.

[48] Z. Khalid, R.A. Kennedy, and P. Sadeghi, "Efficient computation of commutative anisotropic convolution on the 2-sphere," in *6th International Conference on Signal Processing and Communication Systems, ICSPCS'2012*, Gold Coast, Australia, Dec. 2012, p. 7.

[49] R. A. Kennedy, P. Sadeghi, Z. Khalid, and J. D. McEwen, "Classification and construction of closed-form kernels for signal representation on the 2-sphere," in *Wavelets and Sparsity XIV, SPIE international symposium on optics and photonics, invited contribution*, 2013.

[50] Z. Khalid, R. A. Kennedy, P. Sadeghi, and S. Durrani, "Spatio-spectral formulation and design of spatially-varying filters for signal estimation on the 2-sphere," in *Wavelets and Sparsity XIV, SPIE international symposium on optics and photonics, invited contribution*, 2013.

[51] J. R. Driscoll and D. M. Healy, Jr., "Computing Fourier transforms and convolutions on the 2-sphere," *Adv. Appl. Math.*, vol. 15, no. 2, pp. 202–250, June 1994.

[52] R. A. Kennedy, T. A. Lamahewa, and L. Wei, "On azimuthally symmetric 2-sphere convolution," *Digital Signal Processing*, vol. 5, no. 11, pp. 660–666, Sept. 2011.

[53] D. Slepian and H. O. Pollak, "Prolate spheroidal wave functions, Fourier analysis and uncertainity-I," *Bell Syst. Techn. J.*, vol. 40, pp. 43–63, Jan. 1961.

[54] H. J. Landau and H. O. Pollak, "Prolate spheroidal wave functions, Fourier analysis and uncertainity-II," *Bell System Tech J.*, vol. 40, pp. 65–84, Jan. 1961.

[55] H. J. Landau and H. O. Pollak, "Prolate spheroidal wave functions, Fourier analysis and uncertainity-III: The dimension of the space of essentially time- and band-limited signals," *Bell System Tech J.*, vol. 41, pp. 1295–1336, 1962.

[56] D. Slepian, "Fourier analysis and uncertainty-IV: extensions to many dimensions; generalized prolate spheroidal functions," *Bell Syst. Tech. J*, vol. 43, pp. 3009–3057, 1964.

[57] A. Albertella, F. Sansò, and N. Sneeuw, "Band-limited functions on a bounded spherical domain: the Slepian problem on the sphere," *J. Geodesy*, vol. 73, no. 9, pp. 436–447, June 1999.

[58] J. J. Sakurai, *Modern Quantum Mechanics*, Addison Wesley Publishing Company, Inc., Reading, MA, 2nd edition, 1994.

[59] J. D. McEwen and Y. Wiaux, "A novel sampling theorem on the sphere," *IEEE Trans. Signal Process.*, vol. 59, no. 12, pp. 5876–5887, Dec. 2011.

[60] I. H. Sloan and R. S. Womersley, "A variational characterisation of spherical designs," *J. Approx. Theory*, vol. 159, no. 2, pp. 308–318, Aug. 2009.

[61] R. G. Crittenden and N. G. Turok, "Exactly azimuthal pixelizations of the sky," *Arxiv preprint astro-ph/9806374*, 1998.

[62] K. M. Huffenberger and B. D. Wandelt, "Fast and exact spin-s spherical harmonic transforms," *Astrophys. J. Supp.*, vol. 189, no. 2, pp. 255–260, Aug. 2010.

[63] Z. Khalid, R. A. Kennedy, and J. D. McEwen, "An optimal-dimensionality sampling scheme on the sphere with fast spherical harmonic transforms," *IEEE Trans. Signal Process.*, vol. 62, no. 17, pp. 4597–4610, Sept. 2014.

[64] I. H. Sloan and R. S. Womersley, "Extremal systems of points and numerical integration on the sphere," *Adv. Comput. Math.*, vol. 21, no. 1, pp. 107–125, Jul. 2004.

[65] M. J. Mohlenkamp, "A fast transform for spherical harmonics," *J. Fourier Anal. and Appl.*, vol. 5, no. 2-3, pp. 159–184, 1999.

[66] J.A.R. Blais and M.A. Soofi, "Spherical harmonic transforms using quadratures and least squares," in *Computational Science ICCS 2006*, vol. 3993 of *Lecture Notes in Computer Science*, pp. 48–55. Springer Berlin Heidelberg, 2006.

[67] N. Sneeuw, "Global spherical harmonic analysis by least-squares and numerical quadrature methods in historical perspective," *Geophys. J. Int.*, vol. 118, no. 3, pp. 707–716, Sept. 1994.

[68] D. M. Healy, Jr., D. Rockmore, P. J. Kostelec, and Sean S. B. Moore, "FFTs for the 2-sphere - improvements and variations," *J. Fourier Anal. and Appl.*, vol. 9, pp. 341–385, 2003.

[69] K. M. Górski, E. Hivon, A. J. Banday, B. D. Wandelt, F. K. Hansen, M. Reinecke, , and M. Bartelmann, "HEALPix: A framework for high-resolution discretization and fast analysis of data distributed on the sphere," *Astrophysical J.*, vol. 622, no. 2, pp. 759–771, Apr. 2005.

[70] Y. Wiaux, L. Jacques, and P. Vandergheynst, "Fast spin 2 spherical harmonics transforms and application in cosmology," *J. Comput, Phys.*, vol. 226, no. 2, pp. 2359–2371, 2005.

[71] P. J. Kostelec and D. N. Rockmore, "FFTs on the rotation group," *J. Fourier Anal. and Appl.*, vol. 14, pp. 145–179, 2008.

[72] C. AN, X. Chen, I. H. Sloan, and R. S. Womersley, "Well conditioned spherical designs for integration and interpolation on the two-sphere," *SIAM J. Numer. Anal.*, vol. 48, no. 6, pp. 2135–2157, Dec. 2010.

[73] E. Bannai and E. Bannai, "A survey on spherical designs and algebraic combinatorics on spheres," *Eur. J. Comb.*, vol. 30, no. 6, pp. 1392–1425, Aug. 2009.

[74] W. Skukowsky, "A quadrature formula over the sphere with application to high resolution spherical harmonic analysis," *J. Geodesy*, vol. 60, no. 1, pp. 1–14, Mar. 1986.

[75] A. G. Doroshkevich, P. D. Naselsky, O. V. Verkhodanov, D. I. Novikov, V. I. Turchaninov, I. D. Novikov, P. R. Christensen, and Chiang, "Gauss Legendre Sky Pixelization (GLESP) for CMB maps," *Int. J. Mod. Phys. D.*, vol. 14, no. 02, pp. 275–290, Feb. 2005.

[76] X. Chen, A. Frommer, and B. Lang, "Computational existence proofs for spherical t-designs," *Numer. Math.*, vol. 117, no. 2, pp. 289–305, Feb. 2011.

[77] X. Chen, A. Frommer, and B. Lang, "Computational existence proofs for spherical t-designs," *Numer. Math.*, vol. 117, no. 2, pp. 289–305, Feb. 2011.

[78] M. Reimer, *Constructive theory of multivariate functions: with an application to tomography*, BI-Wissenschaftverlag, 1990.

[79] M. Reimer, "Spherical polynomial approximations: a survey," *MATH RES*, vol. 107, pp. 231–252, Nov. 1999.

[80] M. A. Wieczorek and F. J. Simons, "Localized spectral analysis on the sphere," *Geophys. J. Int.*, vol. 162, no. 3, pp. 655–675, Sept. 2005.

[81] M. A. Sharifi and S. Farzaneh, "Regional TEC dynamic modeling based on Slepian functions," *Adv. Space Res*, vol. 56, no. 5, pp. 907–915, Sept. 2015.

[82] K. Jahn and N. Bokor, "Vector Slepian basis functions with optimal energy concentration in high numerical aperture focusing," *Opt. Commun*, vol. 285, no. 8, pp. 2028–2038, Nov. 2012.

[83] A. P. Bates, Z. Khalid, and R. A. Kennedy, "Efficient computation of Slepian functions for arbitrary regions on the sphere," *ArXiv preprint 1608.05479*, Aug. 2016.

[84] A. Albertella and N. Sneeuw, "The analysis of gradiometric data with Slepian functions," *Phys. Chem. Earth Pt. A*, vol. 25, no. 9, pp. 667–672, Dec. 2000.

[85] C. Harig and F. J. Simons, "Ice mass loss in Greenland, the Gulf of Alaska, and the Canadian Archipelago: Seasonal cycles and decadal trends," *Geophys. Res. Lett.*, vol. 43, no. 7, pp. 3150–3159, Apr. 2016.

[86] F. A. Dahlen and F. J. Simons, "Spectral estimation on a sphere in geophysics and cosmology," *Geophys. J. Int.*, vol. 174, pp. 774–807, 2008.

[87] A. Plattner and F. J. Simons, "High-resolution local magnetic field models for the Martian South Pole from Mars Global Surveyor data," *J. Geophys. Res. Planets*, vol. 120, no. 9, pp. 1543–1566, Sept. 2015.

[88] A. P. Bates, Z. Khalid, and R. A. Kennedy, "Slepian spatial-spectral concentration problem on the sphere: Analytical formulation for limited colatitude-longitude spatial region," *IEEE Trans. Signal Process.*, vol. 65, no. 6, pp. 1527–1537, Mar. 2017.

[89] C. Lessig and E. Fiume, "On the effective dimension of light transport," in *Proc. Eurographics Symposium on Rendering 2010*, Saarbrücken, Germany, June 2010, vol. 29, pp. 1399–1403.

[90] W. Zhang, R. A. Kennedy, and T. D. Abhayapala, "Signal estimation from incomplete data on the sphere," in *2008 Australian Communications Theory Workshop*, Jan 2008, pp. 39–44.

[91] R. A. Kennedy, W. Zhang, and T. D. Abhayapala, "Spherical harmonic analysis and model-limited extrapolation on the sphere: Integral equation formulation," in *2008 2nd International Conference on Signal Processing and Communication Systems*, Dec 2008, pp. 1–6.

[92] W. Zhang, R. A. Kennedy, and T. D. Abhayapala, "Iterative extrapolation algorithm for data reconstruction over sphere," in *2008 IEEE International Conference on Acoustics, Speech and Signal Processing*, March 2008, pp. 3733–3736.

[93] L. S. Zhou, C. C. Bao, M. S. Jia, and B. Bu, "Range extrapolation of head-related transfer function using improved higher order ambisonics," in *Sig-*

nal and Information Processing Association Annual Summit and Conference (APSIPA), 2014 Asia-Pacific, Dec 2014, pp. 1–4.

[94] B. Rafaely, "Analysis and design of spherical microphone arrays," *IEEE Transactions on speech and audio processing*, vol. 13, no. 1, pp. 135–143, 2005.

[95] B. Rafaely, B. Weiss, and E. Bachmat, "Spatial aliasing in spherical microphone arrays," *IEEE Transactions on Signal Processing*, vol. 55, no. 3, pp. 1003–1010, 2007.

[96] M. Zaldarriaga and U. Seljak, "All-sky analysis of polarization in the microwave background," *Phys. Rev. D*, vol. 55, pp. 1830–1840, Feb 1997.

[97] A. K. Pradhan and S. N. Nahar, "Atomic astrophysics and spectroscopy," 2011.

[98] C. A. J Fletcher, *Computational techniques for fluid dynamics*, New York, USA, 1988.

[99] F. A. Gilbert, "Inverse problems for the earth's normal modes, mathematical problems in the geophysical sciences," *American Mathematical Society, Providence*, vol. 1, 1971.

[100] J. D. McEwen, "Fast, exact (but unstable) spin spherical harmonic transforms," *All Res. J. Phys.*, vol. 1, no. 1, 2011.

[101] P. J. Kostelec, D. K. Maslen, D. M. Healy, and D. N. Rockmore, "Computational harmonic analysis for tensor fields on the two-sphere," *J. Comput. Phys.*, vol. 162, no. 2, pp. 514–535, Aug. 2000.

[102] K. M. Huffenberger and B. D. Wandelt, "Fast and exact spin-s spherical harmonic transforms," *The Astrophysical Journal Supplement Series*, vol. 189, no. 2, pp. 255, 2010.

[103] M. Reinecke, "libsharp: Library for spherical harmonic transforms," Astrophysics Source Code Library, Feb. 2014.

[104] M. Reinecke and D. S. Seljebotn, "Libsharp - spherical harmonic transforms revisited," *Astron. & Astrophys.*, vol. 554, pp. A112, 2013.

[105] U. Elahi, Z. Khalid, and R. A. Kennedy, "Comparative analysis of geometrical properties of sampling schemes on the sphere," *in 2016 10th International Conference on Signal Processing and Communication Systems (ICSPCS)*, pp. 1–7, Dec 2016.

[106] K. Ivanov and P. Petrushev, "Irregular sampling of band-limited functions on the sphere," *Appl Comput Harmon Anal.*, vol. 37, no. 3, pp. 545 – 562, Nov. 2014.

[107] J. Keiner, S. Kunis, and D. Potts, "Efficient reconstruction of functions on the sphere from scattered data," *J. Fourier Anal. Appl.*, vol. 13, no. 4, pp. 435–458, May 2007.

[108] S. Kunis and D. Potts, "Fast spherical fourier algorithms," *J. Comput. Appl. Math.*, vol. 161, no. 1, pp. 75 – 98, Dec. 2003.

[109] S. Kunis and D. Potts, "Stability results for scattered data interpolation by trigonometric polynomials," *SIAM J. Sci. Comput.*, vol. 29, no. 4, pp. 1403–1419, Feb. 2007.

[110] L. Shen and M. K. Chung, "Large-scale modeling of parametric surfaces using spherical harmonics," in *3D Data Processing, Visualization, and Transmission, Third International Symposium on*, June 2006, pp. 294–301.

[111] C. T. Kelley, *Iterative Methods for Linear and Nonlinear Equations*, Society for Industrial and Applied Mathematics, 1995.

[112] R. Barrett, M. Berry, T. Chan, J. Demmel, J. Donato, J. Dongarra, V. Eijkhout, R. Pozo, C. Romine, and H. van der Vorst, *Templates for the Solution of Linear Systems: Building Blocks for Iterative Methods*, Society for Industrial and Applied Mathematics, 1994.

[113] A. Papoulis, "A new algorithm in spectral analysis and band-limited extrapolation," *IEEE Transactions on Circuits and Systems*, vol. 22, no. 9, pp. 735–742, September 1975.

[114] Y. F. Alem, Z. Khalid, and R. A. Kennedy, "Band-limited extrapolation on the sphere for signal reconstruction in the presence of noise," in *2014 IEEE International Conference on Acoustics, Speech and Signal Processing (ICASSP)*, May 2014, pp. 4141–4145.

[115] J. Meyer and T. Agnello, "Spherical microphone array for spatial sound recording," in *Audio Engineering Society Convention 115*. Audio Engineering Society, 2003.

[116] G. Weinreich and E. B. Arnold, "Method for measuring acoustic radiation fields," *The Journal of the Acoustical Society of America*, vol. 68, no. 2, pp. 404–411, 1980.

[117] T. D. Abhayapala and D. B. Ward, "Theory and design of high order sound field microphones using spherical microphone array," in *2002 IEEE International Conference on Acoustics, Speech, and Signal Processing*, May 2002, vol. 2, pp. II–1949–II–1952.

[118] J. Meyer and G. Elko, "A highly scalable spherical microphone array based on an orthonormal decomposition of the soundfield," in *2002 IEEE International Conference on Acoustics, Speech, and Signal Processing*, May 2002, vol. 2, pp. II–1781–II–1784.

[119] D. L. Alon and B. Rafaely, "Beamforming with optimal aliasing cancellation in spherical microphone arrays," *IEEE/ACM Transactions on Audio, Speech, and Language Processing*, vol. 24, no. 1, pp. 196–210, Jan 2016.

[120] J. Meyer and G. W. Elko, "Handling spatial aliasing in spherical array applications," in *Hands-Free Speech Communication and Microphone Arrays, 2008. HSCMA 2008*. IEEE, 2008, pp. 1–4.

[121] G. Weinreich and E. B. Arnold, "Method for measuring acoustic radiation fields," *The Journal of the Acoustical Society of America*, vol. 68, no. 2, pp. 404–411, 1980.

[122] M. Park and B. Rafaely, "Sound-field analysis by plane-wave decomposition using spherical microphone array," *The Journal of the Acoustical Society of America*, vol. 118, no. 5, pp. 3094–3103, 2005.

[123] A. G. Doroshkevich, P. D. Naselsky, O. V. Verkhodanov, D. I. Novikov, V. I. Turchaninov, I. D. Novikov, P. R. Christensen, and Chiang, "Gauss Legendre Sky Pixelization (GLESP) for CMB maps," *Int. J. Mod. Phys. D.*, vol. 14, no. 02, pp. 275–290, Feb. 2005.

[124] D. S. Seljebotn and H. K. Eriksen, "Sympix: A spherical grid for efficient sampling of rotationally invariant operators," *Astrophys. J., Suppl. Ser.*, vol. 222, no. 2, pp. 17, Apr. 2015.

[125] K. M. Grski, E. Hivon, A. J. Banday, B. D. Wandelt, F. K. Hansen, M. Reinecke, and M. Bartelmann, "Healpix: A framework for high-resolution discretization and fast analysis of data distributed on the sphere," *Astrophys. J.*, vol. 622, no. 2, pp. 759, Apr. 2005.

[126] R. O. Duda and W. L. Martens, "Range-dependence of the hrtf for a spherical head," in *Proceedings of 1997 Workshop on Applications of Signal Processing to Audio and Acoustics*, Oct 1997, pp. 5 pp.–.

[127] J. D. McEwen and Y. Wiaux, "A novel sampling theorem on the sphere," *IEEE Trans. Signal Process.*, vol. 59, no. 12, pp. 5876–5887, Dec 2011.

[128] U. Elahi, Z. Khalid, and R. A. Kennedy, "Spatially constrained anti-aliasing filter using slepian eigenfunction window on the sphere," *in 2018 12th International Conference on Signal Processing and Communication Systems (ICSPCS)*, Dec. 2018.

[129] Z. Khalid, R. A. Kennedy, and S. Durrani, "On the choice of window for spatial smoothing of spherical data," in *Acoustics, Speech and Signal Processing (ICASSP), 2014 IEEE International Conference on*. IEEE, 2014, pp. 2644–2648.

[130] B. Rafaely, "Phase-mode versus delay-and-sum spherical microphone array processing," *IEEE signal processing Letters*, vol. 12, no. 10, pp. 713–716, 2005.

[131] B. Devaraju, *Understanding filtering on the sphere: experiences from filtering GRACE data*, 2015.

[132] F. J. Harris, "On the use of windows for harmonic analysis with the discrete fourier transform," *Proceedings of the IEEE*, vol. 66, no. 1, pp. 51–83, 1978.